Stockholm University

Bachelor Thesis

Degree Project in
Geology 30 hp

Qualitative and quantitative petrography of meta-mafic rocks at Ölme, in the Eastern Segment of the Sveconorwegian orogen

Diana Carlsson

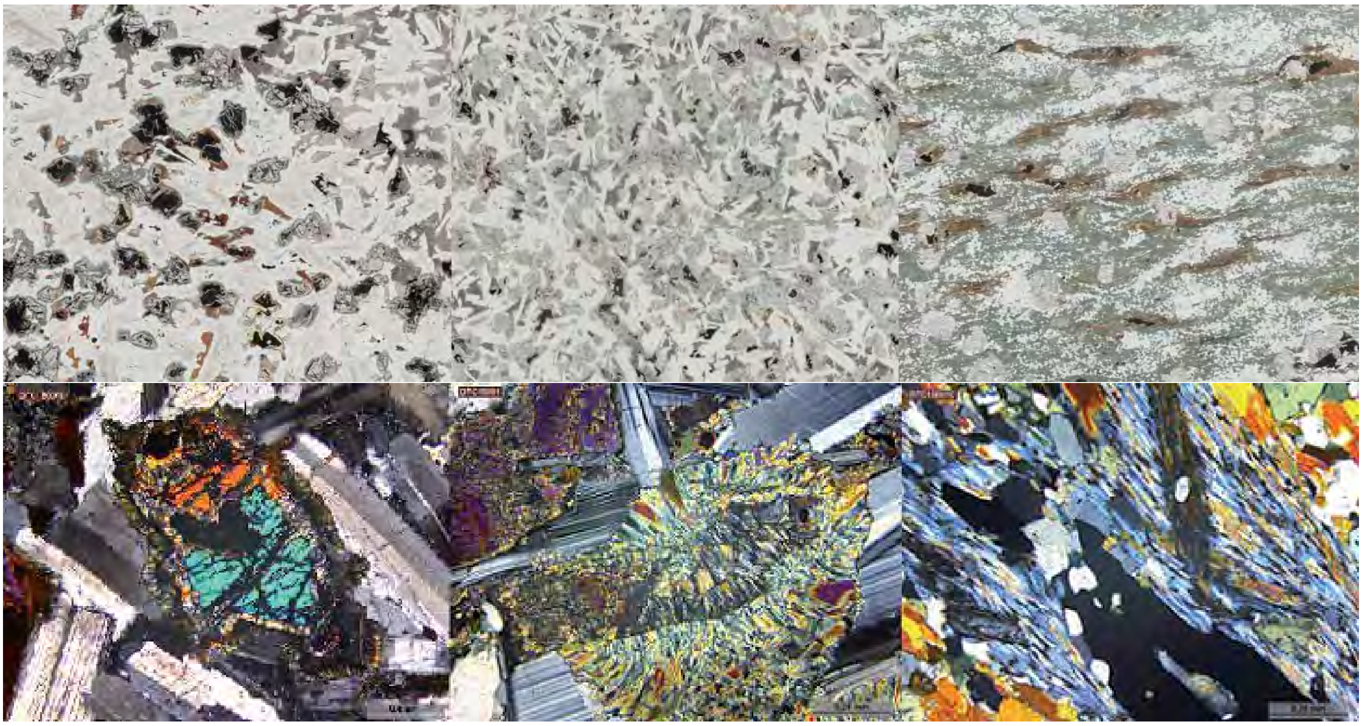

Stockholm 2015

Department of Geological Sciences
Stockholm University
SE-106 91 Stockholm

Abstract

Meta-mafic intrusions with an intrusion age of 1.6-0.9 Ga are found along a north-south trend in the Transitional section of the Eastern Segment in Sweden. These intrusions are garnet-bearing and thus an exception to other meta-mafic intrusions found in Sweden. Meta-mafic intrusions that are garnet-bearing are usually found in the Caledonides to the northeast and in the south west of Sweden where the pressures have been naturally high due to orogenic events or subduction.

The study was conducted on these intrusions around the community of Ölme, to understand the metamorphic and metasomatic history of the area. The focus lies on the transition from magmatic gabbroic intrusions to metamorphosed metagabbros and highly foliated garnet-amphibolites. Average PT estimates was calculated using THERMOCALC and classical geothermobarometry, so that a comparison between the qualitative and quantitative data could be made.

The study indicates metamorphism at amphibolite to upper amphibolite facies conditions for the metagabbros and the garnet-amphibolites.

Average PT-estimates for the garnet-amphibolites gives metamorphic peak temperatures of 680°-730° C with pressures of 9.0-11.0 kbar at the Träfors locality, and metamorphic peak temperatures of 660°-770° C with pressures of 9.5-11.0 kbar at the Skråkvik locality. These results are comparable to research done further to the south on similar intrusions, with temperatures of 700° C and pressures of 10 kbar.

It is concluded that the meta-mafic intrusions at the Skråkvik locality have been metamorphosed in a dry system, in contrast to the Träfors locality which seems to have been affected by more pervasive retrograde metamorphism and fluid-rock interaction. It is also concluded that mafic intrusions can preserve their magmatic textures even under high pressure conditions.

Keywords:
metamorphism, high pressure, amphibolite, granulite, gabbro, metagabbro, garnet-amphibolite, complex coronitic textures, symplectite, Eastern Segment, Transitional section

Abbreviations*

Albite	ab
Apatite	ap
Backscatter Electron	BSE
Biotite	bt
Calcite	cal
Clinopyroxene	cpx
Crossed polarized light	XPL
Epidote	ep
Feldspar	fsp
Garnet	gt
Ilmenite	ilm
Hornblende	hb
Magnetite	mt
Microcline	mc
Muscovite	mu
Opaque minerals/oxides	ox
Orthopyroxene	opx
Plagioclase	pl
Plain polarized light	PPL
Pyrite	py
Pyroxene	px
Quartz	qz
Reflected light	RFL
Saussurite	sau
Sericite	ser
Siderite	sid
Titanite	ttn
Zircon	zrn

*Abbreviations are from THERMOCALC and are not USGS standard

Table of contents

Introduction

Meta-mafic intrusions are found along a north-south trend to the west of the Sveconorwegian deformation zone in the Eastern Segment in Sweden. These intrusions are garnet-bearing and thus an exception to other meta-mafic intrusions found in Sweden. Meta-mafic intrusions that are garnet-bearing are usually found in the Caledonides to the northeast and in the southwest of Sweden where the pressures have been naturally high due to orogenic events or subduction.

The purpose of the study is to do qualitative and quantitative petrography on these meta-mafic intrusions around the community of Ölme in south central Sweden. This can give a better understand of the metamorphic and metasomatic history of the area. The focus of the study is the transition from magmatic gabbroic intrusions to metamorphosed metagabbros and highly foliated garnet-amphibolites, representing a metamorphic overprint with changing temperature, pressure and fluid-rock interaction. Average PT estimates will also be calculated using THERMOCALC and classical geothermobarometry, so that a comparison between the qualitative and quantitative data can be made.

The subject of a detailed petrographic study and quantitative PT have not been made for this area. Previous studies have focused on geochemistry for both the surrounding orthogneiss bedrock and the meta-mafic intrusions, earlier classified as hyperites, and on structural geology (Morthors et al. 1982, Lundegård, 1980). Further to the south in the Eastern Segment, petrography and PT have been made on similar intrusions, the Åker metabasite (Söderlund et al. 2004). This study revealed higher pressures, 10-12 kbar, which might have contributed to the garnet growth in these intrusions. Interesting would be to determine the pressure in Ölme, which would be expected to be high since these intrusions too are garnet-bearing. The mineralogical transition is also seen at the Åker metabasite and the same classification have been used in this study to distinguish between the different types. The classifications used are; unaltered gabbro type I, metamorphosed metagabbro with no foliation, type II and foliated/highly foliated garnet-amphibolites type III and type IV.

The general aspect of this study is to get a better understanding for the metamorphic evolution and the tectonic model at a larger scale. Such models for the Eastern Segement and the Sveconorwegian orogen have been discussed in more detail by Möller et al. (2015) and Slagstad et al. (2013) among others.

Geological setting

The Transitional section of the Eastern Segment, Sveconorwegian orogen

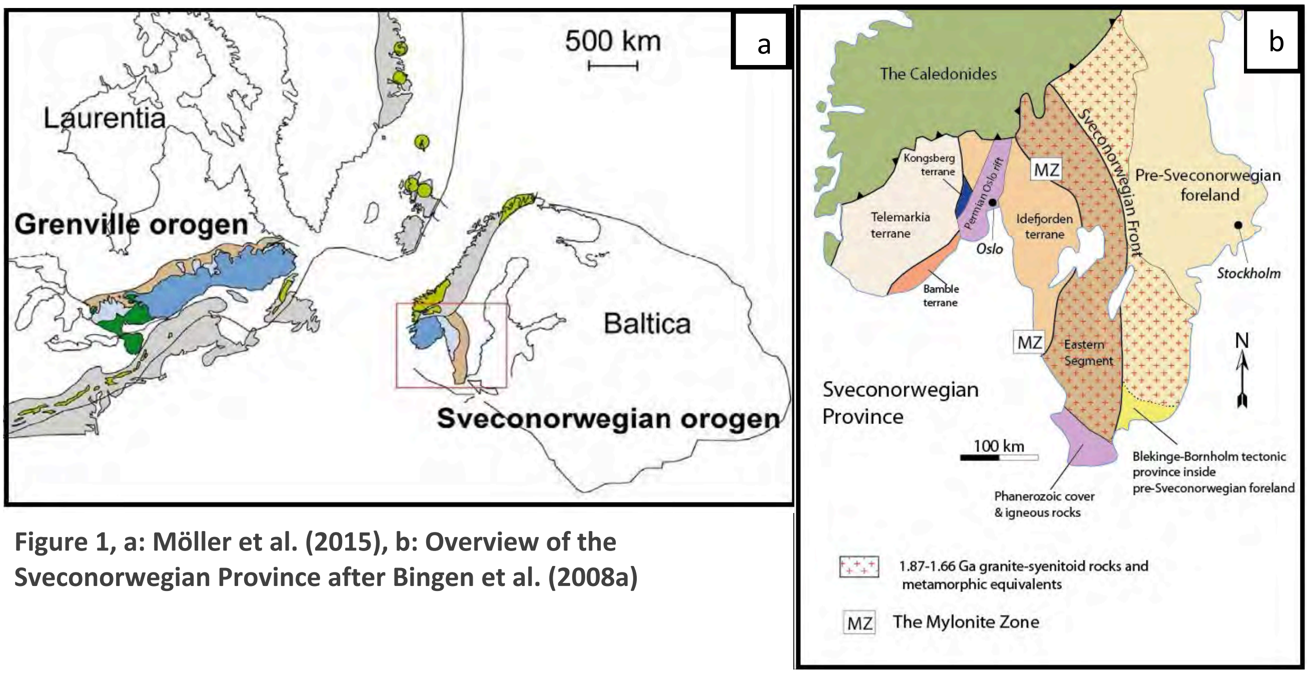

Figure 1, a: Möller et al. (2015), b: Overview of the Sveconorwegian Province after Bingen et al. (2008a)

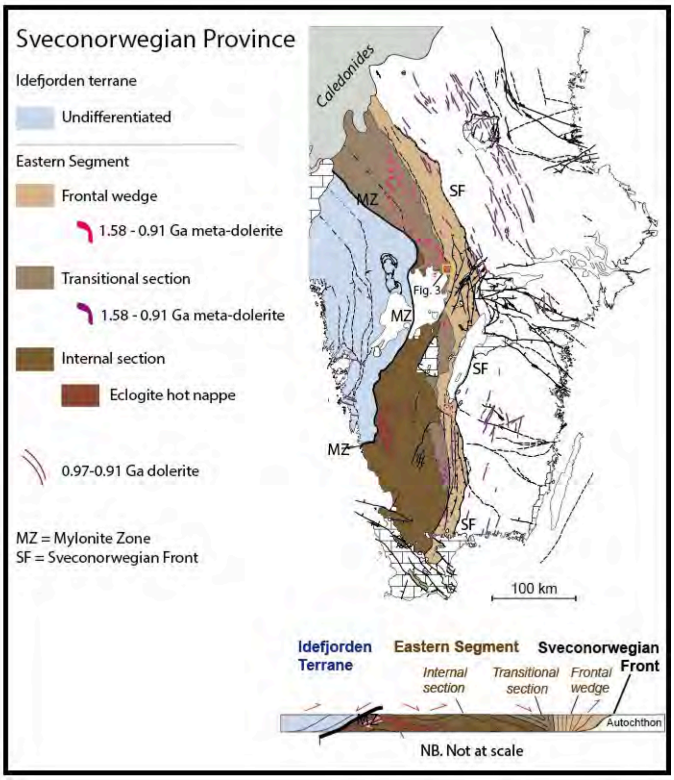

Figur 2, The Sveconorwegian Province (Möller et al. 2015 and SGU database)

Southern Scandinavia belongs to the Sveconorwegian Province, a ca 1.14-0.90 Ga old, > 500 km wide orogenic belt, situated in the western part of the Baltic shield (figure 1a). It has been correlated with the Grenville Province in North America (Lidiak, 1996). Five distinctive orogenic segments have been recognised, these are from west to east: The Telemarkia terrane, the Kongsberg terrane, the Bamble terrane, The Idefjord terrane and the Eastern Segment. These are separated by roughly N-S trending crustal-scale shear zones (figure 1b) (Bingen et al. 2008b). At least four metamorphic events have affected the Sveconorwegian Province between 1.14 and 0.90 Ga (Bingen et al. 2008b, Möller et al. 2015). The earliest metamorphic event, the Arendal phase, is dated at ca. 1.14-1.08 Ga, and affected the central segments (Kongsberg and the Bamble terranes) with metamorphism reaching granulite facies conditions at low to intermediate pressures. It was followed by the 1.05-0.98 Ga Agder phase which included upper greenschist to amphibolite facies conditions across the Idefjorden and the Telemarkia terranes, and high pressure metamorphism at amphibolite to granulite facies conditions in the Idefjorden terrane just west of the Mylonite Zone (Bingen et al., 2008b; Söderlund et al., 2008) (Söderlund et al 2004). The Eastern Segment was affected by late Sveconorwegian metamorphism of the Falkenberg phase, dated to

0.99-0.97 Ga (Bingen et al., 2008b, Möller et al., 2015). This orogenic phase included regional scale metamorphism at upper amphibolite to high-pressure granulite facies conditions and eclogite facies metamorphism in a hot nappe internal to the Eastern Segment followed by wide spread partial melting (Möller 1998; 1999; Möller et al., 2015). The youngest and final metamorphic event, the Dalane phase, occurred between 0.97 and 0.90 Ga, and included high-temperature and low pressure metamorphism associated with anortosite-mangarite-charnockite-granite magmatism and ferroan granite magmatism west of the Mylonite Zone (Bingen et al. 2008a).

The Eastern Segment is the easternmost of five orogenic segments constituting the Sveconorwegian orogen. The eastern boundary of the Eastern Segment is the Sveconorwegian Front, and the western boundary is the Mylonite Zone. The Sveconorwegian Front is the eastern boundary for ductile Sveconorwegian deformation recorded in the Balstic Shield. The Mylonite Zone is a ductile high-strain deformation zone separating the allochthonous units in the west from the parautochthonous Eastern Segment in the east (Bingen et al. 2008b).

The Eastern Segment consists of rocks that were metamorphosed at between 0.99 and 0.96 Ga during the Sveconorwegian orogeny, but that were formed and in places also metamorphosed during older orogenic events. These include 2.0-1.8 Ga metamorphic and igneous Svecofennian rocks, about 1.8-1.7 Ga intrusions of the Transscandinavian Igneous Belt and 1.5-1.4 Ga granite intrusions variously affected by reworking during the 1.47-1.38 Ga Hallandian orogeny (Wahlgren et al., 1994; Söderlund et al., 1999; Möller et al., 20007; Zarins and Johansson 2009). The Eastern Segment thus consists of the same rocks that are found in the remainder of the Baltic Shield, east of the Sveconorwegian orogen and is in this aspect referred to as a parautochthonous segment. This is in contrast to the four other terranes west of the Mylonite Zone that have been tectonically transported and accreted (Wahlgren et al. 1994; Möller et al., 2015).

Based on style and character of the Sveconorwegian metamorphic and deformational imprint, three principal lithotectonic domains can be distinguished in the Eastern Segment, these are: the frontal wedge, the transitional section and the internal section (figure 2). The frontal wedge shows non-penetrative ductile deformation and the metamorphic facies ranges from greenschist in the east to amphibolite facies in the west. Rocks in the transitional section has experienced penetrative ductile deformation at amphibolite facies conditions but have not reached conditions of partial melting. Rocks in the internal section have experienced penetrative ductile deformation and partial melting at upper amphibolite to granulite facies conditions and eclogite facies conditions have been recorded in a distinct tectonic unit inside the internal section (Johansson et al. 1991, Möller et al. 2015).

Geology of Ölme

The area of interest to this study forms part of the transitional section and is located just north of Lake Vänern between Karlstad and Kristinehamn (figure 3). The main rock types are 1.74-1.66 Ga metamorphosed igneous rocks with a granitic to syenitoid composition, intruded by dolerites between 1.58 and 0.91 Ga, which are classified as meta-mafic intrusions in this study. Just to the east, between the Frontal and Transitional section, metamorphosed igneous rocks is found with the same age but with gabbroic to dioritic composition. The Frontal section consists of older 1.82-1.77 Ga metamorphosed igneous rock with the same composition as the main rocks in the Transitional section, but with younger dolerite intrusions, dated between 0.97 and 0.94 Ga. The main rock types belongs to the Transscandinavian Igneous Belt.

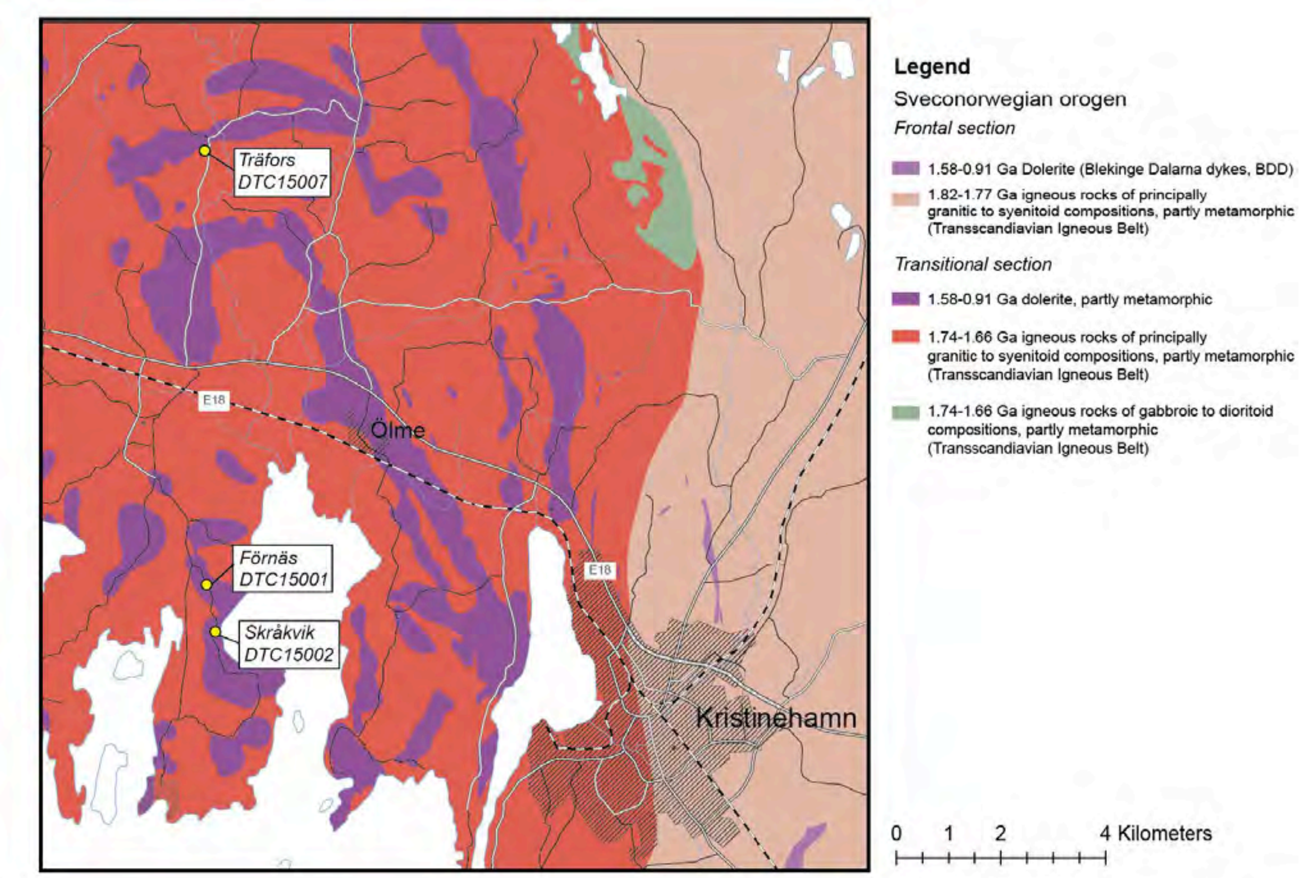

Figure 3, locality map over Ölme area with sampled sites

An early petrogenetic investigation of the meta-mafic intrusions in Värmland was made by Törnebohm (1877) where he in detail distinguished between hyperite and hyperite-diorite based on the relic magmatic textures seen in the recrystallized rocks as well as the mineralogy. Hyperite is an old term that is no longer used as a petrographic term, it was given by the hypersthene orthopyroxenes often found in gabbroic rocks, that weathers with a brownish tint. Törnebohm also noticed a diorite slate along the gneiss contact, but made no further description of this rock type. The diorite slate is interpreted as the foliated garnet-amphibolite that have been studied in this thesis. Högbom (1922) divided the hyperites into three groups; hyperite, hyperite-diorite and hyperite-amphibole. This classification was also used by Morthors et al. (1982). Magnusson (1928, 1933, 1960) noted that the hyperites where younger than the surrounding bedrock but older than the metamorphic event contributing to the gneissic layering. He argued that the recrystallization seen in the hyperites was in fact a result of this later event. Lundegårdh (1977, 1980) made a structural study in the area and found at least three different ductile deformational events: the first event gave rise to folding along NNW trending axes, a second event was characterised by folding along N(NW) trending axes, the last deformation event included folding along E-W trending axes and NNW striking thrust zones.

The geochemical classification of the Ölme intrusions have been discussed in detail by both Morthorst et al. (1982) and Johansson & Johansson (1990), and are thought to be derived from a continental magma source, possibly enriched by mixing with lower crustal material.

U-Pb analyses of baddeleyite of well preserved, unmetamorphosed and undeformed lenses of meta-mafic intrusions in Värmland have given igneous crystallisation ages of these dolerites at 1569±3 Ma (Transitional section, Ölme, Söderlund et al., 2005) and 1568±30 Ma (Björneborg, Frontal section, Wahlgren et al., 1996).

Unpublished U-Pb zircon data from a garnet-amphibolite at Skråkvik, south of Ölme, inferred as a reworked meta-mafic dolerite support a Sveconorwegian age for the dutile deformation and metamorphism of the meta-mafic intrusions (960±12 Ma, SGU unpublished data).

Methods

Sampling and thin section preparation

A total of twenty-eight samples from seven different localities were taken from the studied area. For this study three localities are used, Förnäs, Skråkvik and Träfors (figure 3). Förnäs can be seen as an extension of the Skråkvik locality and lies in the same intrusion according to mapping done by the Geological Survey of Sweden (figure 3). Förnäs were chosen because of its gabbro, which is lacking at the Skråkvik locality. The Förnäs and Skråkvik localities lie approximately 800 meter from each other. To better understand this locality, and as a complement to the metamorphic dating, Skråkvik together with Förnäs where chosen. Träfors was chosen due to its large outcrop with several clear transitions between all three rock types, gabbro, metagabbro and garnet-amphibolite. All the transitions were found within decimetres of each other in the Skråkvik and Träfors locality.

Seventeen of these samples were prepared for thin section. Each sample were sawed perpendicular to the ß-plane (foliation) and parallel to the lineation. Each sample were coarse grinded with Silicon Carbide (SiC 180) abrasive before being sent to the company ABC a Head in Poland for final thin section cut. Each thin section was made without a cover glass so that a scanning electron microscope analysis could be done within this study.

Microscopic examination

A detailed petrographic analysis can be a very important source of data if done properly. Well described mineralogy, mineral reactions, microtextures, deformation and exsolution reactions can help understand the overall history for the rock, metamorphism and fluid-rock interaction.

For each thin section, the following information were documented using mainly a Leica optical polarization microscope or by direct study of the thin section or hand sample:

- main minerals
- accessory minerals < 5%
- the texture of the thin section, grain boundaries and deformation
- dark phases in %
- detailed description of pyroxenes, amphiboles, plagioclase and garnets, with anorthite-albite determination for plagioclase feldspars using the Michel-Levy method (Nesse, 2012)
- foliation: the minerals that define the foliation and description of micas
- detailed descriptions of mineral reactions, reaction textures and inclusions

Both plane polarized and crossed polarized light were used. Reflected light were used to determine oxides. Pictures were taken with a Las Ez camera and edited with the same software. All thin sections, pre- and post-cut were scanned using a Braun FS120 scanner (CyberView X5). Textures and deformation are determined and described according to the approach of Passchier and Trouw (2005).

Scanning Electron Microscope, SEM

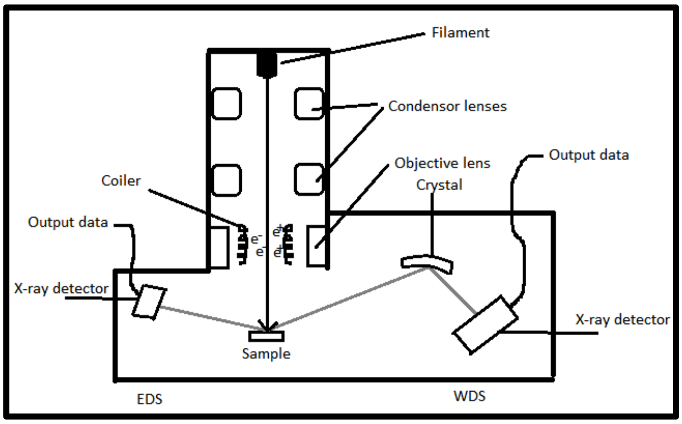

Figure 4, schematic view of Scanning Electron Microscope

Scanning Electron Microscope (SEM) can be used to determine the chemical composition and density of a mineral, as well as making chemical and morphological images of the analysed surface. High energy electrons are created by heating a tungsten filament and are focused with the help of condensor lenses. The electrons are decelerated at a known voltage to attain a certain acceleration towards the prepared sample. When the elements in the sample is struck by the high energy electrons, or the electron beam, several secondary waves are produced. One are the characteristic x-rays. X-rays are dispersed when the inner shell electron in the element has enough energy to leave its orbit, giving rise to an ionized atom. This highly unstable state will be compensated within 0.1 fs, by the outermost energetic electron jumping to the vacant inner shell and thus exciting a measurable x-ray fluorescence photon. In a wavelength dispersive spectrometer, some of these emitted wavelengths hits one or several mounted crystals where the x-rays are reflected depending on the crystal lattice. The reflected x-rays are detected by an x-ray tube that can be set between 0° and 90°. The tube measures the energy of each x-ray and registers the number of x-rays within the same wavelength by scintillation or gas-flow counts, depending on element. The counts are directly proportional to the concentration of the element. By using Bragg's law for constructive interference, the electrons momentum and known densities for an element, the composition of the sample can be determined (Rouessac & Rouessac 2007, Jönsson & Nilsson 2009). Beside the x-rays, low energy secondary electrons and high energy backscatter electrons are also produced when the electron beam hits the sample. These can be detected with a second electron detector, giving rise to 3- and 1-dimensional images of the analysed surface and its composition. Several other secondary particles are dispersed during an electron microprobe analysis, but will not be discussed further in this study.

For this study, a Hitachi S-3400N scanning electron microscope at the Geological Institution, Gothenburg University, was used. The electron microscope has both wavelength-dispersive spectrometers and energy-dispersive spectrometers, and can do both qualitative and quantitative elemental analyses, ranging from Sodium to Uranium. The electron beam was set to 20 kV and the probe current to 6.00 nA at a working distance of 9.6 mm. Calibration was made routinely against a cobalt metal standard. Each analyse was set to 40 seconds. Error of the element oxide is given by (wt.% sigma*compound/wt.%).

Fe^{3+} correction for the amphiboles, garnets and pyroxenes was made according to Droop (1987), where garnets and pyroxenes have been corrected with the equation:

$$F^{3+} = 2X\left(1 - \frac{T}{S}\right)$$

[eq. 1]

Where X is the total oxygen for the mineral, T is the total cation and S is the cation sum from the SEM analyse.

Amphiboles have been corrected with the equation:

$$F^{3+} = 46(1 - 15\psi)$$

[eq. 2]

Where ψ=∑(Si, Ti, Al, Cr, Fe, Mn, Mg, Ca) in the uncorrected formula.

Fe^{3+} is normalized by multiplying it with the difference of T/S (total cation divided by cation sum) and recalculated into Fe_2O_3 by taking 1.1113 x old Feo wt.% x $Fe^{3+}/(Fe^{3+}+Fe^{2+})$. For a detailed discussion, please see Droop (1987).

Geothermobarometry

Solid solution minerals in equilibrium can serve as barometers and thermometers. The key is to find a mineral reaction that has achieved this equilibrium. With SEM data for the minerals of interest, activity can be calculated. This is done with the software AX, by Holland and Powell (1998), in this study.

The activity gives us information about how effectively the mineral will react in a certain reaction. By using the activity, known mineral reactions and experimentally derived thermodynamic datasets within the software THERMOCALC (Powell and Holland, 1994), average temperature and pressure was estimated.

Dynamic equilibrium is considered when the Gibbs free energy is zero. If a change is implied on the system, the system will respond to reduce that change, also known as Le Chatelier's principle. This principle is used by THERMOCALC when calculating average PT.

The Gibbs free energy for a reaction at any pressure or temperature is given by:

$$\Delta G_{reaction} = \sum (n_{products} G_{products} - n_{reactants} G_{reactants})$$

[eq. 3]

Where *G* is given in J/mol. This equation can also be applied to the difference in volume, *ΔV,* and the difference in entropy, *ΔS*.

Changes in the Gibbs free energy for a reaction for a particular pressure and temperature is given by:

$$d\Delta G = \Delta V dP - \Delta S dT$$

[eq. 4]

Where *d* is the change, *Δ* is the difference, *V* is the volume (m^3), *S* the entropy (J/mol-K), T is given in °K and P is given in Pa.

Changes in the Gibbs free energy for a phase that do not vary with pressure and temperature is given by:

$$G = H - TS$$

Where H is the enthalpy (J/mol). [eq. 5]

Equation 4 and 5 can be integrated and incorporated with values from equation 3 for both the Gibbs free energy, the volume and the entropy as well as the gas law to better correspond to natural system containing both gas and fluids. THERMOCALC calculates the average intersection between the barometers and thermometers derived from a combination of reworked equivalents of equation 4 and 5 and the activity for the minerals:

$$\Delta G = 0 = a + bT + cP + RTlnK$$

[eq. 6]

Where a=ΔH, b=ΔS, c=ΔV, R is the ideal gas constant (J/mol-K) and K the equilibrium constant for the reaction. The equilibrium constant is based on the activities for the reactants and products for the reaction. The K-value for the general reaction $reactant_1+Xreactant_2=Yproduct_1+product_2$ is calculated with:

$$K = \frac{a_{r1} * a_{r2}^{X}}{a_{p1}^{Y} * a_{p2}} \qquad \text{[eq. 7]}$$

For a more detailed discussion, please see the Thermodynamics section in Winter (2014).

Dynamic equilibrium between minerals can be seen in the textures and grain boundaries in the microscopic study. This can also be confirmed with SEM data where chemical profiles along the minerals should show little or no variation in chemical zoning. Dynamic equilibrium can also be seen in microdomains between certain minerals, even though the rock seems to be in an overall disequilibrium. PT-estimates can still be done in such rocks, but caution should be taken. A clear understanding for these microdomains and local equilibrium should be argued for.

PT data calculated by THERMOCAL have been evaluated based on the diagnostics after Powell and Holland (1994). These are the sig fit, e* and HAT value, corresponding to the control of uncertainties of enthalpy and activity input data, the difference between measured and calculated activity normalized to the uncertainty and the end-members influence on the least-squares results.

Results

Locality and macroscopic descriptions

A detailed locality and macroscopic description of the localities are found in appendix A.

Förnäs

Sample DTC15001, coordinates N6577986, E0440702

Förnäs is a small road side outcrop which is, approximately 10 meters wide. The outcrop has a brownish weathering on the blasted surface, and a "bulgy" appearance, where mafic domains are standing out as large varts < 40 mm, on the natural surface.

The hand sample has a dark greenish colour with a purple tint and an isotropic texture. It is medium grained and contains black pyroxene, green mafic minerals and plagioclase laths. The plagioclase has a somewhat purple colour and might have been slightly hydrothermally or metamorphically affected. This rock was classified as a gabbro, but re-classification to a metagabbro was done after the thin section study.

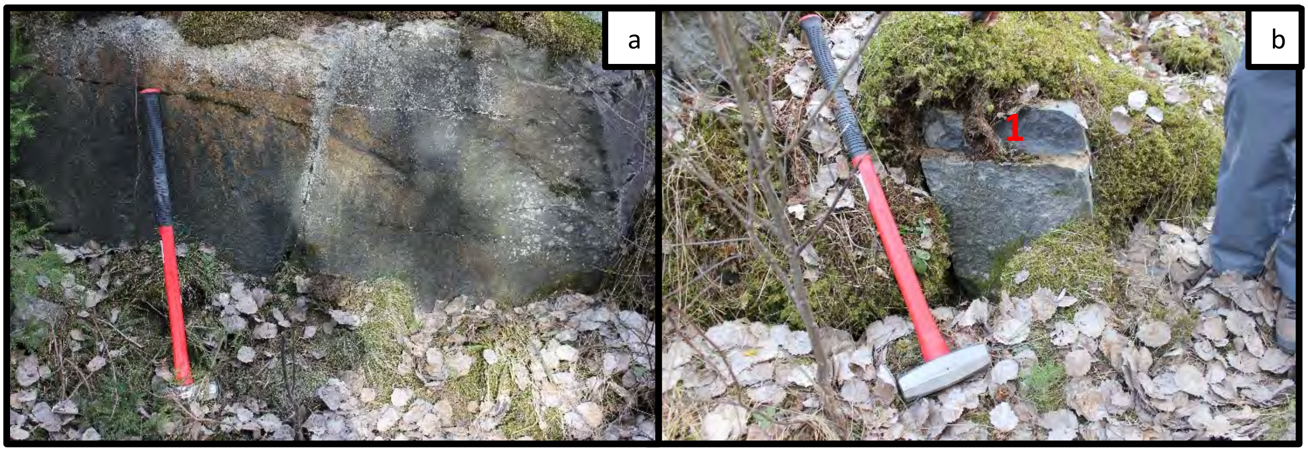

Figure 5, a: Förnäs outcrop with metagabbro, possible pyroxenes have weathered with a rusty brown colour, the picture is taken towards the east, scale of sledge hammer ~1 m in height b: Sample outcrop DTC15001

Skråkvik

Samples DTC15002, coordinates N6577089, E0440868

Skråkvik is a road side outcrop which is approximately 25 meters wide. This outcrop has a clear transition from more well preserved magmatic textures in the metagabbro to highly metamorphosed amphibolites. This transitions goes from south to north and the metamorphic grade changes over a few decimetres. The metagabbro has small brownish weathering spots, probably from weathered orthopyroxenes, while the garnet-amphibolite has a more evenly brown weathered surface.

Zircon dating has been made at this locality, determining the metamorphic overprint to about 960±12 Ma. Younger fine grained, mafic intrusions where found at the outcrop, trending in the NNE-SSW direction and dipping to the west (figure 6b). These are probably younger than 960±12 Ma metamorphic overprint since they cut the foliation seen in the surrounding bedrock. At the northern end of this outcrop a fine grained mafic rock is found which contains < 11 mm large garnets (figure 6d). The rock is highly foliated with a gneissic texture and aligned garnet are seen on the weathered surface.

The metagabbros at this locality are medium grained and have an isotropic texture. They have a dark green colour with a tint of purple towards reddish/brown, plagioclase is found both as laths and recrystallized with a brownish colour. Garnets < 2 mm small are found in both the plagioclase and in contact with the mafic minerals. Biotite domains are sparse.

The garnet-amphibolites are often unevenly grained, have an anisotropic texture, with larger aggregates of mafic minerals and plagioclase. The rocks have a dark green colour, occasionally with a light purple tint, recrystallized plagioclase is found as aggregates and has a white/brownish colour. Biotite is common as both larger domains < 7 mm and as individual crystals. The biotite is somewhat aligned in all the samples.

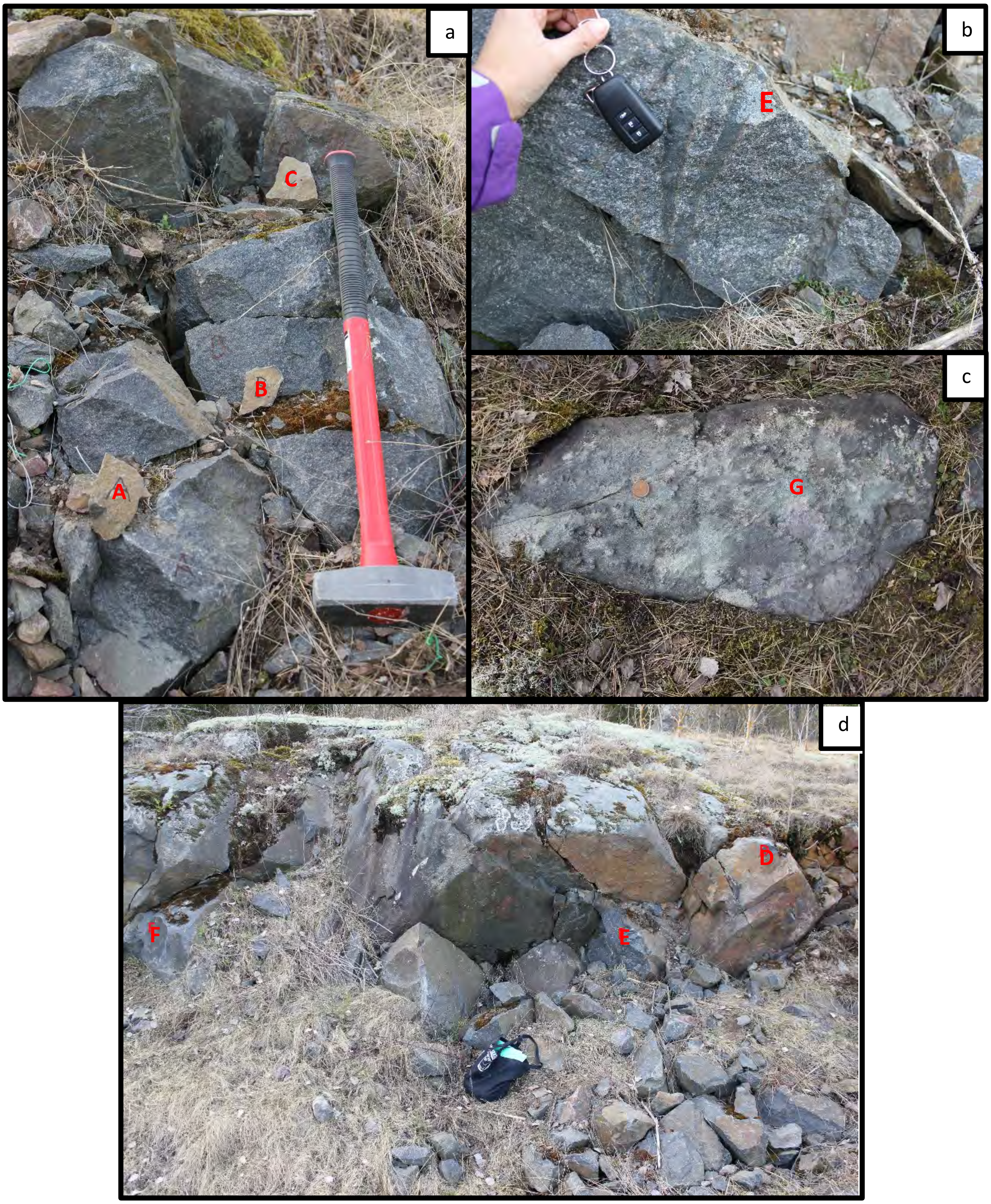

Figure 6, a: sample outcrop A-C b: diabase intrusion, sample E, c: garnet-amphibolite, sample G, d: sample outcrop, D-F, containing metagabbro with different metamorphic grades, the picture is taken towards the west, scale of bag ~30 cm

Träfors

Samples DTC15007, coordinates N6586280, E0440666 to N6586364, E0440710

Träfors is a large, partly new outcrop behind a farm house. It is approximately 85-90 meters wide. This outcrop shows a clear transition from well preserved gabbro to metagabbro with preserved magmatic textures to highly foliated amphibolites. This transitions goes from SSW to NNE and the metamorphic grade changes over a few decimetres. A schistose chlorite zone, about 40 cm wide and 200 cm long, was found where striated rocks have been pressed out, slightly bowl shaped, between the metagabbros. Melting between the orthogneiss and the meta-mafic intrusions is seen 150 meters west of the Träfors locality, but no melting textures is found in the studied locality.

The gabbro is fine grained with a dark mafic matrix and isotropic texture. It has rusty brown weathering surface and dark larger plagioclase laths are occasionally seen in the sample.

The metagabbro at this locality ranges from fine to coarse grained and has an isotropic texture. They have a dark black colour with a green or reddish tint. The metagabbros contain dark black or green mafic minerals and in the coarse grained samples well developed amphiboles are seen. Plagioclase is often recrystallized with a brownish/purple colour, but large plagioclase laths are seen in the coarse grained samples. Both biotite domains and garnets are < 2 mm and are found in the medium to coarse grained samples.

The garnet-amphibolites also ranges from fine to coarse grained and have an anisotropic texture. They have a dark black colour with a reddish, purple or greenish tint. The garnet-amphibolites often have a dark black or green mafic matrix with large recrystallized plagioclase aggregates, < 15 mm. In some samples the mafic minerals and the plagioclase are elongated parallel to the foliation. Biotite domains < 3 mm and garnets < 5 mm are common. Biotite is also often well aligned in the samples.

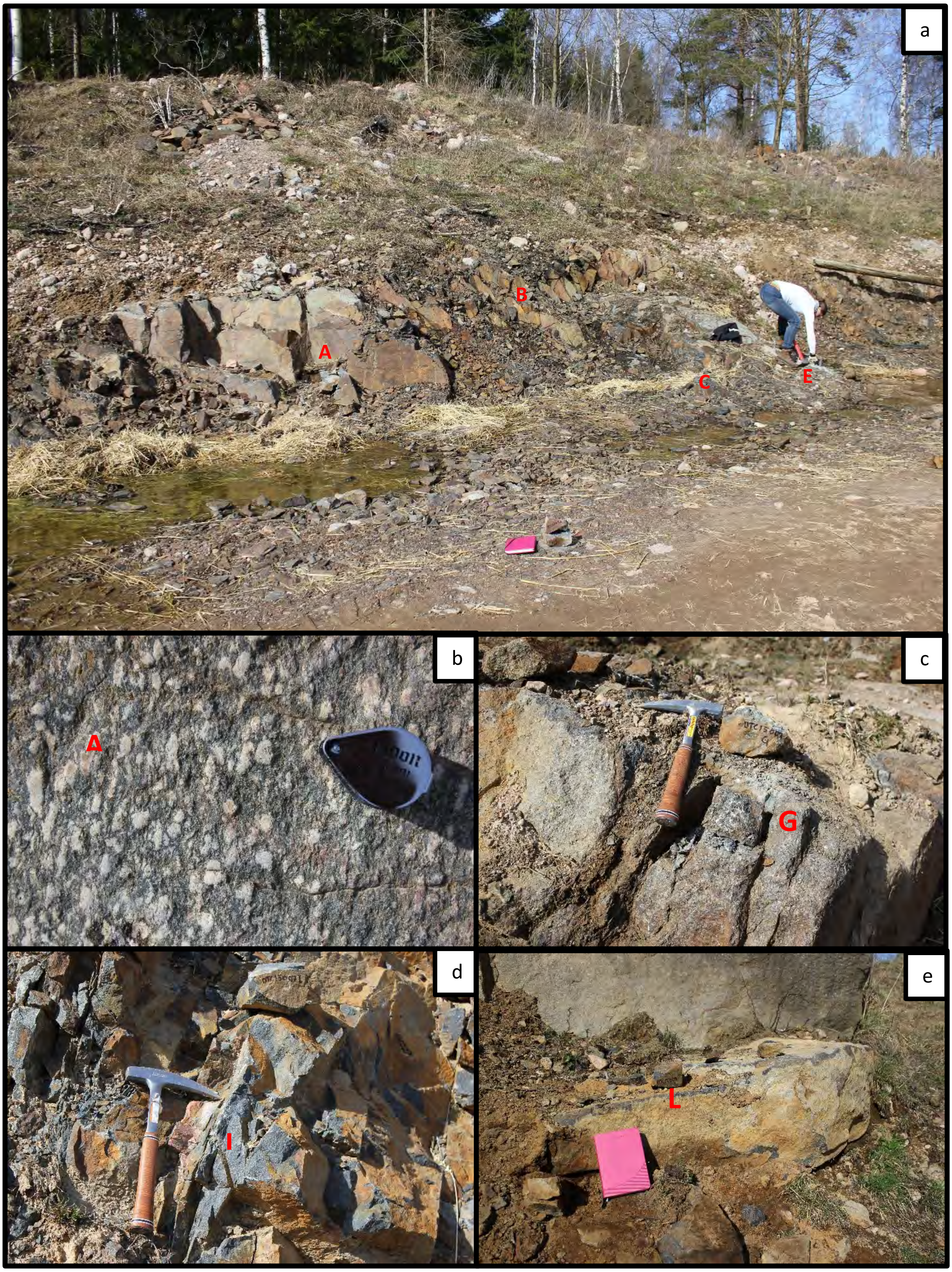

Figure 7, a: Sample outcrop A-C, E, the picture is taken towards the north west, b: garnet-amphibolite, sample A, c: metagabbro, sample G, d: garnet-amphibolite, sample I, e: gabbro, sample L

Petrography and SEM analysis

A detailed petrographic description for each thin section is found in appendix B. SEM data and chemical profiles are found in appendix C and D.

SEM was conducted on six of the seventeen samples, one gabbro, two metagabbros and three garnet-amphibolites. The SEM data is used to confirm chemical composition of minerals found in the petrographic study, to do a mineralogical comparison of the rock types and to calculate PT-estimates in the next section.

Gabbro, type I

Gabbro is only found at the Träfors locality. It has a typical coronitic appearance in the thin section with inequigranular texture and polygonal grain boundaries.

Olivine

Olivine crystals have a composition of fosterite$_{30-40}$, they have a prismatic habit where some shows a complex coronitic texture with ferrosilite and ferrotschermakite as inner and outer rim where olivines are surrounded by plagioclase. Olivines surrounded by augite tends to have a rim consisting of ferrosilite that has been affected by the augite composition. Fractures are common and are filled with opaque minerals, orthopyroxene and possible chlorite or serpentinite.

Plagioclase

Plagioclase laths have a composition of anorthite$_{50-60}$, labradorite, and chemical zoning is not seen even though the crystals have a clear concentric zoning in the microscope (figure 8b).

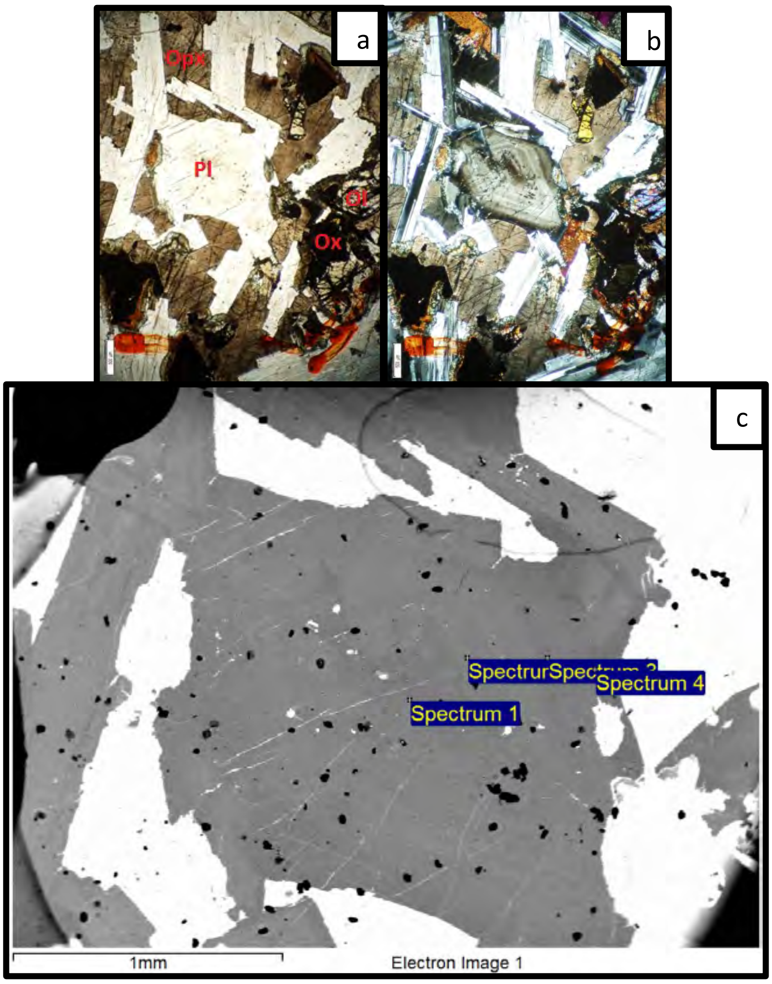

Figure 8, a: PPL - (orange colour is from the pen marking), b: XPL – concentric zoning in pl, pl laths with albite twin (orange colour is from the pen marking), BSE – Pl with no clear chemical zoning

Clinopyroxene

Clinopyroxene is found as interstitial magmatic crystals and have an augitic composition. Chemical zoning in some of the pyroxenes are seen where the core has a composition of an orthopyroxene and the rim has a composition of clinopyroxene. Thin exsolution lamellae of orthopyroxenes and oxides occur in some crystals. Clinopyroxene crystals is found as both early prismatic crystals and later interstitial crystals.

Orthopyroxene

Orthopyroxene is found as both interstitial magmatic crystals and as rims in the complex coronitic textures. Both types have a composition of enstatite$_{50-60}$, where the magmatic orthopyroxene usually has a lower enstatite component. No zoning have been observed but small exsolution lamellae of augite are common, indicating higher temperature and slow cooling (Nesse 2009). Orthopyroxene is a late interstitial crystallized phase.

Amphibole

Hornblende is found only as late interstitial rims in the complex coronitic textures. It has a composition of pargasite to ferro-pargasite but with depleted Na content. Hornblende is also found as rims around the opaque minerals, where intergrowth formations are common, containing small crystals with Si, Al, Fe and Mg rich minerals, with accessory Ca, Mn and Zn. These crystals have not been identified.

Biotite

Biotite is sparse in the gabbro where they are found as late interstitial crystalized minerals, often as rims around the opaque minerals, and rimmed by late orthopyroxene. This is seen in both the petrographic study and confirmed with the SEM. Reaction rims are evolved by replacement of previous minerals and are considered as isolated features (Passchier and Trouwe, 2005). The biotite has a different colour in comparison to the biotite found in both the metagabbros and the garnet-amphibolites where the SEM analysis confirms high Fe and Ti content as consistent with the biotite rimming ilmenite in most cases. The biotite has a composition of annite44.

Opaque minerals

The opaque minerals are ilmenite, magnetite and pyrite. They often have a radiating corona of biotite and an outer rim of hornblende where the opaque minerals are surrounded by plagioclase. Magnetite is found as symplectite formations together with interstitial orthopyroxene (figure 9). Since orthopyroxene is a late interstitial mineral, it normally crystalizes by the following reaction:

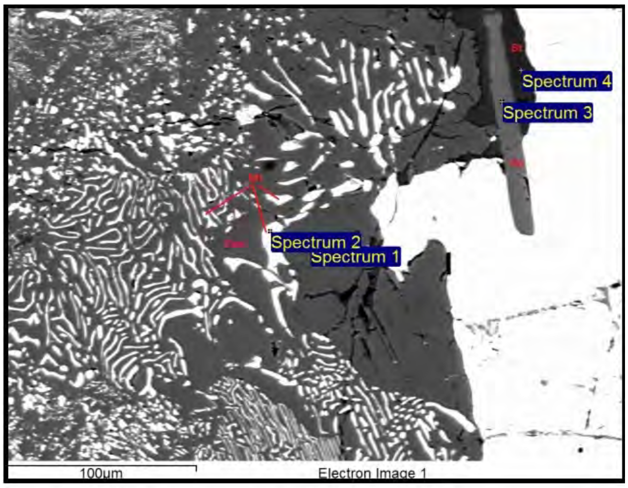

Figure 9, BSE - Symplectite formation between mt and opx

$$\underset{\text{olivine}}{(Fe,Mg)_2SiO_4} + SiO_2 \Longrightarrow \underset{\text{orthopyroxene}}{(Fe,Mg)_2Si_2O_6} \qquad [R1]$$

Additional reactions must have occurred in this rock:

$$\underset{\text{olivine}}{6(Fe,Mg)_2SiO_4} + O_2 \Longrightarrow \underset{\text{fayalite}}{3Mg_2SiO_4} + \underset{\text{magnetite}}{2Fe_3O_4} + 3SiO_2 \qquad [R2]$$

$$\underset{\text{fayalite}}{Mg_2SiO_4} + \underset{\text{quartz}}{SiO_2} \Longrightarrow \underset{\text{enstatite}}{Mg_2Si_2O_6} \qquad [R3]$$

Where free O_2 is given by early penetrating water into the hot gabbro.

Metagabbro, type II

Metagabbro is found at all three localities. The main difference lies in the overall texture with a more coronitic and relict igneous textures found at Förnäs and Skråkvik. For all localities, the metagabbros have a seriate texture that is coarse grained with both polygonal and interlobate grain boundaries.

Amphibole

Hornblende is found ranging between tschermakite to pargasite and their ferro counterparts. Pargasite is found closer to the possible recrystallized olivine, and tschermakite is found at the rim in contact with plagioclase. Again there is intergrowth formations at the outer edge of the rim, but the minerals are too small to analyse in the SEM. Overall they seem to have less Al and more Si than the surrounding amphibole. Hornblende could be either metamorphic or late interstitial magmatic at the inner parts of the rims.

$$\underset{\text{orthopyroxene}}{(Mg,Fe)SiO_3} + \underset{\text{clinopyroxene}}{Ca(Mg,Fe)Si_2O_6} + 2(\underset{\text{plagioclase}}{(Ca,Na)Al_2Si_2O_8}) + H_2O = \underset{\text{hornblende}}{(Ca,Na)_{2\text{–}3}(Mg,Fe,Al)_5(Al,Si)_8O_{22}OH_2} + SiO_2 \qquad [R4]$$

Plagioclase

Plagioclase laths are mostly subhedral, they have a composition of anorthite$_{40\text{-}70}$ with a chemical zoning ranging between labradorite in the core and andesine at the rim.

Garnet

Garnets are common in the metagabbros. They occur both as rims and as coronas, often around the opaque minerals. There are two types of garnets present. Type 1 has a typical sieve texture that seems to be in apparent textural disequilibrium with the surrounding minerals. These garnets are found as cores in larger garnets or as rims around other minerals. Type 2 has a clear euhedral habit with very few inclusions, if any. These garnets suffer however from fractures more often than type 1 does. Garnets that are close to biotite seems to be in apparent textural equilibrium with the surrounding minerals, this is probably due to the Al exchange that the biotite and garnet might have. Since biotite is crystallized late, and these garnets lack inclusions, this indicates that the type 2 garnets crystallized at the same time or later than the biotite. From the SEM-analysis we have that the type 2 garnets have a chemical zoning with a Mg/Mn rich core and a Fe rich rim. Suggesting retrograde crystallization where biotite is present.

$$\underset{\text{augite}}{CaFeSi2O_6} + \underset{\text{anorthite}}{CaAl_2Si_2O_8} \Longrightarrow \underset{\text{garnet}}{(CaFe)_3Al_2Si_3O_{12}} + SiO_2 \qquad [R6]$$

Biotite

Biotite is a late crystallizing mineral often found as thick rims around the opaque minerals when in contact with plagioclase, or in symplectite formations with the opaque minerals. In the metagabbros biotite is found as annite$_{41}$. The following reaction for biotite is possible:

$$\underset{\text{k-feldspar}}{KalSi_3O_8} + 3FeO + H_2O \Longrightarrow \underset{\text{annite}}{KFe_3(AlSi_3O_{10})(OH)_2} \qquad [R5]$$

Where FeO comes from ilmenite or augite.

Orthopyroxene

Orthopyroxene is found as possible recrystallized olivines surrounded by a hornblende rim. They have a composition of enstatite$_{60}$, which is higher than the orthopyroxenes found in the gabbro.

$$\underset{\text{olivine}}{(Mg,Fe)_2SiO_4} + SiO_2 \Longrightarrow \underset{\text{ferrosilite}}{2(Mg,Fe)SiO_3} \qquad [R7]$$

Clinopyroxene

Clinopyroxene is augitic with a clear blue colour indicating high Ti content. This was confirmed by the SEM where the clinopyroxene in the metagabbros has higher amount of Ti in comparison to the gabbro. The clinopyroxenes that are surrounded by plagioclase have a clear rim of hornblende. Intergrowth formations between clinopyroxene, hornblende and quartz are common in the metagabbros, indicating the presence of fluids and lower temperature at a later stage. Orthopyroxene and oxide lamellae is common in the clinopyroxenes.

Hornblende rim around clinopyroxenes could have recrystallized by the following reaction:

$$\underset{\text{augite}}{5CaFeSi_2O_6} + \underset{\text{anorthite}}{2CaAl_2Si_2O_8} + 2H_2O + 3FeO \Longrightarrow \underset{\text{ferrotschermakite}}{2Ca_2Fe_4Al_2Si_2O_{22}(OH)_2} + 3CaO \qquad [R8]$$

Where FeO comes from ilmenite or augite.

Opaque minerals

The opaque minerals are ilmenite and pyrite, determined by microscopy analysis. Magnetite was not seen, but might occur. The opaque minerals often have a radiating corona of biotite and an outer rim of hornblende where enclosed by plagioclase, similar to the opaque minerals in the gabbro. They are also seen as inclusions in the pyroxenes, giving them a dusty appearance.

Garnet-amphibolite, type III and IV

Garnet-amphibolite is found at the Skråkvik and Träfors localities. They have no magmatic texture or replacement textures left, and where foliation is defined by hornblende, biotite, and at the Träfors locality also chlorite and titanite. The texture is seriate with fine to medium grained crystals, where dynamic recrystallization ranges from fine to coarse grained with mostly medium to high deformation. Grain boundaries are interlobate with minor polygonal grain boundaries in the type III, whilst type IV only has polygonal grain boundaries.

Amphibole

Hornblende is found as interstitial crystals often as cumulates along the foliation. They have a composition of pargasite to ferro-pargasite being somewhat depleted in Na and Ca but enriched with Fe and Mg. Overall the Al and Na content increases with increasing metamorphic grade from type I to type IV based on the petrographic analysis and the SEM data. The Al enrichment and Fe decrease is indicated by the petrographic analysis based on the colour of the hornblende. For hornblende the relationship is Fe^{3+} and Ti substitution for Al, where blue-green hornblende has high Fe^{3+} and Ti but low Al and brown-green hornblende has low Fe^{3+} and Ti but high Al (Frost and Frost (2014)).

A possible reaction for hornblende could be:

$$\underset{\text{anorthite}}{2CaAl_2Di_2O_8} + \underset{\text{augite}}{3CaFeSi_2O_6} + \underset{\text{albite}}{NaAlSi_3O_8} + 2H_2O + 5FeO \Longrightarrow \underset{\text{Fe-pargasite}}{NaCa_2Fe_4Al_3Si_6O_{22}(OH)_2} + \underset{\text{Fe-tschermakite}}{Ca_2Fe_4Al_2Si_7O_{22}(OH)_2} + CaO \qquad [R9]$$

Plagioclase

Plagioclase ranges from subhedral to anhedral habit where sericitization and saussuritization increases with increasing anorthite composition. Type III has a composition of $anorthite_{30\text{-}40}$ while type IV has a composition of $anorthite_{20\text{-}30}$, both belonging to oligoclase. The decrease of anorthite composition is clearly seen from type I to type IV.

Garnet

Garnets are mostly euhedral and fractures are common. Sieve textures are more common in type III but do occur in type IV, consistent with type 1 garnets found in the metagabbros. In type IV the garnets seems to be in apparent textural equilibrium with the surrounding minerals, consistent with type 2 garnets found in the metagabbros. Overall the garnets have less inclusions than the metagabbros where very little chemical zoning between the core and rim is found. Again with a retrograde indication of crystallization where Fe and Mg is higher in the core than in the rim. Garnets may have crystallized by the following reaction:

$$\underset{\text{anorthite}}{36CaAl_2Si_2O_8} + \underset{\text{augite}}{31CaFeSi_2O_6} + \underset{\text{ilmenite}}{32FeTiO_3} + 2H_2O \Longrightarrow \underset{\text{titanite}}{32CaTiSiO_5} + \underset{\text{garnet}}{30(Ca,Fe)3Al_2Si_3O_{12}} + \underset{\text{zoisite}}{4Ca_2Al_3Si_3O_{12}(OH)} \quad [R10]$$

Biotite

Biotite is found as interstitial crystals often as cumulates along the foliation. They have a composition of $annite_{43}$. There is a clear decrease in Fe and Ti from type I to type IV. The general relationship for biotite is that the colour reflects Fe and Mg content, where a green-brown colour indicates a Mg-rich composition with high $Fe^{3+}/(Fe^{2+}+Fe^{3+})$, and red-brown indicates a Fe-rich composition with low $Fe^{3+}/(Fe^{2+}+Fe^{3+})$ and is also Ti-bearing (Lalonde and Bernard, 1993).

Chlorite

Chlorite is found with a Berlin blue colour indicating high Fe content. Based on the SEM data, this could be an orthochamosite, a polytype of chamosite, which is probably an alteration product from the breakdown of pyroxenes, amphiboles, biotite and/or garnets. The chlorite is retrograde and has probably crystallized during late uplift and fluid access.

$$\underset{\text{annite}}{K(Mg,Fe)_3AlSi_3O_{10}(OH)_2} + H_2O + \underset{\text{ferrotschermakite}}{Ca_2Fe_4Al_2Si_7O_{22}(OH)_2} = \underset{\text{chamosite}}{((Mg,Fe)_5Al)(AlSi_3)O_{10}(OH)_8} + \underset{\text{k-feldspar}}{KAlSi_3O_8} + CaO + \overset{\text{quartz}}{SiO_2} \quad [R11]$$

Where CaO comes from anorthite.

Titanite

Titanite is common in the garnet-amphibolites. They occur as thin rims around the opaque minerals and more often as cumulates along the foliation. These could have crystallized according to the following reaction:

$$\underset{\text{k-feldspar}}{KalSi_3O_8} + \underset{\text{ilmenite}}{3FeTiO_3} + \underset{\text{quartz}}{2SiO_2} + H_2O + 3CaO \Longrightarrow \underset{\text{annite}}{KFe_3(AlSi_3O_{10})(OH)_2} + \underset{\text{titanite}}{3CaTiSiO_5} \quad [R12]$$

Opaque minerals

The opaque minerals are ilmenite and pyrite, determined by microscopy analysis. Magnetite was not seen, but might occur. They are found in large clusters, as individual crystals and very often as inclusions in other minerals.

Geothermobarometry

PT-estimates have been calculated for both the Skråkvik and Träfors locality. At the Skråkvik locality the PT-estimates have been done on the garnet-amphibolite, DTC15002D, and at the Träfors locality PT-estimates have been done on both the gabbro, DTC15007L, and the garnet-amphibolite DTC15007I. Average PT with THERMOCLAC has only been done on the garnet-amphibolites. These three samples have been chosen due to apparent textural equilibrium in the microscopic study and little chemical zoning in the minerals from the SEM analysis.

Data from three microdomains in each garnet-amphibolite have been used for the average PT with Thermocalc and classical thermobarometry. All reactions suggested by Thermocalc have been used for the average PT-estimates. A total of three-five runs with correction for PT in AX was made for each sample, where quartz and water are given as additional end-members. H_2O activity is considered 1 for the garnet-amphibolites based on the macroscopic and petrographic study. Correction for Fe^{3+} is made for garnet, amphibole and pyroxene where applicable.

THERMOCALC

THERMOCAL output data and PT-estimates per domain is found in appendix E.

Table 1, average PT from Thermocalc, H_2O(a) = 1.0

	DTC15002D average PT-estimates					**DTC15007I average PT-estimates**			
	Fe3+ uncorrected		*Fe3+ corrected*			*Fe3+ uncorrected*		*Fe3+ corrected*	
	core	rim	core	rim		core	rim	core	rim
P kbar	9,5	10,4	9,5	10,3	**P kbar**	9,8	9,8	9,9	9,8
P (sd)	1,4	1,5	1,4	1,5	**P (sd)**	1,5	1,4	1,5	1,5
T °C	731	767	732	769	**T °C**	776	778	777	778
T (sd)	90	95	90	95	**T (sd)**	101	100	101	101

Classical geothermobarometry

PT-estimates for the garnet-amphibolites are calculated using Kohn and Spears (1990) Pl-Gt-Hb-Qz geobarometer, Graham and Powells (1984) Gt-Hb geothermometer and Hodges and Spears (1982) Gt-Bt geothermometer. These estimates have been done on three microdomains in each sample and are based on the garnet rim, since these are considered to be in more equilibrium with the surrounding minerals than the garnet core. PT-estimates per domain is found in appendix F.

Skråkvik

Garnet-amphibolite, DTC15002D

Fe^{3+} uncorrected

PT-estimates using Graham and Powells (1984) Gt-Hb thermometer yields temperatures between 648°-672° C and Hodges and Spears (1982) Gt-Bt thermometer yields temperatures between 729°-793° at a pressure of 10 kbar. For these temperature intervals, Kohn and Spears (1990) Pl-Gt-Hb-Qz barometer yields pressures between 9.0-12.5 kbar. (Figure 11a).

Fe^{3+} corrected

PT-estimates using Graham and Powells (1984) Gt-Hb themometer yields temperatures between 657°-692° C and Hodges and Spears (1982) Gt-Bt thermometer yields temperatures between 745°-821° at a pressure of 10 kbar. For these temperature intervals, Kohn and Spears (1990) Pl-Gt-Hb-Qz barometer yields pressures between 9.0-12.5 kbar. (Figure 11b).

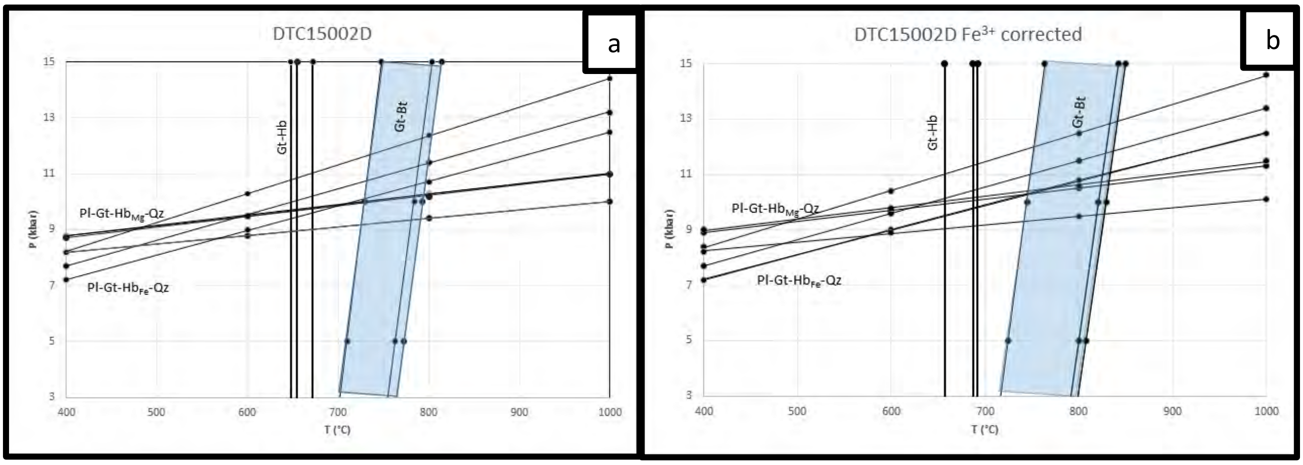

Figure 10, PT-estimates based on Kohn and Spears (1990) Pl-Gt-Hb-Qz geobarometer, Graham and Powells (1984) Gt-Hb geothermometer and Hodges and Spears (1982) Gt-Bt geothermometer.

Träfors

Garnet-amphibolite, DTC15507I

Fe^{3+} uncorrected

PT-estimates using Graham and Powells (1984) Gt-Hb thermometer yields temperatures between 661-772 C and Hodges and Spears (1982) Gt-Bt thermometer yields temperatures between 695-780 at a pressure of 10 kbar . For these temperature intervals, Kohn and Spears (1990) Pl-Gt-Hb-Qz barometer yields pressures between 9.0-11 kbar. (Figure 12a).

Fe^{3+} corrected

PT-estimates using Graham and Powells (1984) Gt-Hb thermometer yields temperatures between 687-810 C and Hodges and Spears (1982) Gt-Bt thermometer yields temperatures between 706-816 at a pressure of 10 kbar. For these temperature intervals, Kohn and Spears (1990) Pl-Gt-Hb-Qz barometer yields pressures between 9.5-11 kbar. (Figure 12b).

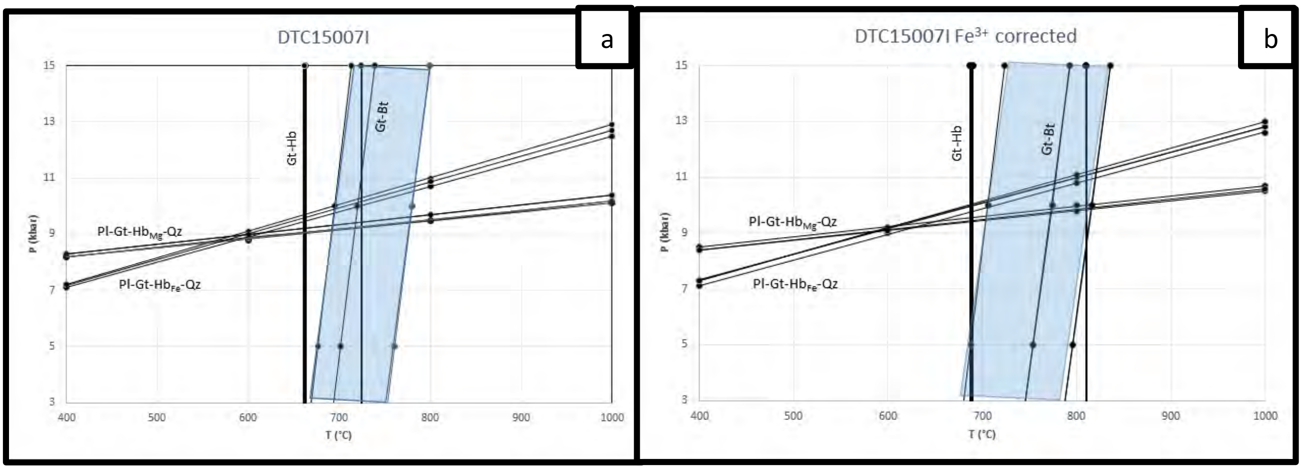

Figure 11, PT-estimates based on Kohn and Spears (1990) Pl-Gt-Hb-Qz geobarometer, Graham and Powells (1984) Gt-Hb geothermometer and Hodges and Spears (1982) Gt-Bt geothermometer.

Gabbro, DTC16007L

PT-estimates for the average crystallization in the gabbro have been calculated using Holland and Blundys (1994) Pl-Hb geothermometer, with pressure calculated on Andersson and Smith (1995), and Wood and Bannos (1973) Cpx-Opx geothermometer. Estimates where done on four domains and gives the following data:

Table 2, average PT-estimates

	Holland and Blundy	Wood and Banno	
Average T (°C)	826	1023	
SD (T)	25	67	
Average P (kbar)	8.4		**Anderson and Smith**
SD (P)	1		

Discussion

Petrography and textures

The gabbro have several interesting textures. One is the complex coronitic texture where olivine surrounded by plagioclase have given rise to synantectic minerals, representing equilibrium steps. This could be either due to slow cooling of the magma, or a deep syntectonic metamorphic event (Bard 1986). A common reaction for these synantectic minerals are:

$$\underset{\text{olivine}}{4(Fe,Mg)_2SiO_4} + \underset{\text{plagioclase}}{4((Ca,Na)Al_2Si_2O_8)} + H_2O \Longrightarrow \underset{\text{orthopyroxene}}{(Mg,Fe)SiO_3} + \underset{\text{clinopyroxene}}{Ca(Mg,Fe)Si_2O_6} + \underset{\text{spinel}}{MgAl_2O_4} + \underset{\text{garnet}}{(Ca,Fe)3Al_2Si_3O_{12}} + \underset{\text{hornblende}}{(Ca,Na)_{2\text{–}3}(Mg,Fe,Al)_5(Al,Si)_8O_{22}OH_2} \tag{R13}$$

No garnets or spinel minerals have been identified during the petrographic or SEM analysis of these reaction rims, indicating that this texture might be magmatic rather than metamorphic. No textures or minerals implies that melting has occurred, olivine should thus have recrystallized under subsolidus conditions giving rise to the complex coronitic textures.

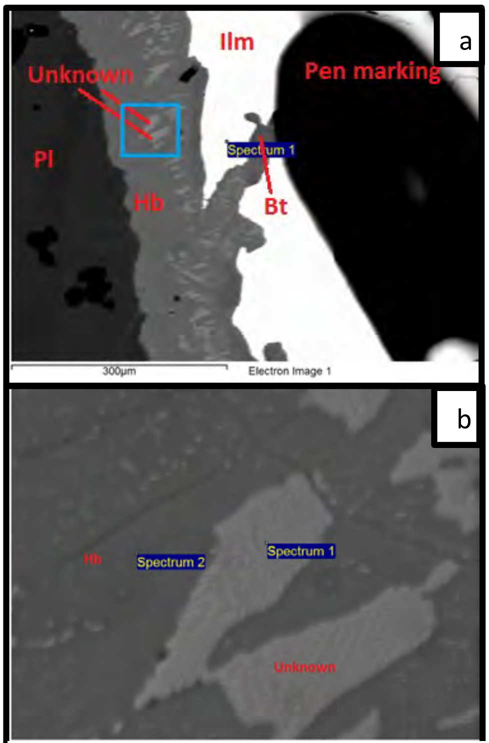

Figure 12, a: BSE, b: BSE - close up of blue area in picture 49a

Another interesting texture is the amphibole reaction rim found around the opaque minerals, where intergrowth formations between the amphibole and unidentified minerals are seen. After consultation with Thomas Zack (Senior Lecturer), Johan Hogmalm (Principle Research Engineer) and Andreas Karlsson (Research assistant) at Gothenburg University, several interpretations have been discussed. One is that these are atypical garnets with no clear habit, suggesting a later metamorphic overprint that is not seen in any other mineral assemblage in the thin section. This is also consistent with what Söderlund et al. (2004) found for their gabbro at the Åker metabasite. If there is a metamorphic overprint, the complex coronitic textures might also be metamorphic rather than magmatic. Another interpretation could be that these crystals are depleted endmembers of the amphibole group and could be considered as a mixture between the hornblende and the bordering mineral.

Symplectite textures are also seen between the magnetite and orthopyroxene in the gabbro. Similar symplectite textures between magnetite, orthopyroxene and pleonaste is found at the Rymmen gabbro (Claeson, 1998) and was interpreted as magmatic cooling textures. However, no member of the spinel group was found during the SEM analyse. These textures could instead indicate early hydration reactions and diffusion occurring over vast distances (Efimov and Malitch, 2012), since magnetite and orthopyroxene does not necessary have to lie in direct contact, rather than being a late metamorphic alteration.

Orthopyroxene replacement of biotite indicates a backwards reaction with K^+ release and dehydration of the biotite. This could indicate later reheating or decompression of a dry system with no melting. If the system was subjected to early hydration, giving rise to the symplectite formations between orthopyroxene and magnetite, together with biotite, a later reheating without melt giving rise to late recrystallized orthopyroxene seems likley. This gabbro is in such case metamorphic.

Recrystallization of inclusions is found in several garnets. The most evident is in metagabbro sample DTC15002D, where two relict plagioclase laths have been partly recrystallized into garnet. In the garnet-amphibolite sample, DTC15002G, we see a textural sector zoning (figure 13). The cause for this texture is still being debated, one possibility is that the garnet has grown during chemical disequilibrium, where the crystal faces grow faster than the edges giving the garnet a branched appearance. During a later stage the garnets have grown in or close to equilibrium giving them their typical prismatic habit (Ben-Jacob and Garik, 1990).

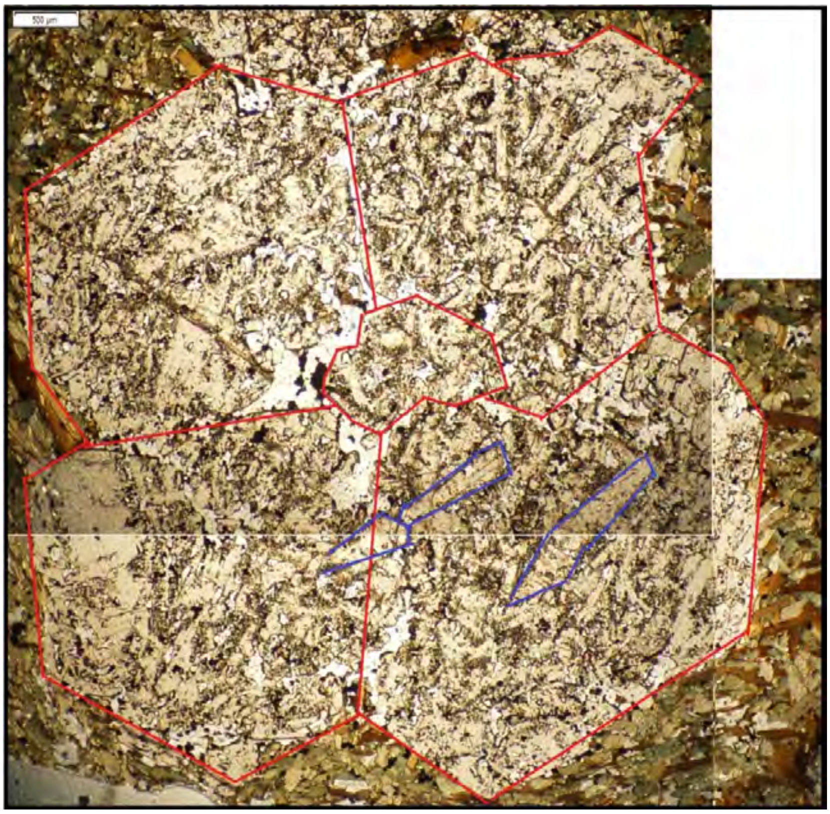

Figure 13, picture collage of a large garnet in DTC15002G with textural zoning. Red lines are interpretation of branched appearance and blue lines are interpretation of possible recrystallized inclusions

Myrmekitization is seen in two metagabbro samples, DTC15002B and DTC15007G, indicating anhydrous conditions or lower temperature and pressure (Collins, 1998). Myrmekite occurs during cooling and is nucleated along grain boundaries where K^+ is removed and Ca^{2+}, Na^+ and/or Si^{4+} is added. This can be done by magma intrusion for example (Wirth and Voll, 1987). At the Skråkvik locality, small mafic intrusions are found, which could have contributed with the extra heat needed for this texture while at the Träfors locality, where more fluids are present, myrmekite seems to have developed during a late stage with low temperature and pressure.

Skeletal textures are found in the garnet-amphibolites from the Träfors locality. The SEM analysis confirms that the crystals are clinopyroxenes, probably aegerine-augite but that the surrounding mas is illite, a member of the mica group, rather than serpentine as though in the microscopic study. The 60° cleavage seen in the BSE image (figure 14) could be the 461 plane for the aegirine-augite crystals, since the SEM data does not support an amphibole. It could also be that part of the aegirine-augite has recrystallized into amphibole. Based on the petrographic study, the former is more likely. This texture could indicate a discontinuous reaction where serpentinization of olivine occurred in an early stage followed by recrystallization into clinopyroxene and micas with decreasing temperature and increasing fluids.

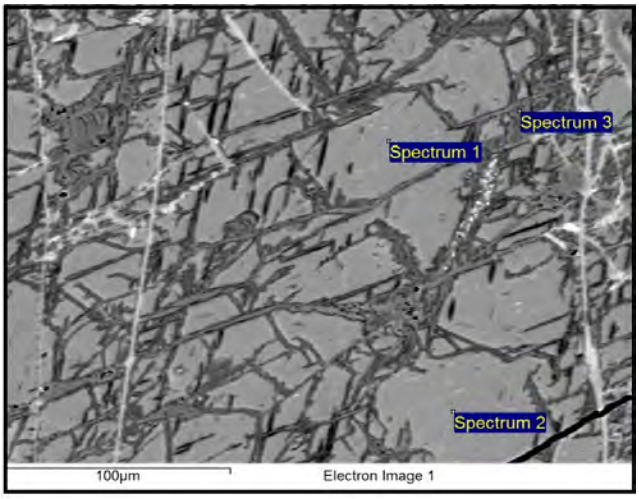

Figure 14, skeletal texture in DTC15007A

Another interesting result is the Fe and Ti decrease, from type I to type IV, in both biotite and horblende. The Fe probably has gone into garnet, amphiboles or chlorite and the Ti into the clinopyroxenes or titanite. This enrichment is seen both in the petrographic study based on the colour of the biotite and hornblende and in the SEM analyses. Since Ti and Fe are relatively light elements in the transitional series, they are often found in mafic and ultramafic rocks, where Ti often follows Fe during magmatic crystallization. However, prograde metamorphism makes Ti an immobile element but the contrary appears during retrograde metamorphism at the amphibolite and granulite facies. During metasomatism, Ti contributes to magnetite rich rocks. Magnetite have only been confirmed in the gabbro from the Träfors locality, but might occur in both the metagabbros and garnet-amphibolites. If so, magnitite is not abundant and metasomatism is modest.

PT and Tectonic history

PT-estimates calculated with classical geothermobarometry for the gabbro in Träfors was made on four domains. These domains cannot be seen as equilibrated microdomains and the results are highly uncertain. The calculated results could be interpreted as an average crystallization temperature and pressure for this sample. The poor quality of these data is due to PT for the gabbro not being a part of the original project and enough SEM analyses was not taken for this sample. A new study with clear microdomains should be made to give more accurate results.

If the gabbro is interpreted as magmatic, since no garnets or spinel could be clearly identified, PT-estimates could indicate an intrusion depth of some 25-35 km below the crust. However, if the gabbro is interpreted as metamorphic, the PT-estimates are no longer applicable, and the rock has been metamorphosed at upper amphibolite to lower granulite facies conditions based on the orthopyroxene replacement of biotite and the symplectite formation between orthopyroxene and magnetite.

Interesting is that the gabbro still have its magmatic texture preserved, and the metagabbros have relict magmatic textures, even though the intrusions have experienced high pressure conditions. This indicates that temperature has a larger impact on metamorphic evolution than pressure has.

There is a negligible difference between the PT-estimates for the garnet-amphibolites based on ferrous and ferric iron. Ferric iron was found in the garnets, while the hornblende only contained ferrous iron. The ferric iron in the garnets indicates that continuous solid solution between grossular and andradite is possible. Such an exchange indicates higher metamorphic temperatures >700° C (Nesse, 2009). A problem with determining ferrous and ferric iron is that general calculations, as used in this study, does not give an accurate result. Many geobarothermometers are calibrated based on H_2O-content and cation site valances giving a certain Fe^{2+}/Fe^{3+} ratio. This is especially true for complex mineral groups such as phyllosilicates and amphiboles. Although less complex minerals can also give errors due to factors such as Si^{4+}/Al^{3+}. If a different ratio is assumed in the study, it can highly affect the final results. More accurate results could be attainable by determining ferrous and ferric iron by wet-chemical analysis instead.

Average PT-estimates by THERMOCALC seems to overall coincide better with the Gt-Bt geothermometer by Hodges and Spear (1982). This could suggest that the later crystalized biotite is in better equilibrium than the earlier crystalized amphibole. Classical geothermobarometry shows more scatter for the Skråkvik locality than the same PT-estimates for the Träfors locality. This scatter could be due to late mafic intrusions found at the Skråkvik locality, which might have affected the surrounding bedrock with additional heat, disrupting the reaction of amphibole. Also there seems to be more chemical zoning in the garnets from the Skråkvik locality in comparison to the Träfors locality. Consideration should as well be taken for retrograde exchange reactions that can occur between biotite and Fe-Mg rich minerals surrounding the analysed crystal. The lower PT is then the closure temperature rather than the metamorphic peak temperature (Winter, 2014). In such case, the higher average PT given by THERMOCALC might be better coinciding with the metamorphic peak temperature. Also two types of garnets have been found, where the late crystalized type 2 often is the one in more textural equilibrium. In such case the PTs symbolises a late metamorphic overprint, rather than the metamorphic peak.

Diagnostics from THERMOCALC shows that the HAT value for grossular and pyrope is too high, indicating a high influence on the PT-estimates. Since no reactions were found without either, and all other diagnostics such as sig fit and e* being within the given intervals, this activity was kept during the calculation of average PT. The high influence from these minerals could be that the Gt-Bt thermometer used by Ferry and Spear (1978) is calibrated after synthetic minerals, which might not be perfectly consistent with a natural system. Additional components such as high Ti and Fe content have been found in mainly biotite and chlorite. These can also give rise to complex AX relationships that are non-ideal, indicating an equilibrium outside the calibrated limits. Due to Fe-Mg exchange between minerals, the high HAT and based on the petrographic analysis, PT-estimates from the classical geothermobarometry seem to better coincide with actual PTs.

The PT-estimates for the garnet-amphibolites are consistent with previous studies made in this area and for meta-mafic intrusions in the Eastern Segment. Study of the Åker metabasite, further to the southwest along the Sveconorwegian Deformation zone, has given somewhat lower temperatures of 600°-630° C and similar pressure of 10-12 kbar. Other studies in the Eastern Segment have yielded temperatures between 680°-800° C (Söderlund et al. 2004), and Wang et al. (1996) found similar coronitic textures with temperatures of 700° C with prograde metamorphism for meta-mafic intruions in the southern part of the Eastern Segment. Just south of lake Vänern, Söderlund et al. (2008) classified mafic intrusions, with the same textures and mineral assemblage as found here, to have metamorphosed under upper amphibolite to granulite facies. Their PT-estimates shows temperature of ~700° C and pressure of ~10 kbar.

Two possible P-T paths can be argued for; 1) The meta-mafic rocks intruded under high pressure followed by slow cooling and retrograde metamorphism due to uplift and fluid-rock interaction 2) the meta-mafic rocks intruded under high pressure, was subjected to hydration in an early stage, followd by reheating with dehydration, uplift and late fluid-rock interaction.

The dating for the metamorphic overprint at 960 Ma is consistent with the Sveconorwegian orogenic event. Möller et al. have represented a tectonic model with the Eastern Segment subducting to the west under the accreated terrains of Telemarkia and Idefjorden. This have given rise to internal folding of the Eastern Segment between the Sveconorwegian Deformation Zone and the Mylonite zone. The Transitional section can thus be correlated with the tectonic history of an imbricated thrust stack, representing a fan-like structure in cross section as given by Wahlgren et al. (1994). They suggest that imbrication of the Transitonal section and the Frontal wedge started in early Sveconorwegian, about 1.57 Ga. This gave rise to the mafic intrusions that where later metamorphosed under higher pressure due to subduction. This model does not give any direct suport for a later reheating event.

If the model proposed by Slagstad et al. (2013) with a back-arc extension is considered, the mantle upwelling found to the west of the Eastern Segment could have contributed to a reheating event. A reheating event could also have been local for this area as a result of uplift and decompression of the rocks.

Previous studies for both the surrounding orthogneiss and the mafic intrusions have given amphibolite facies conditions for the Transitional section with no melting. During the fieldstudy, two localities about 350 meters southwest of Träfors and 1.8 km south of Träfors shows melting textures and segregation of felsic and mafic minerals in the orthogneiss. Based on the findings in this study and fieldobservations, there seems to be some uncertainty about the temperature and the metamorphic grade. More research is needed to confirm if the melting found in the area is on a local scale or a more regional scale.

The hydrothermal fluids is likely to have been derived from the surrounding orthogneiss bedrock and a transition within the meta-mafic intrusion should be evident with decreasing corona and symplectite formation in the central part, where none or little fluids have gained access. Further studies of the contact between the intrusions and the surrounding bedrock would be of interest to get a better understanding of the hydrothermal fluids and their movement in the area. It would also be interesting to do a T-t path as given by Dodson (1986) to get a better understanding of the cooling history and the tectonic environment.

Error sources

During thin section preparation, stress can be built in the minerals when cutting the sample. This can be minimized by polishing the sample in several stages. Another problem could be that the interpretation of the ß-plane and the foliation is not correct, giving us minerals that differs in the colours during microscopy. Colour deviations can also occur if the thin section is too thick or too thin, which was the case for some of the samples. Mainly the samples where too thin along the edges of the thin section.

Microscopy is limited since the observations made are for only a small part of a larger bedrock. For the same locality the protolith, hydrothermal fluids and intrusions can affect the composition and metamorphic overprint of the rock. To minimize interpretation errors, detailed mapping and selective sampling can be helpful.

Geothermobarometry contains several error sources. Barometers and thermometers usually work better for some type of rocks and are often calibrated after a certain composition or are based on synthetic minerals differing from natural systems. Disequilibrium or poly-metamorphic overprints can also influence PT outcome, as well as retrograde effects and slow cooling, usually found in high grade rocks or plutonic systems. A good understanding for the studied sample, both on a macro and micro scale is crucial.

Conclusion

The study indicates metamorphism at amphibolite to upper amphibolite facies conditions for the metagabbros and the garnet-amphibolites.

Average PT-estimates for the garnet-amphibolites gives metamorphic peak temperatures between 680°-730° C with pressures between 9.0-11.0 kbar at the Träfors locality, and metamorphic peak temperatures between 660°-770° C with pressures between 9.5-11.0 kbar at the Skråkvik locality.

Based on the petrographic and PT study, it is concluded that the meta-mafic intrusions at the Skråkvik locality have been metamorphosed in a dry system in contrast to the Träfors locality. The intrusions at the Träfors locality seems to have been affected by late hydrothermal fluid alterations and more pervasive retrograde metamorphism. It is also concluded that mafic intrusions can preserve their magmatic textures even under high pressure conditions.

Acknowledgements

I would like to thank Jenny Andersson at the Swedish Geological Survey in Uppsala for her time in the field, her engagement and personal appreciation at the microscopy and all the interesting discussions and feedback.

I would also like to express my gratitude to Professor Alasdair Skelton at Stockholm University for his feedback during this project and his help with the PT estimates. Beside this thesis I would like to thank him for three interesting years at the Department of Geological Sciences, his motivation and knowledge. He has without doubt contributed to my keen interest in metamorphic rocks.

Beside my advisors I would like to thank Krister Junghan and Dan Zetterberg at Stockholm University for all technical help, lab assistance and interesting coffee discussions during my time at the department.

At Gothenburg University I would like to thank Thomas Zack, Andreas Karlsson and Johan Hogmalm for their professional input during the SEM analyses.

And last but not least, a special thank you to my husband Martin and my family, without whom I would not be able to do this project.

References

Articles

ANDERSON, J.L., SMITH, D.R., (1995) *The effect of temperature and oxygen fugacity on Al-in-hornblende barometry,* AM MINERAL vol. 80, pp. 549-559

BEN-JACOB, E., GARIK, P., (1990), *The formation of patterns in non-equilibrium growth*, Nature, vol. 343, pp. 523-530

BINGEN, B., ANDERSSON, J., SÖDERLUND, U., MÖLLER, C., (2008a), *The Mesoproterozoic in the Nordic countries*, Episodes, vol. 31, no 1

BINGEN, B., NORDGULEN, Ö., VIOLA, G., (2008b), A fourphase model for the Sveconorwegian orogeny, SW Scandinavia, Norwegian Journal of Geology, pp. 43-72

BURKHARDT, M., (1992), *Calcite twins, their geometry, appearance and significance as stress-strain markers and indicators of tectonic regime: a review*, Journal of Structural Geology, vol. 15, issue 3-5, pp. 351-368

CLAESON, D.T., (1998), *Coronas, reaction rims, symplectites and emplacement depth of the Rymmen gabbro, Transscandinavian Igneous Belt, southern Sweden*, Mineralogical Magazine, vol. 62(2), pp. 743-757

DODSON, M.H., (1986), *Closure profiles in cooling systems*, Material Science Forum, vol. 7, pp. 145-154

DOOP, G.T.R, (1987), *A general equation for estimating Fe^{3+} concentrations in ferromagnesian silicates and oxides from microprobe analyses, using stoichiometric criteria*, Mineralogical Magazine, vol. 51, pp. 431-435

EFIMOV, A.A., MALITCH, K.N., (2012), Magnetite-orthopyroxene symplectites in gabbros of the Urals: A structural track of olivine oxidation, Geology of Ore Deposits, vol. 54 (7), pp. 531-539 (translated from Zapiski Rossiiskogo Mineralogicheskogo Obshchestva 2010, vol. 139 (5), pp. 18-28)

FERRY, J. M., SPEAR, F. S., (1978), *Experimental Calibration of the partitioning of Fe and Mg Between Biotite and Garnet,* Contributions to Mineralogy and Petrology, vol. 66, pp. 113-117

GRAHAM, C.M., POWELL, R., (1984), *A garnet-hornblende geothermometer: calibration, testing, and application to the Pelona Schist, Southern California,* J. metamorphic Geol., vol. 2, pp. 13-31

HAGESKOV, B., (1980), *The Sveconorwegian structures of the Norwegian part of the Kongsberg-Bamble-0stfold segment*, GFF vol. 102, pp. 150-155, cited in Morthorst et al. 1982

HOLLAND, T., BLUNDY, J., (1994) *Non-ideal interactions in calcic amphiboles and their bearing on amphibole-plagioclase thermometry*, Contrib. Mineral Petrol. Vol. 116, pp. 433-447

HOLLAND, T.J.B., POEWLL, R., (1998), *An internally consistent thermodynamic data set for phases of petrological interest*, Journal of Metamorphic Geology, v. 16, p. 309–343

HODGES, K.V., SPEAR, F.S., (1982), *Geothermometry, geobarometry and the Al2SiO5 triple point at Mt. Moosilauke, New Hampshire,* American Mineralogist, vol. 67, pp. 1118-1134

HÖGBOM, A., (1922) *Berggrunden. In Beskrivning till kartbladet Väse*, SGU Aa 151, cited in Morthorst et al. 1982

HÖGDAHL, K., ANDERSSON, U.B., EKLUND, O., (2004), *The Transscandinavian Igneous Belt (TIB) in Sweden:a review of its character and evolution*, Geological survey of Finland, Special Paper 37

JOHANSSON, L., JOHANSSON, Å., (1990), *Isotope geochemistry and age relationships of mafic intrusions along the Protogine Zone, southern Sweden*, Precambrian Research vol. 48, pp. 395-414

JOHANSSON, L., LINDH, A., MÖLLER, C., (1991), Late Sveconorwegian (Grenville) high-pressure granulite facies metamorphism in southwest Sweden, J. Metamorph. Geol. 9, 283–292, cited in Möller, C., and Söderlund, U. (1997)

KOHN, M.J., SPEAR, F.S., (1990), *Two new geobarometers for garnet amphibolites, with applications to southeastern Vermont*, American Mineralogist, vol. 75, pp. 89-96

LALONDE, A., BERNARD, P., (1993), Composition and color of biotite from granites; Two useful properties in the characterization of plutonic suites from the Hepburn internal zone of Wopmay Orogen, Northwest territories, Canadian Mineralogist, vol. 31, 203-217

LIDIAK, E.G., (1996) *Geochemistry of subsurface Proterozoic rocks in the eastern Midcontinent of the United States: Further evidence for a within-plate tectonic setting,* Geological Society of America Special Papers, vol. 308, pp. 45-66

LINDH, A., SCHÖBERG, H., ANNERTZ, K., (1994), *Disturbed radiometric ages and their bearing on interregional correlations in the SW Baltic Shield*, Lithos vol. 31, pp. 65-79

LLNDEGÅRDH, P.H., (1977), *The Gräsmark Formation in western central Sweden,* SGU C 732, cited in Morthorst et al. 1982

LUNDEGÅRDH, P.H., (1980a), *The gneissic granites and allied rocks in central and northwestern Värmland, western Sweden,* SGU C 777, pp. 3-23, cited in Morthorst et al. 1982

LUNDEGÅRDH, P.H., (1980b), *The Östmark Formation and neighbouring rocks in the Proterozoic of Värmland, western Sweden*, GFF 102, 137-140, cited in Morthorst et al. 1982

LUNDEGÅRDH , P.H., GORBATSCHEV, R., LINDH, A., (1982), *Berggrundskarta över Värmlands län. Statens industriverk, mineralbyrån . With an explicative note in Swedish,* cited in Morthorst et al. 1982

MAGNUSSON, N.H., (1928), *Aktuella problem från Värmlands gnejsurberg*; *with comments of Johansson, Holmquist, Sundius and Benedicks,* GFF, pp. 810-816, cited from Morthorst et al. 1982

MAGNUSSON, N.H., (1933), *Berggrunden, In Beskrivning till kartbladet Karlstad*, SGU Aa 174, cited from Morthorst et al. 1982

MAGNUSSON, N. H., (1960), *Age determinations of Swedish precambrian rocks,* Geol. Foren. Stockh. Forh. vol. 82, pp. 407-432, cited from Morthorst et al. 1982

MORTHORST, JR. ZECK, H.P., LUNDEGÅRDH, P.H., (1982), *The Proterozoic Hyperites in southern Värmland, western Sweden. Sveriges geologiska undersökning*, Ser. Ba, No. 30, pp.1-104, Uppsala

MÖLLER, C., (1998), Decompressed eclogites in the Sveconorwegian (-Grenvillian) orogen of SW Sweden: petrology and tectonic implications, J. metamorphic Geol. Vol. 16, pp. 641-656

MÖLLER, C., SÖDERLUND, U., (1997), Age constraints on the regional deformation within the Eastern Segment, S. Sweden: Late Sveconorwegian granite dyke intrusion and metamorphic deformational relations, GFF, vol. 119, pp. 1- 12

MÖLLER, C., ANDERSSON, J., DYCK, B., LUNDIN, I.A., (2015), *Exhumation of an eclogite terrane as a hot migmatitic nappe, Sveconorwegian orogen*, Lithos, Article in press

POWELL, R., HOLLAND, T., (1994), *Optimal geothermometry and geobarometry*, American Mineralogist, vol. 79, pp. 120-133

SLAGSTAD, T., ROBERTS, N.M.W., MARKER, M., RØHR, T.S., SCHIELLERUP, H., (2013), *A non-collisional, accretionary Sveconorwegian orogen,* Terra Nova, v. 25, pp. 30-37

SKIÖLD, T, (1976), *The interpretation of the Rb-Sr and K-Ar ages of late Precambrian rocks in south-western Sweden,* GFF vol. 98, pp. 3-29, cited in Morthorst et al. 1982

SMELLIE, J.A.T., (1974), *Formation of atoll garnets from the aureole of the Ardara pluton, Co. Donegal, Ireland*, Mineralogical Magazine, vol. 39, pp. 878-888

SÖDERLUND, U., HELLSTRÖM, F.A., KAMO, S.L., (2008), *Geochronology of high-pressure mafic granulite dykes in SW Sweden: tracking the P-T-t path of metamoprhism using Hf isotopes in zircon and baddeleyite*, J. metamorphic. Geol., vol. 28, pp. 539-560

SÖDERLUND, U., ISACHSEN, C.E., BYLUND, G., HEAMAN, L.M., PATCHETT, J., VERVOORT, J.D., ANDERSSON, U.B., (2005) *U–Pb baddeleyite ages and Hf, Nd isotope chemistry constraining repeated mafic magmatism in the Fennoscandian Shield from 1.6 to 0.9 Ga*, Contrib Mineral Petrol vol. 150, pp. 174-194

SÖDERLUND, P., SÖDERLUND, U., MÖLLER, C., GORBATSCHEV, R., RODHE, A., (2004), *Petrology and ion microprobe U-Pb chronology applied to a metabasic intrusion in southern Sweden: A study on zircon formation during metamorphism and deformation*, Tectonics, vol. 23, TC5005

TÖRNEBOHM, A.E., (1877), *Om Sveriges vigtigare diabas- och gabbroarter*. Kongl. Svenska Vetenskapsakademiens handlingar 14:13, Stockholm, cited in Morthorst et al. 1982

WAHLGREN, C.H., CRUDEN, A.R., STEPHENS, M.B., (1994), *Kinematics of a major fan-like structure in the eastern part of the Sveconorwegian orogen, Baltic Shield, south-central Sweden*, Precambrian Research, vol. 70, pp. 67-91

WANG, X-D., LAURENCE, M.P., LINDH, A., (1996a), *$^{40}Ar/^{39}Ar$ geochronological constraints from the southernmost part of the Eastern Segment of the Sveconorwegian orogen: Implication for timing of granulite-facies metamorphism*, GFF, vol. 188, pp. 1-8

WANG, X-D., LINDH, A., (1996), *Temperature-pressure investigation of the southern part of the Southwest Swedish Granulite Region*, European Journal of Mineralogy, vol. 8, pp. 51-67 , cited in Wang et al. 1996a

WIDENFALK, L., (1969), Electron micro-probe analyses of myrmekite plagioclase and coexisting feldspars, Lithos 2, 295- 309

WIRTH, R., VOLL, G., (1987), Cellular intergrowth between quartz and sodium-rich plagioclase (myrmekite) – an analogue of discontinuous precipitation in metal alloys, Journal of Materials Science, vol. 22, pp. 1913-1918

WOOD, B.J., BANNO, S., (1973) Garnet--orthopyroxene and orthopyro×ene-clinopyroxene relationships in simple and complex systems, Contrib. Mineral. Petrol. Vol. 42, pp. 109-124

ZARINS, K., JOHANSSON, Å., (2008), U–Pb geochronology of gneisses and granitoids from the Danish island of Bornholm: new evidence for 1.47–1.45 Ga magmatism at the southwestern margin of the East European Craton, International Journal of Earth Sciences vol. 98, pp. 1561–1580

Litterature

BARD, J.P., (1986), Microtextures of igneous and metamorphic rocks, D. Reidel Publishing Company, ISBN-13:

978-90-277-2313-0COLLINS, L.G., (1998), Primary microcline and myrmekite formed during progressive metamorphism and Kmetasomatism of the Popple Hill gneiss, Grenville Lowlands, northwest New York, USA, ISSN 1526-5757

JÖNSSON, G., NILSSON, E., (2009), Tillämpad atomfysik, Teach Support, ISBN: 978-91-972499-4-2

NESSE, W.D., (2009), Introduction to mineralogy, Oxford University Press, International edition, ISBN 978-0-19- 539114-5

PASSCHIER, W.C., TROUW, R.A.J, (2005), Microtectonics, Springer, 2nd edition, ISBN-10: 3-540-64003-7, ISBN-13: 978-3- 540-64003-5

ROUESSAC, F., ROUESSAC, A., (2007), *Chemical Analysis, Modern Instrumentation Methods and Techniques,* John Wiley & Sons, Ltd., Second edition, ISBN: 978-0-470-85902-5

WINTER, J.D., (2014), *Principles of Igneous and Metmorphic Petrology*, Pearson New International Edition, Second edition, ISBN-10: 1-292-02153-5, ISBN-13: 978-1-292-02153-9

Appendix A: Macroscopic description

Locality:	Area:	N	E	Field classification	Weathering:	Color:	Grain size	Minerals:	Foliation:
DTC15001	Förnäs	6577986	440702	Gabbro	Brownish weathering	Dark greenish with a purple tint	Medium grained	Black pyroxene, green mafic minerals, strawish white plagioclase and somewhat recrystallized purple plagioclase?	-
DTC15002A	Skråkvik	6577089	440868	Metagabbro	Brownish weathering	Dark with a purple tint	Medium grained	Dark green mafic minerals, strawish brown plagioclase and recrystallized with brownish plagioclase. Very small garnets < 1 mm found in the dark matrix or occasionally with minor plagioclase.	-
DTC15002B	Skråkvik	6577089	440868	Metagabbro	Brownish weathering	Dark greenish with a brownish tint	Unevenly grained with larger recrystallized reddish plagioclase in a medium grained mafic matrix	Dark green mafic minerals, some strawish dark brown plagioclase and recrystallised brownish plagioclase. Small biotite domains and very small garnets < 1 mm found in the dark matrix.	-
DTC15002C	Skråkvik	6577089	440868	Metagabbro	Brownish weathering	Dark green with a redish tint	Unevenly grained. Contact between coarse grained garnet-amphibolite and fine grained basaltic intrusion with large garnets. Larger recrystallized plagioclase and small garnets in a fine grained mafic matrix	Dark green/black minerals, recrystallised white/reddish plagioclase aggregates < 15 mm, occasionally strawish dark plagioclase, small garnets < 2 mm found with plagioclase, and occasionally biotite domains < 4 mm.	-

DTC15002D	Skråkvik	6577089	440868	Garnet-amphibolite	Brownish weathering, "spotty" appearance on half the sample with dark and light crystal aggregates.	Dark black/green	Unevenly grained. Contact between a coarse grained garnet-amphibolite and a fine grianed basaltic intrusion. Larger recrystallized plagioclase crystals in a fine mafic matrix on half the sample. The other half is coarse grained.	Dark black very fine grained minerals with a greenish tint, larger recrystallized dark/reddish plagioclase crystals < 6 mm, biotite "veins" probably from the contact with the coars grained part. Occasionally small garnets < 1 mm in contact with plagioclase occasionally in dark matrix.	Slightly?
DTC15002E	Skråkvik	6577089	440868	Diabase intrusion in garnet-amphibolite	Brownish weathering, dark red/brownish weathered minerals, occasionally elongated, plagioclase? Spotty in the coars grained part.	-	Unevenly grained. Contact between a coarse grained garnet-amphibolite and a fine grianed basaltic intrusion. Large aggregates of mafic minerals and plagioclase, very fine grained in the young diabase intrusion.	Dark black/greenish mafic minerals, larger aggregates of white/brownish plagioclase, small garnets < 2 mm in contac with the plagioclase and alot of biotite crystals. The diabase intrusion contains clasts from the coarse grained part.	The coarse grained part has a foliation
DTC15002F	Skråkvik	6577089	440868	Garnet-amphibolite	Greenish/brown weathering	Dark green with a light purple tint	Medium to coarse grained	Dark green amphibole, somewhat aligned biotite and also biotite domains are found < 7 mm, recrystallized brownish plagioclase, small garnets < 1 mm found in the dark matrix.	Slightly
DTC15002G	Skråkvik	6577089	440868	Garnet-amphibolite	Rusty brown with large garnet varts	Black/greenish	Unevenly grained with a very fine grained mafic matrix and large phorphyroblast garnets.	Dark mafic minerals, biotite, quartz and large garnets < 11 mm.	Schistose

DTC15007A	Träfors	6586280	0440666	Garnet-amphibolite	Reddish/brown weathering		Unevenly grained with large recrystallized red plagioclase and fine to medium grained mafic elongated matrix.	Dark mafic minerals, alot of biotite, , large plagioclase cyrstals < 15 mm, most of them have a brick-red color and a few are blue/green. Few small garnets < 1mm is found in the dark matrix.	A clear foliation plane is found in the sample
DTC15007B	Träfors			Garnet-amphibolite	Brown weathering	Dark black	Very fine grained with plagioclase and garnets crystals	Dark mafic matrix with alot of well aligned biotite, many small garnets < 2mm, red elongated parts possible recrystallized plagioclase and perhaps with garnets inside. Most garnets are found in the mafic matrix. White/brownish plagioclase crystals are seen.	A clear foliation plane is found in the sample, schistose
DTC15007C	Träfors			Garnet-amphibolite	Spotty with green and white elongated crystals filled with rusty garnets.	Dark black with a reddish tint	Fine to medium grained	Dark mafic matrix with alot of well aligned biotite and many small garnets < 4 mm, red/brownish recrystallized plagioclase,	A clear foliation plane is found in the sample, schistose towards gneissic
DTC15007D	Träfors			Metagabbro	Brownish weathering	Dark black with a greenish tint	Fine to medium grained	Dark green mafic minerals, white/brownish recrystallized plagioclase and some dark plagioclase laths.	-
DTC15007E	Träfors			Metagabbro	Greenish/brown weathering	Dark black with a greenish and redish tint	Medium to coarse grained	Dark green mafic minerals, brownish/red recrystallized plagioclase, biotite and small garnets < 1 mm in both the dark matrix and in contact with the plagioclase.	-
DTC15007F	Träfors			Metagabbro	Brownish weathering	Dark black/green	Very fine grained with larger plagioclase aggregates	Dark black mafic minerals, small biotite domains < 1 mm, reddish/white recrystallized plagioclase	Slight?

DTC15007G	Träfors			Metagabbro?	Brown/reddi sh weathering		Very coarse grained	Large green amphiboles, both white and dark recrystallized plagioclase and also large plagioclase laths are visible. Yellow quartz and biotite domains, small garnets less < 2 mm.	
DTC15007H	Träfors			Garnet-amphibolite	Spotty with green and white elongated crystals and biotite domains.	Greenish with a purple tint	Fine to medium grained	Fine dark green mafic matrix, biotite domains < 2 mm are common, small garnets < 1 mm are common, white/reddish/brown recrystallized plagioclase and dark thin plagioclase laths.	Slightly
DTC15007I	Träfors			Metagabbro/ Garnet-amphibolite	Brownish weathering	Dark black	Very fine grained	Fine dark matrix with small white plagioclase crystlas, biotite and minor small garnets < 0.5 mm.	Slightly
DTC15007J	Träfors			Garnet-amphibolite	Spotty with dark green and white aggregates	Black with a greenish tint	Medium grained	Black mafic minerals, white/brownish recrystallized plagioclase, biotite and many garnets < 2 mm	-
DTC15007K	Träfors			Garnet-amphibolite	Spotty with dark green and white aggregates and garnets	Deep black with a reddish tint	Medium grained	Black/dark green mafic crystals, biotite domains < 3 mm, recrystallized white/brownish plagioclase and also very thin plagioclase laths. Garnets are very common and < 5 mm.	Slightly
DTC15007L	Träfors	6586364	0440710	Gabbro	Rusty brown weathering	Deep black	Fine to medium grained	Black mafic crystals, occasionally larger, dark plagioclase laths are very common	
DTC15007M	Träfors	6586280	0440666	Chlorite schist	Dark green	Dark green	Fine grained	Dark green chlorite	Highly

Appendix B: Thin section descriptions

Förnäs

Metagabbro, type II - DTC15001

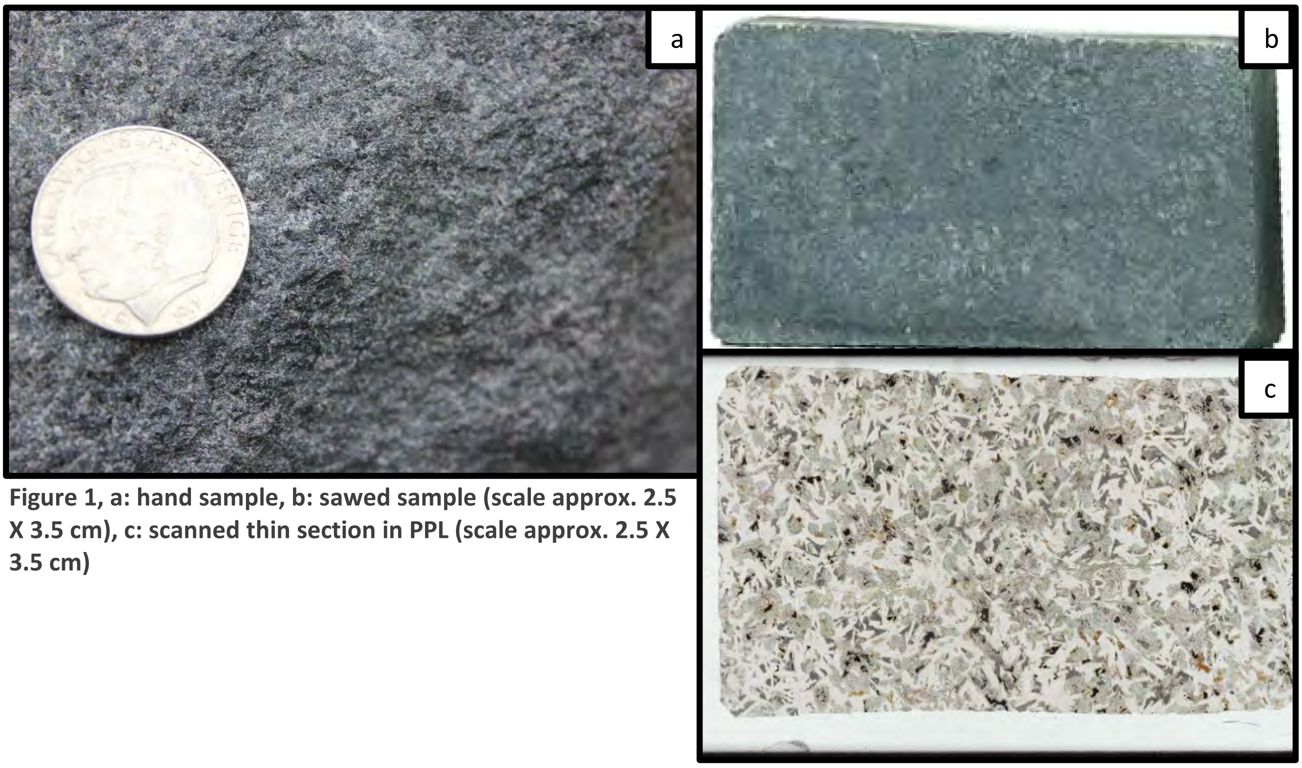

Figure 1, a: hand sample, b: sawed sample (scale approx. 2.5 X 3.5 cm), c: scanned thin section in PPL (scale approx. 2.5 X 3.5 cm)

The main minerals are plagioclase, pyroxene, amphibole, opaque minerals and garnet, with biotite, hornblende, apatite and zircon as accessory minerals. There is about 25% dark phases in the sample.

The sample has a seriate texture with both polygonal and interlobate grain boundaries. The magmatic texture is preserved were possible relict olivine crystals have been totally recrystallized into orthopyroxene in the core and amphibole at the rim.

Plagioclase laths are common and have a composition of Anorthite$_{40\text{-}50}$. Augitic clinopyroxenes have a dark bluish colour, are common in the sample and have a euhedral habit. Exsolution lamellae of orthopyroxene, probably pigeonite, and oxides are common along the {100} cleavage plane. Exsolution of the oxides make the crystals somewhat dark grainy in both PPL and XPL. The pyroxenes have been recrystallized to hornblende at the edges.

Garnet is common, they occur as euhedral individual crystals and as coronas around opaque minerals and relict olivine crystals. Few individual crystals have a sieve texture in the core with a more equilibrated rim. Biotite is sparse to fairly common, they have a green-brown colour and occurs both as individual crystals and as coronas around the opaque minerals. The opaque minerals are ilmenite and to a lesser extent pyrite, where the ilmenite has a euhedral to anhedral habit while the pyrite are smaller than the ilmenite crystals, with anhedral habit. Zircons are few with a prismatic habit and occurs in the plagioclase or as crystals with radiation rims in the biotite. Possible baddeleyite, euhedral with no reaction towards zircon is found in the plagioclase.

Fluid inclusions and thin acicular zoisite crystals are seen along the grain boundaries of the plagioclase, often aligned.

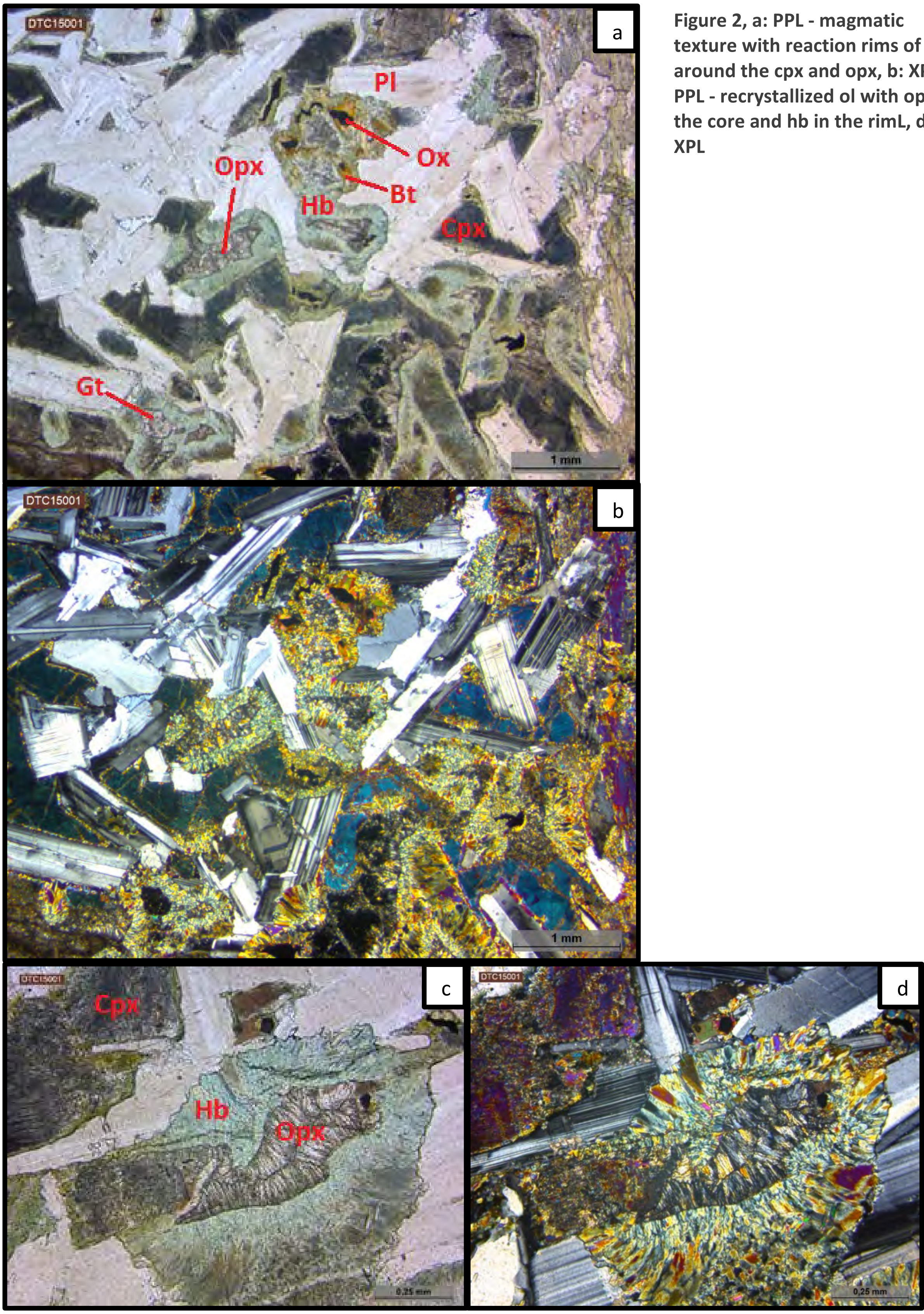

Figure 2, a: PPL - magmatic texture with reaction rims of hb around the cpx and opx, b: XPL, c: PPL - recrystallized ol with opx in the core and hb in the rimL, d: XPL

Skråkvik

Metagabbro, type II - DTC15002A

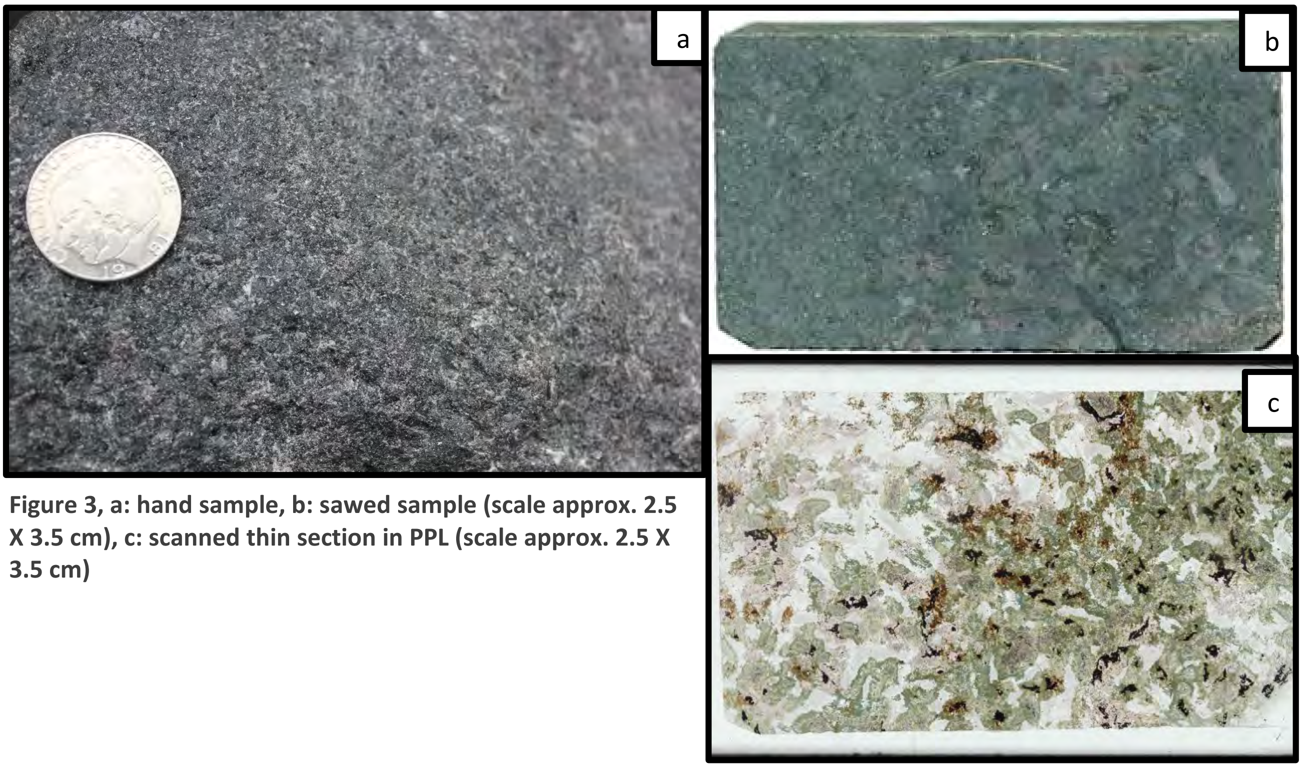

Figure 3, a: hand sample, b: sawed sample (scale approx. 2.5 X 3.5 cm), c: scanned thin section in PPL (scale approx. 2.5 X 3.5 cm)

The main minerals are hornblende, plagioclase, opaque minerals, biotite, garnet, pyroxene and quartz with accessory minerals apatite, siderite and zircon. There is about 40% dark phases in the sample.

The sample has a seriate texture with polygonal and interlobate grain boundaries. Replacement textures are seen where pyroxenes have recrystallized at the edges to hornblende. Coarse grained dynamic recrystallization is seen with a slight deformation grade.

Large subhedral plagioclase laths and anhedral plagioclase with a composition of anorthite$_{30\text{-}40}$ are common. Thin narrow albite twins, pericline twins, Carlsbad twins and sparse sericitization are characteristic for the plagioclase. Concentric zoning occurs. Augitic clinopyroxenes have a bluish colour, an anhedral habit and are commonly rimmed by hornblende. Clinopyroxenes are fairly common in the sample. Hornblende occurs as green-brown aggregates and as coronas around other minerals where intergrowth formations of hornblende, clinopyroxenes and quartz are common. Biotite occur as brown-red aggregates, randomly oriented and often in contact with or as radiating structures around the opaque minerals. Biotite is fairly common in the sample.

Garnet is found as rims around the opaque minerals and as individual anhedral crystals, often in aggregates. They appear zoned with a sieve textured core and an outer rim with few or none inclusions (figure 4c). Garnet is common in the sample. The opaque minerals are ilmenite and pyrite where both have a euhedral to anhedral habit. Ilmenite is more common than pyrite but both often occur in close contact. The opaque minerals are found in large domains.

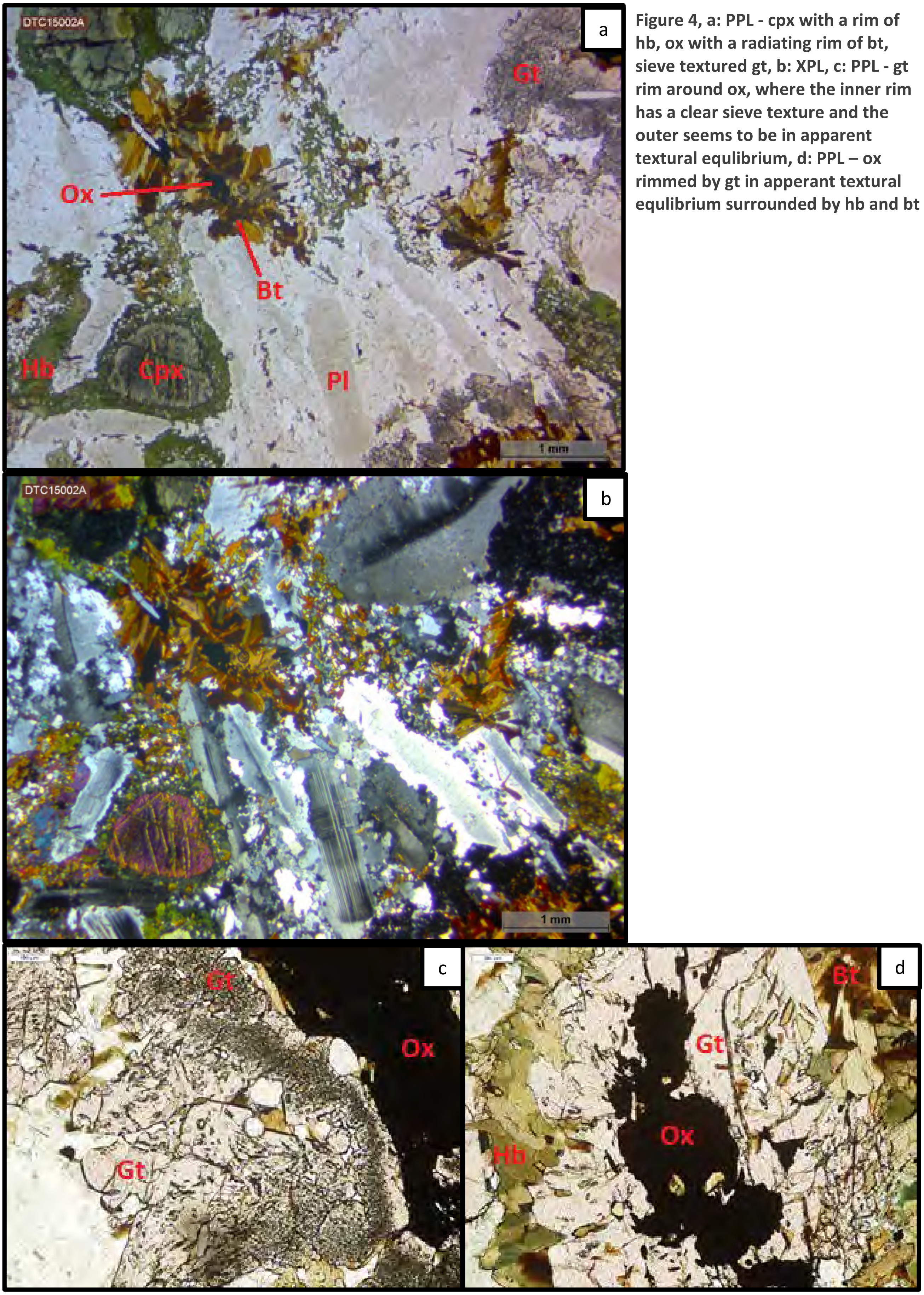

Figure 4, a: PPL - cpx with a rim of hb, ox with a radiating rim of bt, sieve textured gt, b: XPL, c: PPL - gt rim around ox, where the inner rim has a clear sieve texture and the outer seems to be in apparent textural equlibrium, d: PPL – ox rimmed by gt in apperant textural equlibrium surrounded by hb and bt

Metagabbro, type II - DTC15002B

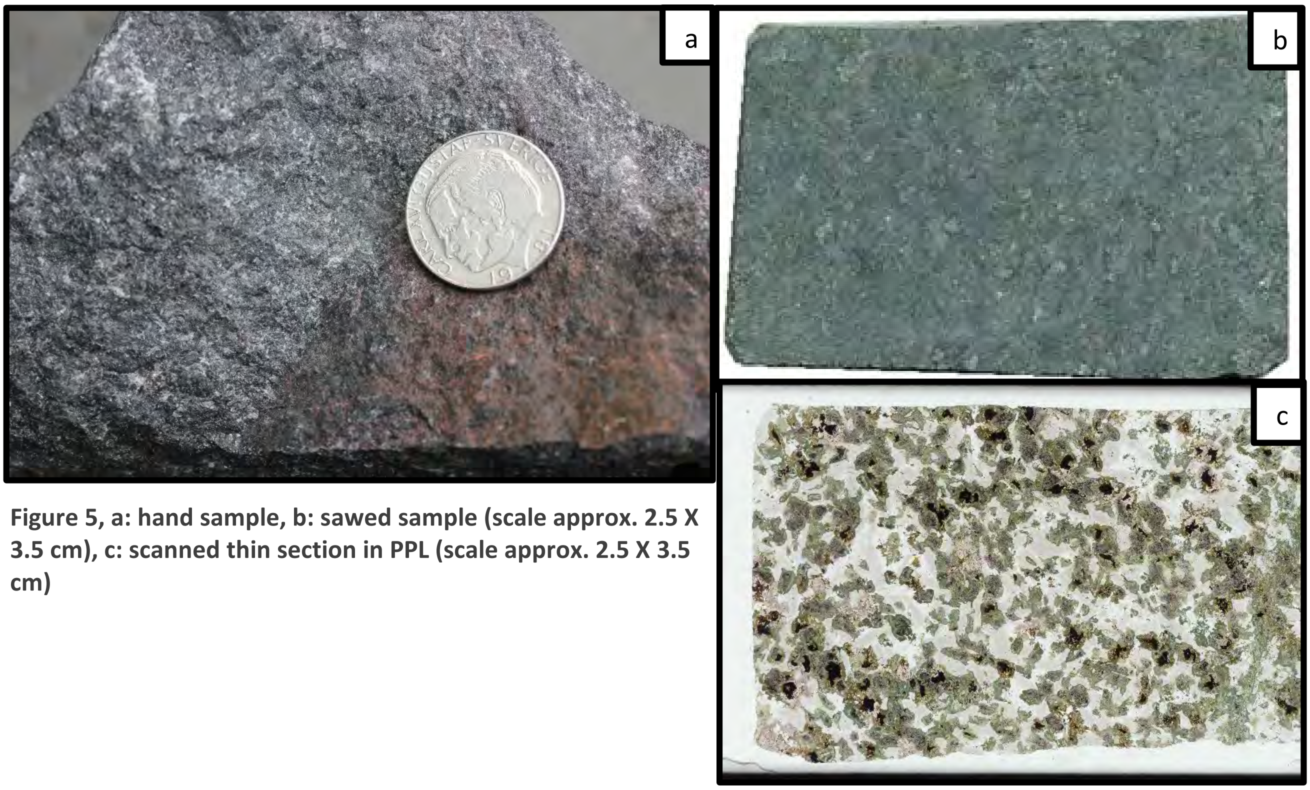

Figure 5, a: hand sample, b: sawed sample (scale approx. 2.5 X 3.5 cm), c: scanned thin section in PPL (scale approx. 2.5 X 3.5 cm)

The main minerals are plagioclase, hornblende, opaque minerals, biotite, pyroxene and quartz with accessory minerals siderite, apatite and zircon. There is about 45% dark phases in the sample.

The sample has a seriate texture with interlobate grain boundaries. Replacement textures are seen with pyroxene in the core and hornblende at the rim.

Anhderal plagioclase laths are common and have a composition of anorthite$_{30-40}$. Albite and Carlsbad twins are common where saussuritization and myrmekitization with quartz in the plagioclase is sparse. Antiperthite is sparse while tartan twinning of microcline is fairly common in the sample**.** Augitic clinopyroxenes have a bluish colour, an anhedral habit and are rimmed by hornblende. Oxide exsolution lamellae are very common along the {100} cleavage plane. Hornblende is found with both brown-green and blue-green colour, as intergrowth formations with pyroxene and quartz or as coronas around the opaque minerals and the biotite. Hornblende is common in the sample. Biotite occurs as brown-red aggregates, as radiating formations and is fairly common in the sample.

Garnet is found as thick coronas around the opaque and mafic minerals, they are often zoned with a sieve textured core and a more equilibrated rim. Inclusions are very common consisting mostly of plagioclase and biotite. The opaque minerals are ilmenite and pyrite, both occur as large anhedral crystals in close contact. The ilmenite often shows skeleton textures or are found in small fine grained domains (figure 13d).

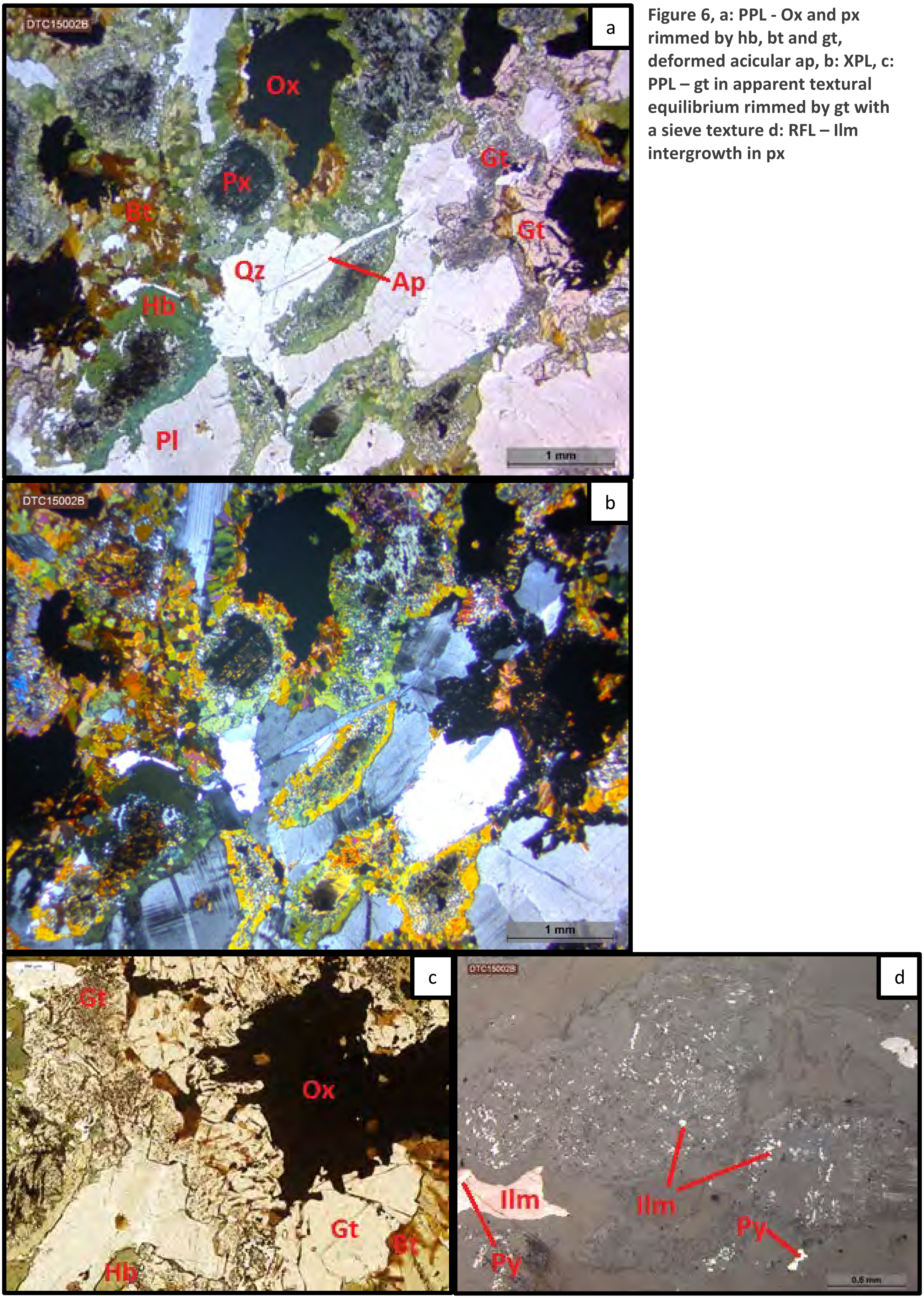

Figure 6, a: PPL - Ox and px rimmed by hb, bt and gt, deformed acicular ap, b: XPL, c: PPL – gt in apparent textural equilibrium rimmed by gt with a sieve texture d: RFL – Ilm intergrowth in px

Metagabbro, type II - DTC15002C

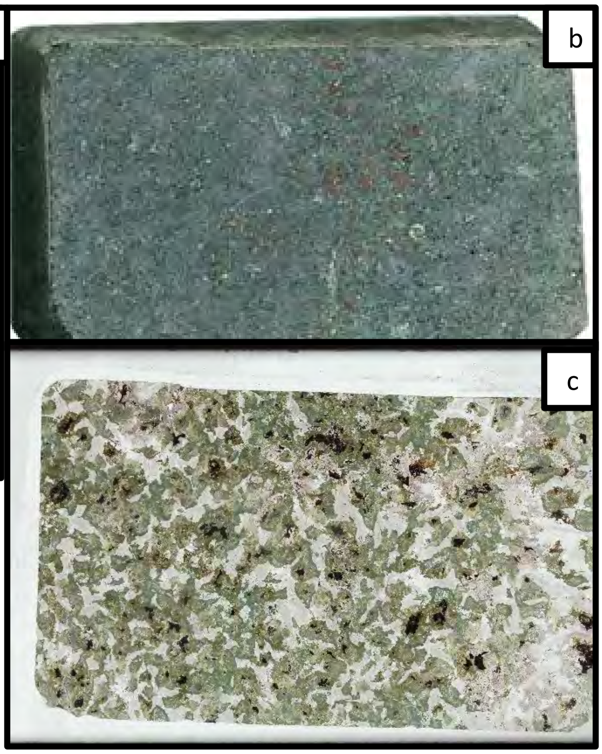

Figure 7, a: hand sample, b: sawed sample (scale approx. 2.5 X 3.5 cm), c: scanned thin section in PPL (scale approx. 2.5 X 3.5 cm)

The main minerals are hornblende, plagioclase, opaque minerals, garnets, pyroxene, biotite and quartz with accessory minerals calcite and siderite. There is about 50% dark phases in the sample.

The sample has a seriate texture with both polygonal and interlobate grain boundaries. Replacement textures are seen with recrystalized pyroxene in the core and hornblende at the rim.

The sample contains some plagioclase laths, where most plagioclase has an anhedral habit. Plagioclase has a composition of anorthite$_{30-40}$, where thin narrow albite twins, Carlsbad twins and pericline twins occur occasionally. Saussuritization is sparse. Augitic clinopyroxenes have a light bluish colour, are porphyroblastic with an anhedral habit and are rimmed with hornblende. Clinopyroxene is fairly common in the sample. Hornblende has a green-brown to green-blue colour, occur as large aggregates, as intergrowth formations with pyroxene and quartz and is common in the sample. Biotite has a brown colour, occur as randomly oriented aggregates and as radiating formations around the opaque minerals. Biotite is sparse in the sample.

Garnet is common, occur as euhedral crystals in aggregates, where inclusions are common. There are two types of garnets, type 1 has smaller euhedral habit which seems to be in apparent textural equilibrium with the surrounding minerals. Type 2 has an anhedral habit or occur as coronas, with a sieve textured core and with a narrow rim of more equilibrated garnet. Overall, these garnets contains more fractures than in previous samples. The opaque minerals are ilmenite and pyrite, with an euhedral and anhedral habit. The opaque minerals occurs either in close contact or as individual crystals, often together with hornblende, biotite and garnet. Acicular long apatite are often bent (figure 15c).

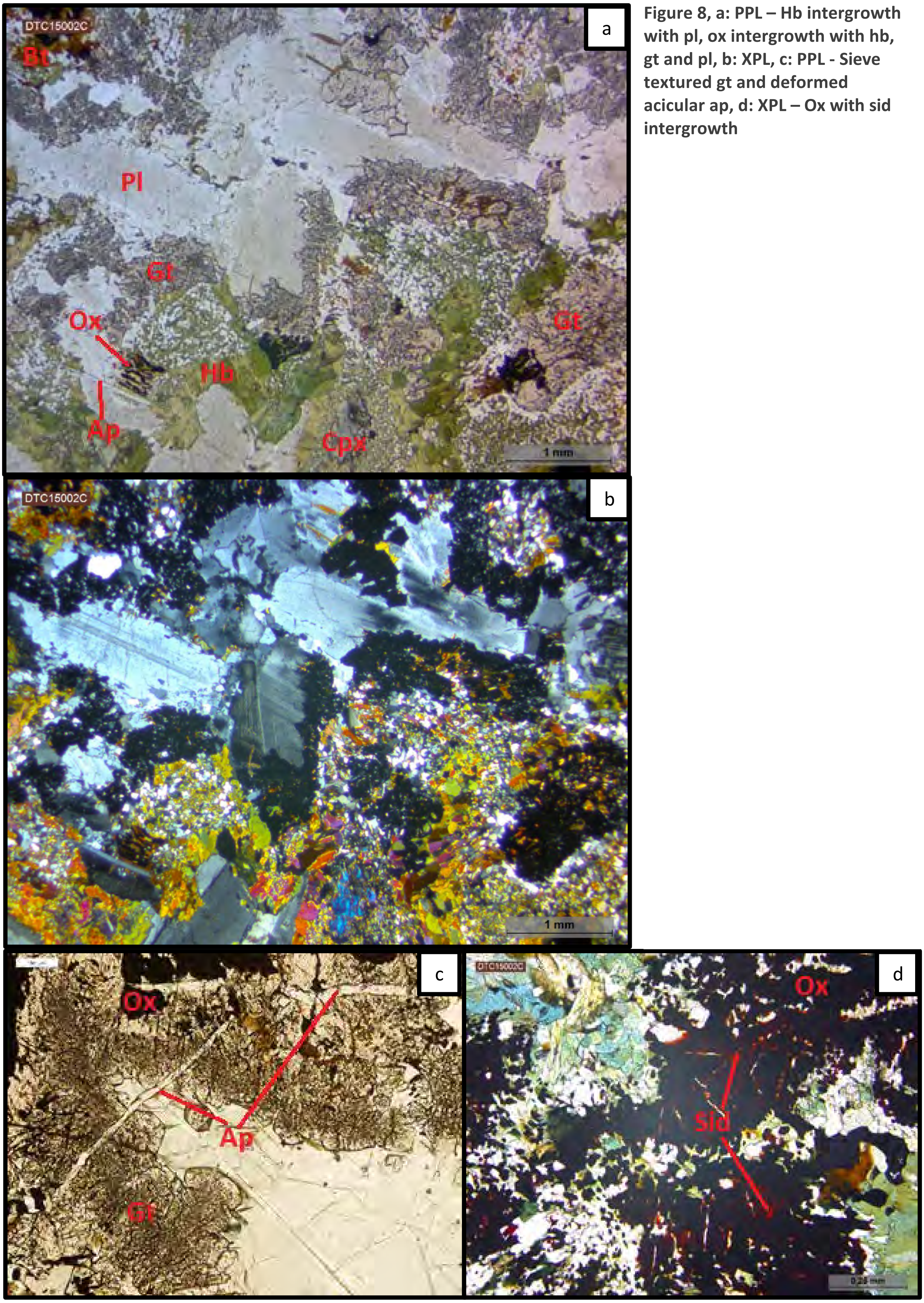

Figure 8, a: PPL – Hb intergrowth with pl, ox intergrowth with hb, gt and pl, b: XPL, c: PPL - Sieve textured gt and deformed acicular ap, d: XPL – Ox with sid intergrowth

Garnet-amphibolite, type IV - DTC15002D

Figure 9, a: hand sample, b: sawed sample (scale approx. 2.5 X 3.5 cm), c: scanned thin section in PPL (scale approx. 2.5 X 3.5 cm)

This sample consists of a younger mafic intrusion in a garnet-amphibolite.

Garnet-amphibolite

The main minerals in the garnet-amphibolite are hornblende, biotite, quartz, garnet, opaque minerals and plagioclase with accessory minerals apatite, calcite and epidote. There is about 40% dark phases in this par of the thin section.

The sample has a seriate texture with polygonal grain boundaries and foliation is defined by aligned biotite and hornblende. Cleavage domains are parallel with a rough to smooth shape, where dynamic recrystallization is coarse grained with high deformation grade.

Plagioclase occurs as euhedral crystals with a composition of anorthite20-30. Albite twins and pericline twins are visible, where sericitization is sparse to fairly common. Hornblende has a green-brown colour, occur as larger aggregates and is common. Biotite has a brown-red colour, occur as aligned aggregates often together with the opaque minerals and hornblende. Biotite is common.

The garnets in the garnet-amphibolite seems to be in apparent textural equilibrium with the surrounding minerals, where they are also smaller than in the intrusion. Pressure shadows in the direction of the foliation are common in the intrusion.

The opaque minerals are ilmenite and pyrite. They occur as larger anhedral or acicular crystals along the foliation. Ilmenite is more common than pyrite.

Mafic intrusion

The main minerals in the mafic intrusion are hornblende, garnet and plagioclase with accessory minerals biotite and calcite. There is more than 50% dark phases in this part of the thin section.

The sample has a seriate texture with interlobate grain boundaries. Foliation is defined by alignment of all minerals with domains that have medium size crystals, mostly plagioclase and biotite where small crystals are aligned around the garnets. Cleavage domains and foliation are continuous, where the dynamic recrystallization is fine grained and clustered with medium deformation grade.

Plagioclase occurs as larger anhedral plagioclase laths and smaller anhedral crystals with a composition of anorthite30-40. The crystals show Carlsbad twins that are badly sericitized and concentric zoning is also visible in the plagioclases. Hornblende has a green-brown colour, occur as individual crystals evenly distributed. Hornblende is common in the whole sample. Biotite has a brown-red colour, occur as individual crystals or as aggregates without a clear alignment. Biotite is fairly common.

Poikiloblastic garnets are common in the whole sample. They occur as large euhedral crystals, often with a sieve textured core and an inclusion free rim. In some garnets there are relict plagioclase laths that is partly recrystallized into fairly inclusion free garnets (figure 10f). The opaque minerals are ilmenite and pyrite. They are small and evenly distributed, with ilmenite more abundant than pyrite but where the pyrite crystals are larger than the ilmenite. Some larger crystals are seen in close relationship with the garnets.

Evidence of fluid-rock interaction is seen along the grain boundary edges of the hornblende. A continuous crack runs through the whole sample, where calcite seems to be common as filling material. The calcite is highly deformed. Occasionally calcite is found in smaller domains with a fibrous habit.

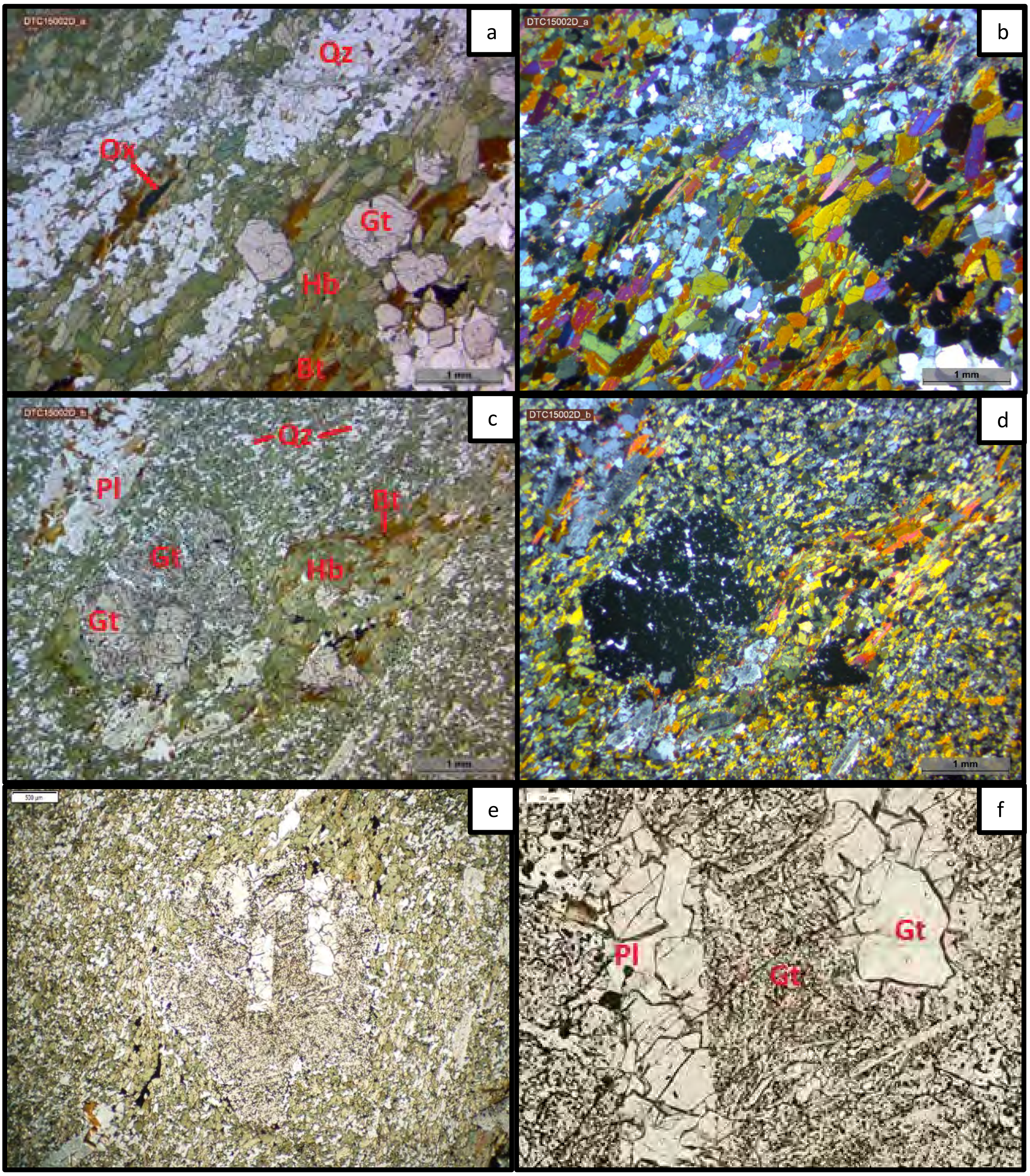

Figure 10, a: PPL – minerals seems to be in apparent textural equilibrium, b: XPL, c: PPL – sieve textured gt with recrystallized inclusions where the new gt seems to be in better textural equilibrium than surrounding gt, e: PPL – sieve textured gt with pl laths as partly recrystallized inclusions, f: PPL – close up of 17e, the pl laths are partly recrystallized in to more equilibrated gt than surrounding sieve textured gt

Metagabbro - DTC15002E

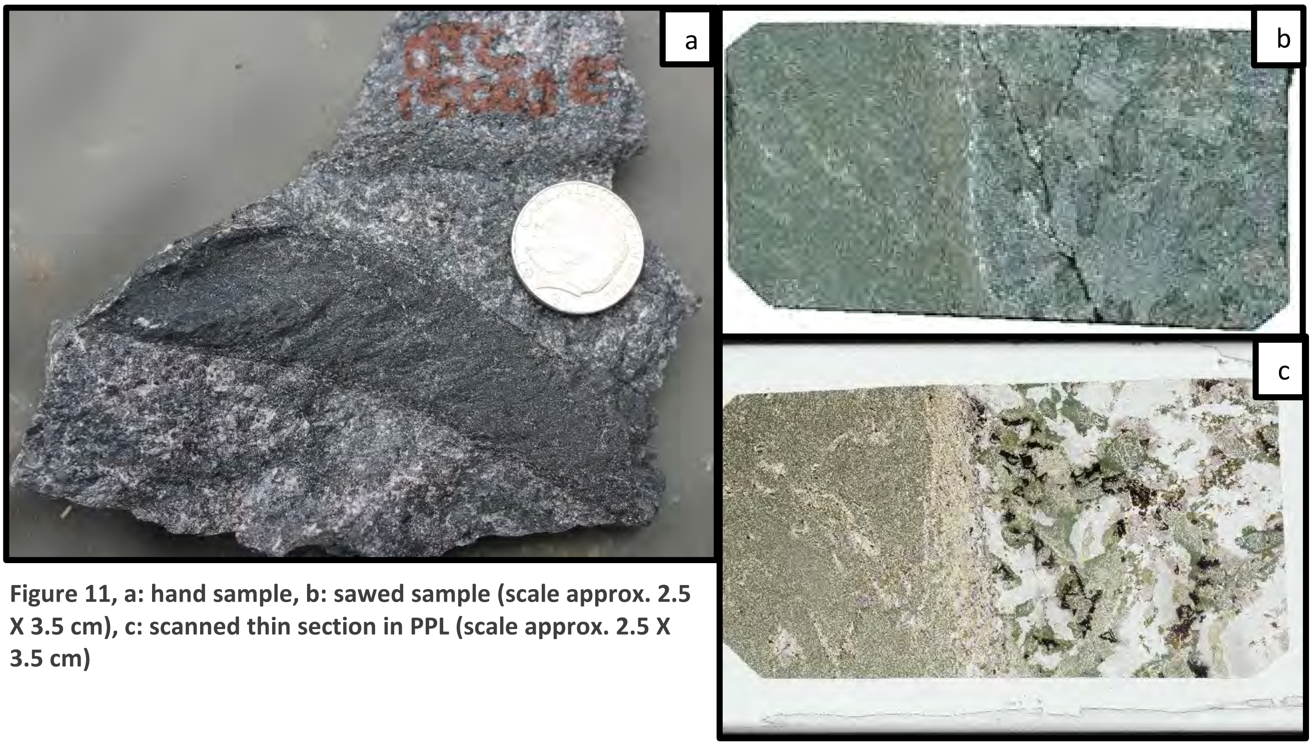

Figure 11, a: hand sample, b: sawed sample (scale approx. 2.5 X 3.5 cm), c: scanned thin section in PPL (scale approx. 2.5 X 3.5 cm)

This sample contains a mafic intrusion into a metagabbro.

Metagabbro

The main minerals in the metagabbro are hornblende, plagioclase, biotite, opaque minerals, garnet and quartz with accessory minerals apatite and calcite. There is about 35% dark phases in the metagabbro.

The sample has a seriate texture with mostly polygonal grain boundaries. No foliation is defined and diffuse replacement textures seems preserved. A micro shear zone occurs between the intrusion and the original rock (figure 12a), containing aligned biotite as pressure shadows around the garnets, parallel to the foliation.

Large plagioclase laths, subhedral to anhedral and has a composition of anorthite$_{30\text{-}40}$. Albite twins, both thick and small/narrow are common in all plagioclase. Hornblende has a green-blue colour, occurs as large aggregates and is common. Biotite has a brown colour, occurs as aggregates together with the opaque minerals. Biotite is fairly common to common in the whole sample, with higher abundance in the shear zone.

Garnet is common in the metagabbro, they have a euhedral habit and often occurs in aggregates or as rims around other minerals. The garnets often have a sieve texture with only individual crystals having achieved apparent textural equilibrium. The opaque minerals are ilmenite and pyrite, they occur as anhedral crystals in the metagabbro. Ilmenite is commonly larger and more abundant than pyrite.

Mafic intrusion

The main minerals in the intrusion are hornblende, biotite and plagioclase with accessory minerals garnet, opaque minerals and calcite. There is more than 50% dark phases in the intrusion.

The sample has a seriate texture with polygonal grain boundaries. Foliation is defined by aligned biotite, where cleavage domains are anastomosing with a rough shape in the intrusion.

Plagioclase laths are commonly large, subhedral to anhedral and has a composition of anorthite$_{40\text{-}50}$. Albite twins, both thick and small/narrow are common in all plagioclase. The plagioclase in the intrusion are severely saussuritized showing a sieve texture. Hornblende has a green-blue colour, are evenly distributed and fine grained. Hornblende is common in the whole sample. Biotite has a brown colour, occurs as individual small crystals, occasionally as smaller aggregates. Biotite is fairly common to common in the whole sample, with higher abundance in the shear zone.

Garnets are sparse, they occur as individual euhedral crystals and have a sieve texture throughout. The opaque minerals are ilmenite and pyrite, they occur as anhedral crystals but can also be found as euhedral crystals in the intrusion. The opaque minerals often occur together with hornblende and biotite, with the pyrite being larger but ilmenite is more abundant.

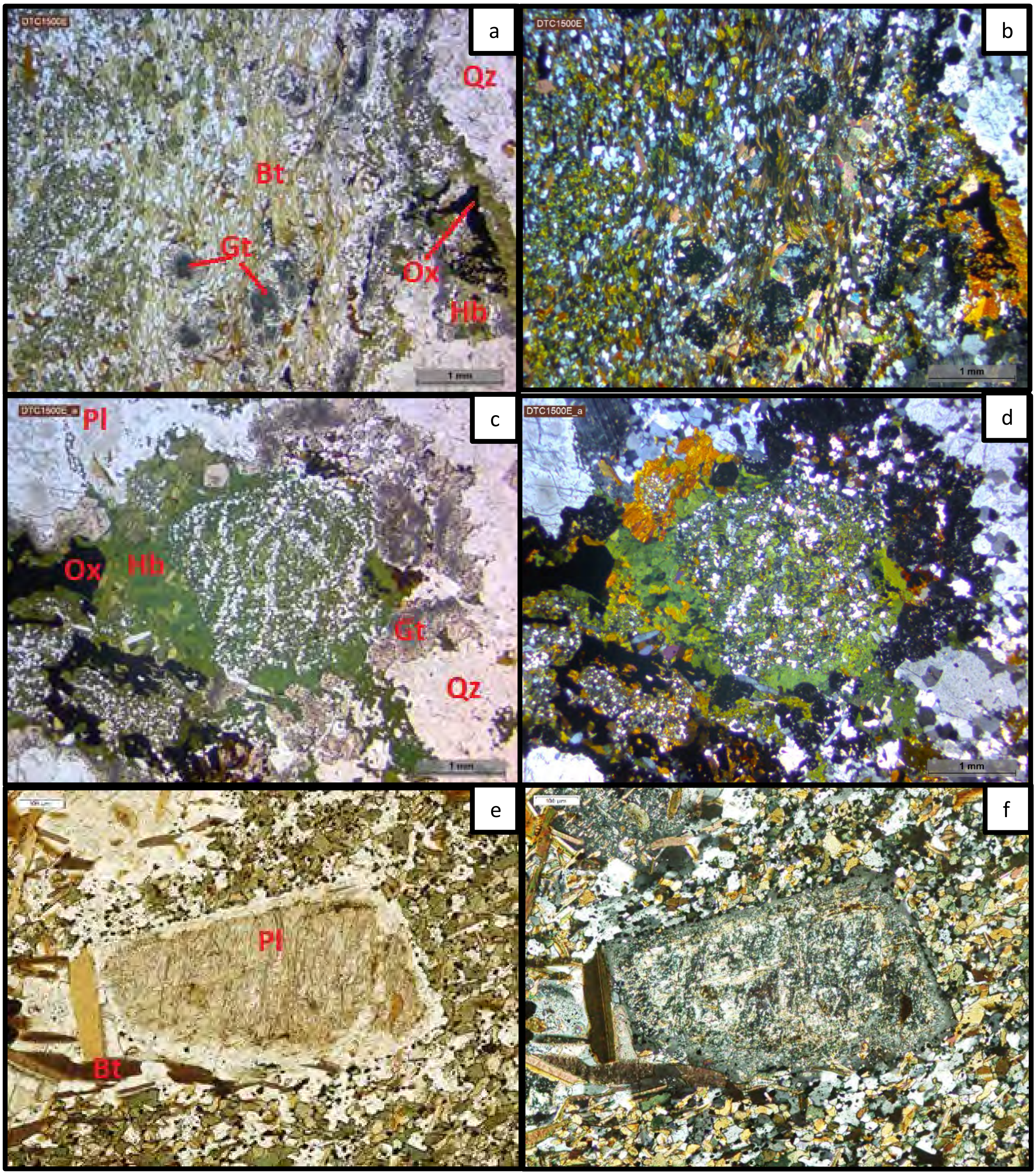

Figure 12, a: PPL – shear zone between the garnet-amphibolite and the intrusion, gt have a typical sieve textured core and a rim that seems to be in more apparent textural equilibrium, b: XPL, c: Hb intergrowth with pl and qz, d: XPL, e: PPL – sieve textured pl surrounded by a fine matrix of hb, ox, bt and qz, f: XPL

Garnet-amphibolite, type III - DTC15002F

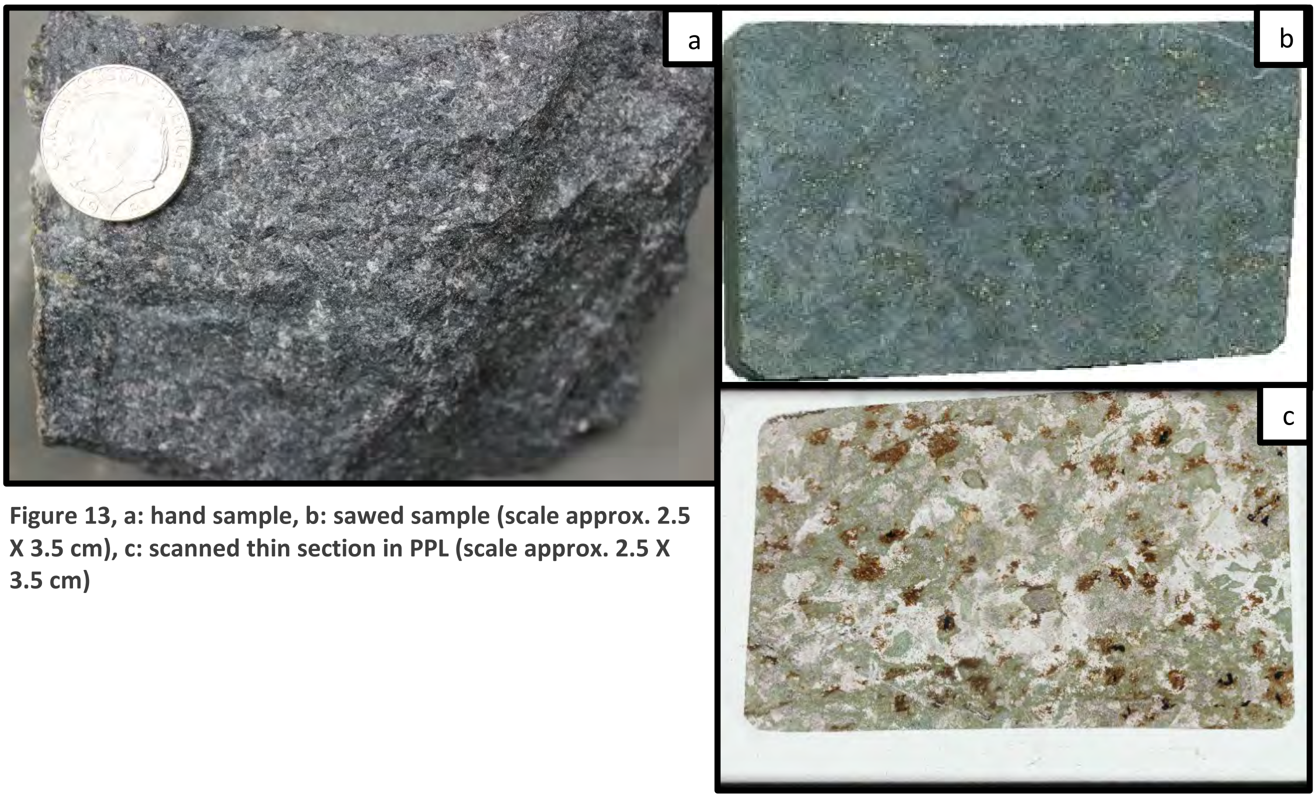

Figure 13, a: hand sample, b: sawed sample (scale approx. 2.5 X 3.5 cm), c: scanned thin section in PPL (scale approx. 2.5 X 3.5 cm)

The main minerals are hornblende, plagioclase, garnet, biotite, pyroxene and quartz with accessory minerals opaque minerals, calcite and amphibole. There is about 45% dark phases in the sample.

The sample has a seriate texture with polygonal towards interlobate grain boundaries. The sample is coarse grained with medium deformation and where granoblastic domains of plagioclase is present.

Occasionally subhedral plagioclase laths occur, but plagioclase is mostly found as anhedral crystals. The plagioclase has a composition of anorthite$_{30-40}$, albite twins are common and pericline twins are sparse. Sericitization occurs sparsely. Pyroxene is highly recrystallized at the edges into hornblende, and intergrowth formations are common. The pyroxene is probably clinopyroxenes, but are too dark to determine with a microscope due to oxide exsolution. Pyroxenes are fairly common to common in the sample. Hornblende is brown-green and occur as aggregates in larger domains. Oxide inclusions are common in some hornblende. Hydrothermal alteration is seen along the edges of the hornblende crystals where secondary hornblende has recrystallized after the metamorphic event, these occur in random orientations in contrast to the aligned hornblende. Hornblende is common in the sample. Biotite has a brown-red colour, occur in aggregates with no clear alignment and is fairly common to common in the sample.

Garnets have a euhedral habit, occur in aggregates and occasionally as rims or coronas, often along the edges of hornblende or in the plagioclase. Fractures are common in the garnets and some have a sieve texture. The opaque minerals are ilmenite and pyrite, where ilmenite occur as large euhedral crystals in contact with biotite and the pyrite is found as small crystals, often as stains in hornblende, garnet or other minerals.

Fractures are highly affected by fluids where low grade hydrous minerals, such as calcite, are found along the veins.

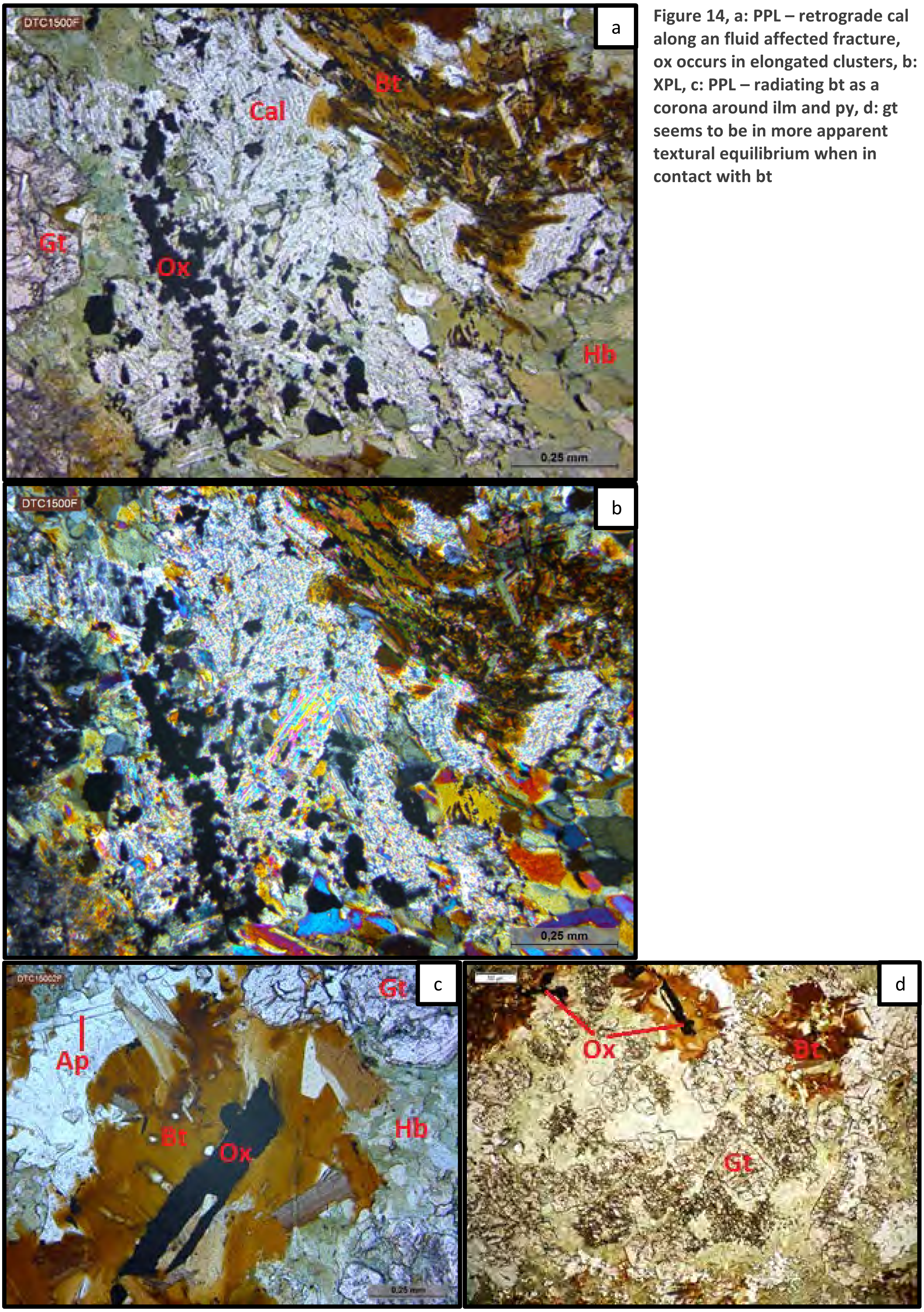

Figure 14, a: PPL – retrograde cal along an fluid affected fracture, ox occurs in elongated clusters, b: XPL, c: PPL – radiating bt as a corona around ilm and py, d: gt seems to be in more apparent textural equilibrium when in contact with bt

Garnet-amphibolite, type IV - DTC15002G

Figure 15, a: hand sample, b: sawed sample (scale approx. 2.5 X 3.5 cm), c: scanned thin section in PPL (scale approx. 2.5 X 3.5 cm)

The main minerals are hornblende, garnet, biotite, plagioclase and opaque minerals with accessory minerals quartz and titanite. There is more than 50% dark phases in the sample.

The sample has a seriate texture with polygonal grain boundaries. Foliation is defined by aligned hornblende and biotite where the cleavage domains are anastomosing with a smooth shape.

The plagioclase has a subhedral habit with a composition of anorthite$_{30\text{-}40}$. Albite twins are common and intergrowth formations with hornblende and quartz are sparse. Hornblende has a green-brown colour, occur in both large and small aggregates and is common in the sample. Biotite has a brown-red colour, occur as individual crystals, preferably in contact with the garnets, and is fairly common in the sample.

Garnets have a poikiloblastic texture, with inclusions consisting mostly of quartz, plagioclase, opaque minerals and titanite. They have a syntectonic deformation with strain caps, no internal foliation, and pressure shadows in the direction of foliation are common. The larger garnets seems to have a textural sector-zoning where relict mineral grains that have recrystallized into garnet is seen (figure 23c). The opaque minerals are ilmenite and pyrite, where ilmenite is more abundant than pyrite. They occur as small euhedral crystals that are evenly distributed throughout the sample.

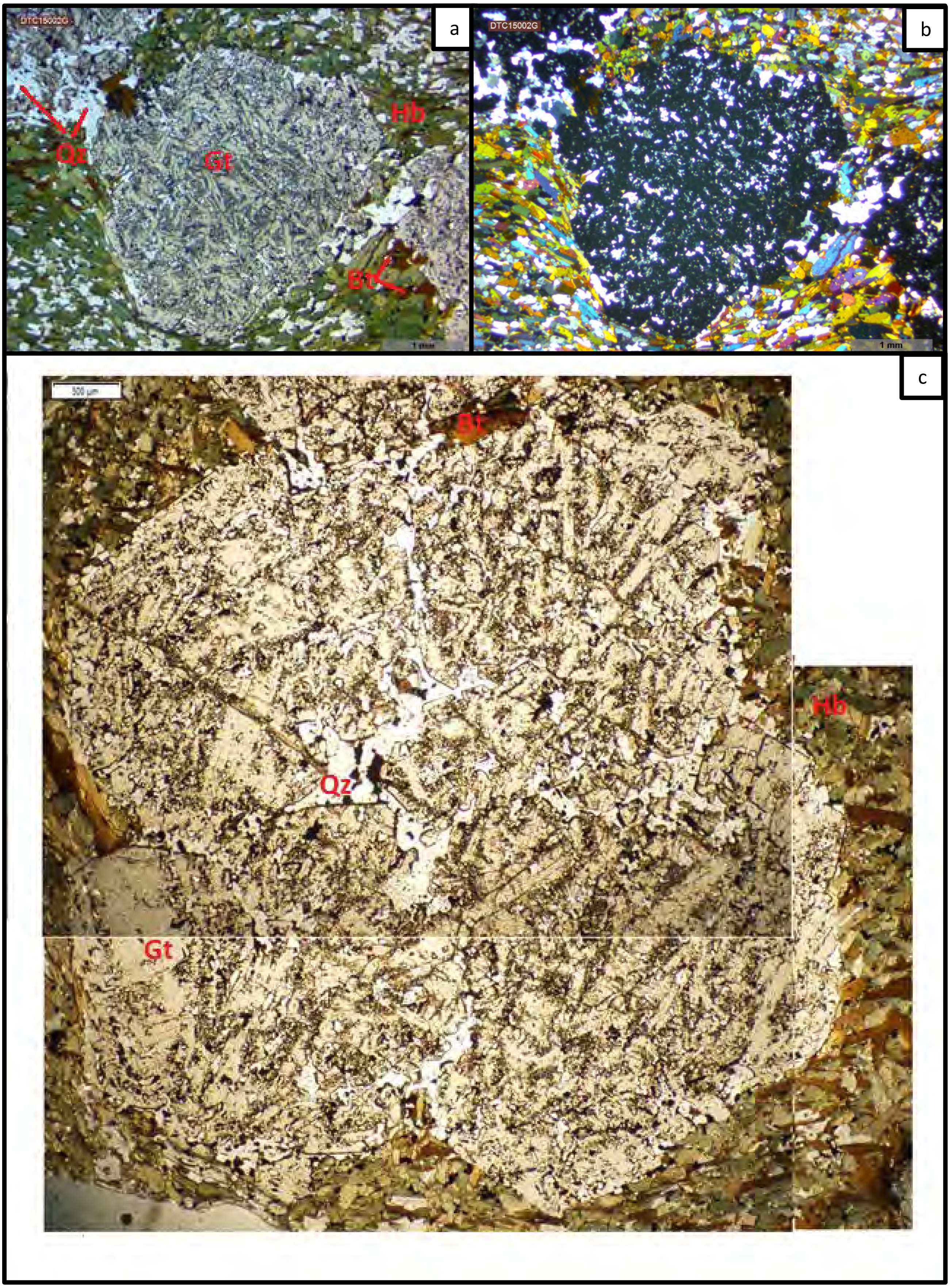

Figure 16, a: PPL – gt with textural zoning showing pressure shadows along the foliation, b: XPL, c: PPL – photo collage, large gt with textural zoning in several steps

Träfors

Garnet-amphibolite, type IV - DTC15007A

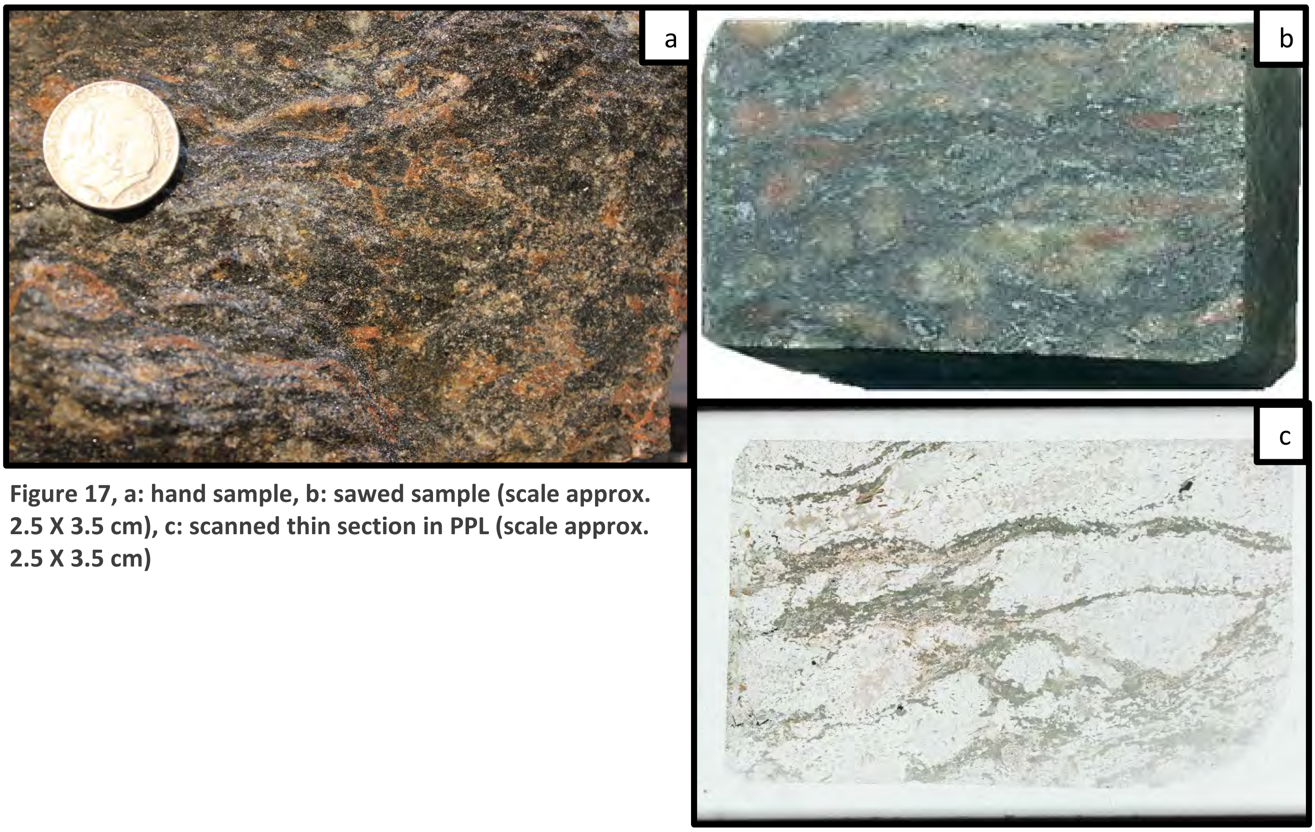

Figure 17, a: hand sample, b: sawed sample (scale approx. 2.5 X 3.5 cm), c: scanned thin section in PPL (scale approx. 2.5 X 3.5 cm)

The main minerals are plagioclase, hornblende, quartz, pyroxene and *serpentine?* with accessory minerals titanite, apatite, calcite, biotite, opaque minerals, garnet and chlorite. There is about 15% dark phases in the sample.

The sample has a seriate texture with polygonal grain boundaries. Foliation is defined by hornblende, chlorite, biotite, olivine and titanite where cleavage domains are anastomosing with a smooth shape. The dynamic recrystallization is fine grained and clustered with a high deformation grade. Large subhedral to anhedral crystals, preferably in domains.

The plagioclase has a composition of anorthite$_{20\text{-}30}$, thin albite twinning is common where some larger crystals contains deformed and somewhat wavy twinning. The pyroxenes are clinopyroxenes where skeletal textures, with possible phyllosilicate mineral around the clinopyroxenes, are common. Hornblende has a green-brown colour, occur as both individual grains or as aggregates. Hornblende is common in the sample. Biotite has a brown-green colour, occur as individual crystals and is sparse in the sample. Along hydrothermal fluid veins or high deformation zones, the biotite is severely chloritized into Berlin blue chlorite.

Garnets occur as individual crystals, with euhedral habit when found as individual crystals or with anhedral habit when found in aggregates. The crystals are often fractured but seems to be in apparent textural equilibration. Garnet is sparse in the sample and often occur together with hornblende. Titanite occurs as aggregates, often in contact with the opaque minerals, or in elongated domains along the foliation. Apatite is common, it is found as both large acicular and subhedral crystals with a sky blue colour, often as inclusions in plagioclase. The opaque minerals are pyrites that are found with both acicular, prismatic or anhedral habit. Pyrite is often found together with titanite, hornblende and olivine.

One large anhedral quartz crystal in the centre of the thin section contains several inclusions of prismatic apatite, acicular biotite and anhedral plagioclase (figure 25b). Pressure shadow is visible along the foliation around the crystal.

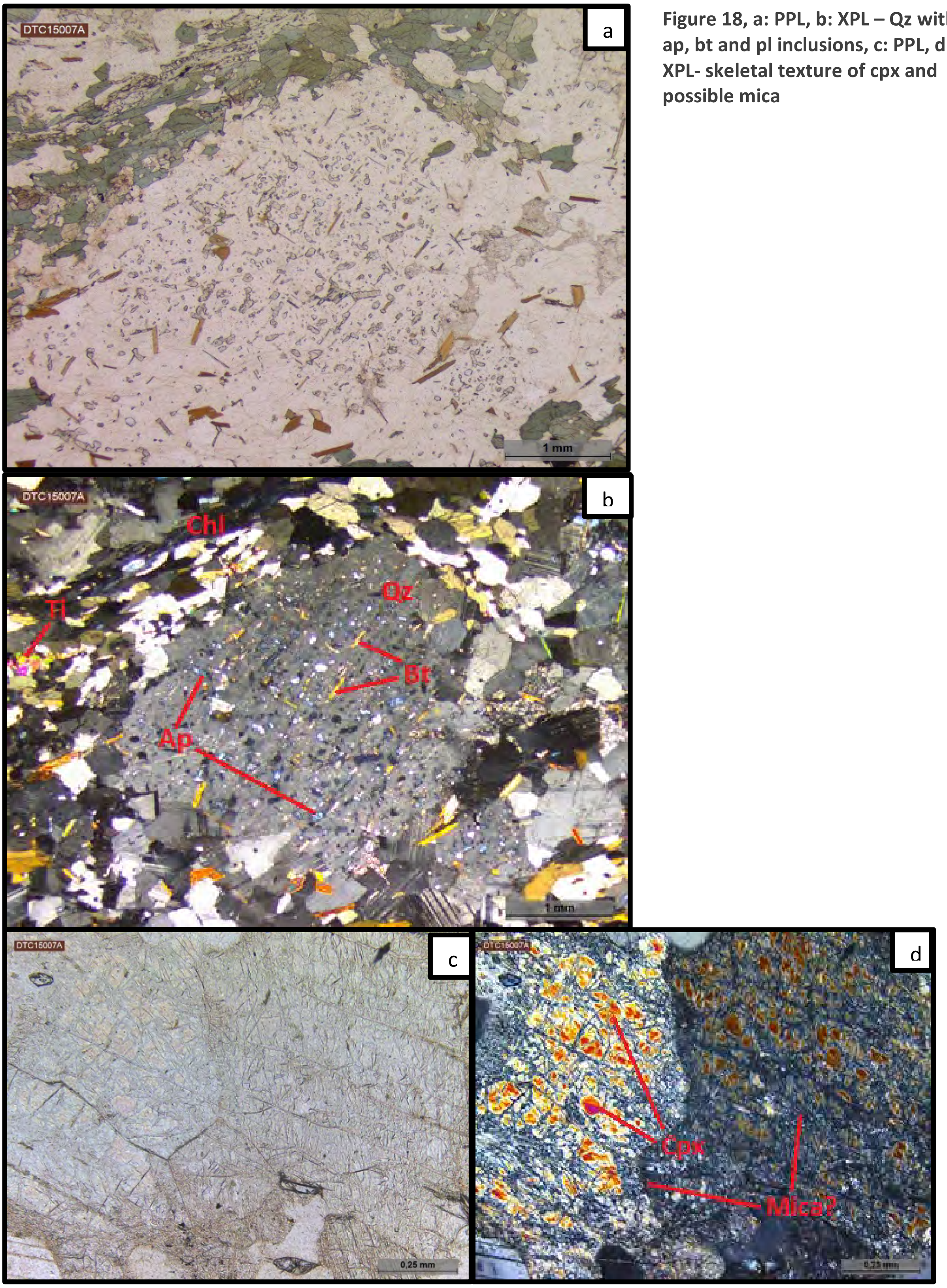

Figure 18, a: PPL, b: XPL – Qz with ap, bt and pl inclusions, c: PPL, d: XPL- skeletal texture of cpx and possible mica

Garnet-amphibolite, type IV - DTC15007C

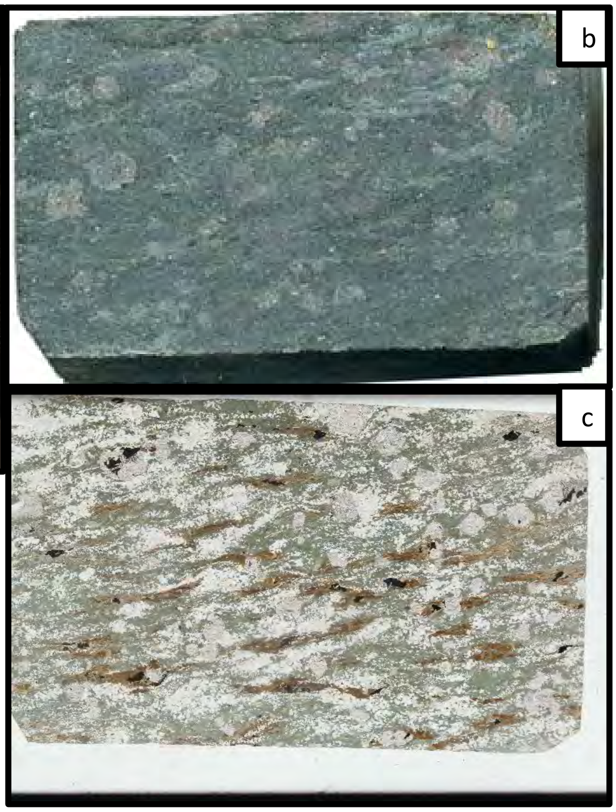

Figure 19, a: hand sample, b: sawed sample (scale approx. 2.5 X 3.5 cm), c: scanned thin section in PPL (scale approx. 2.5 X 3.5 cm)

The main minerals are hornblende, biotite, garnet, opaque minerals, plagioclase and chlorite with accessory minerals quartz, apatite and siderite. There is about 40% dark phases in the sample.

The sample has a seriate texture with polygonal grain boundaries. Foliation is defined by hornblende, biotite and chlorite where cleavage domains are anastomosing with a rough to smooth shape. Dynamic recrystallization is fine grained and clustered with a high deformation grade.

Plagioclase has a composition of anorthite$_{30\text{-}40}$, they have a subhedral to anhedral habit and occur in domains. Albite twinning is found sparsely. The plagioclase are mostly sericitized, where modest saussuritization is present along the grain boundaries. Some crystals are severely saussuritized. Hornblende has a green-brown colour, is found in aggregates and is common in the sample. Biotite has a brown-red colour and is found as aligned aggregates along the foliation. Larger domains are often severely chloritized into Berlin blue chlorite. Biotite is common in the sample.

Garnet is found as porphyroblastic euhedral crystals. Inclusions are sparse, consisting mostly of strained quartz, plagioclase, apatite and opaque minerals. One larger garnet has a criss cross pattern of opaque minerals and siderite. Pressure shadows are common where the garnets have a syntectonic rotation with a dextral shear. The opaque minerals are ilmenite and pyrite, where ilmenite is found as large anhedral crystals, often with a skeleton texture. Pyrite is also anhedral but are smaller than the ilmenite.

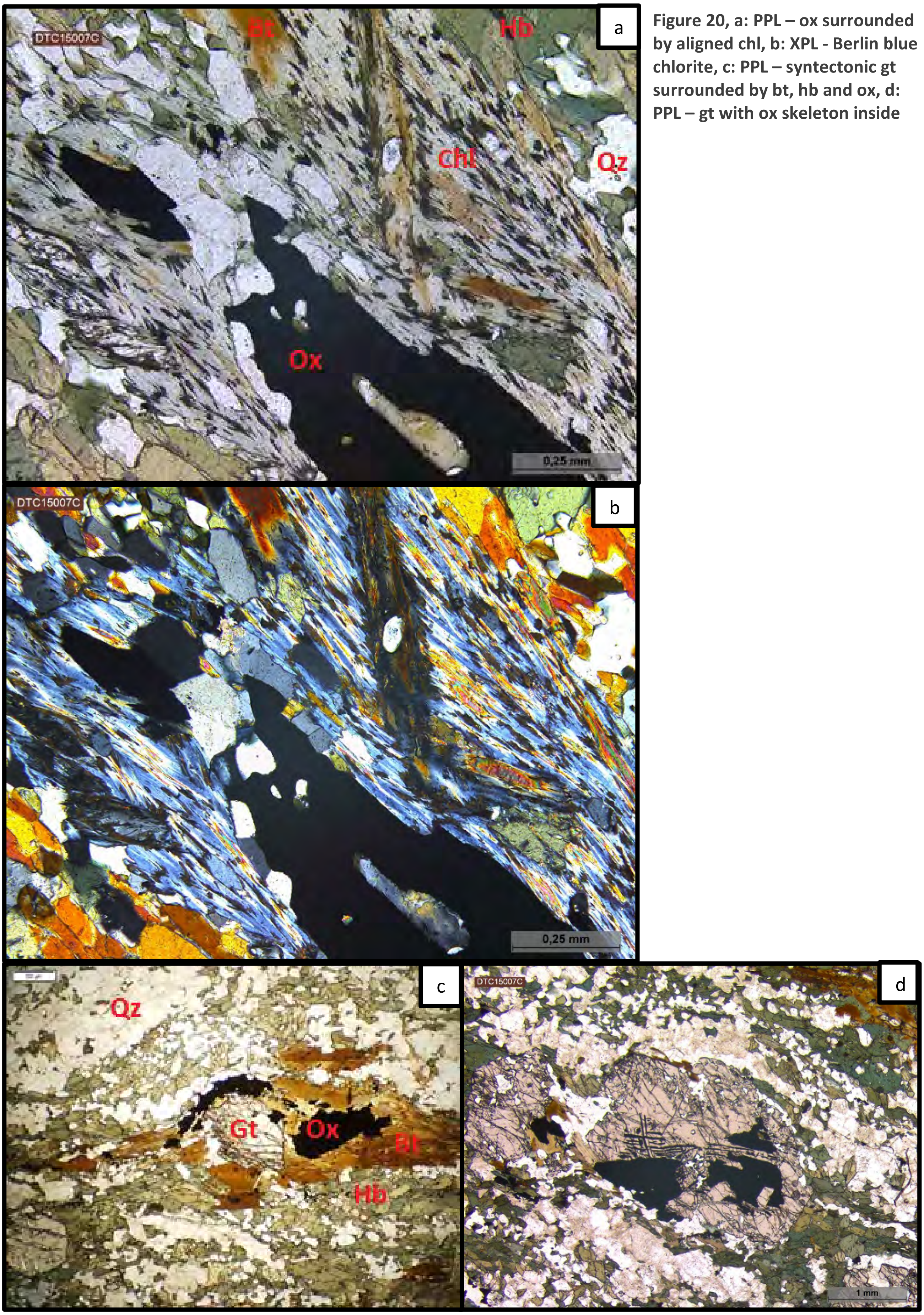

Figure 20, a: PPL – ox surrounded by aligned chl, b: XPL - Berlin blue chlorite, c: PPL – syntectonic gt surrounded by bt, hb and ox, d: PPL – gt with ox skeleton inside

Garnet-amphibolite, type III - DTC15007F

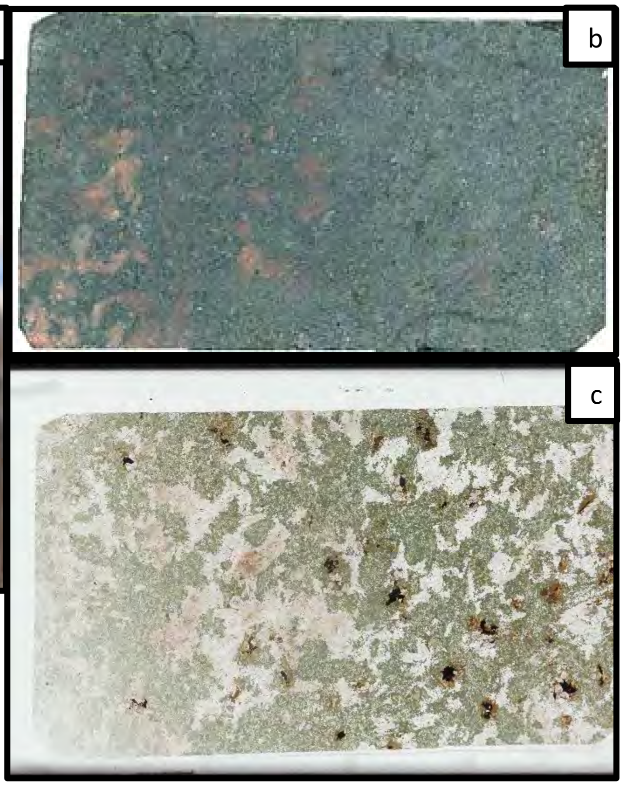

Figure 21, a: hand sample, b: sawed sample (scale approx. 2.5 X 3.5 cm), c: scanned thin section in PPL (scale approx. 2.5 X 3.5 cm)

The main minerals are hornblende, garnet, plagioclase, biotite, opaque minerals and quartz with accessory minerals apatite, chlorite, titanite and siderite. There is about 40% dark phases in the sample.

The sample has seriate texture with polygonal grain boundaries. Granoblastic domains of plagioclase and opaque minerals occur. The dynamic recrystallization is fine grained and clustered with low deformation grade.

Plagioclase has a subhedral to anhedral habit, with a composition of anorthite$_{30}$. Some plagioclase are severely saussuritized, albite twins are common and pericline twins are sparse. Hornblende has a green-brown colour, occur as small crystals in large aggregates and is common in the sample. Biotite has a brown-red colour, occur as coronas around the opaque minerals and occasionally as individual crystals together with hornblende. Some crystals are modest to severely chloritized into Berlin blue chlorite. Biotite is sparse in the sample.

Garnets occur as individual crystals or in smaller aggregates, often together with hornblende and the opaque minerals. They have a euhedral habit and is common in the sample. The opaque minerals are mostly ilmenite, but small pyrite do occur. Ilmenite is found as anhedral crystals with skeletal textures, often together with biotite and hornblende.

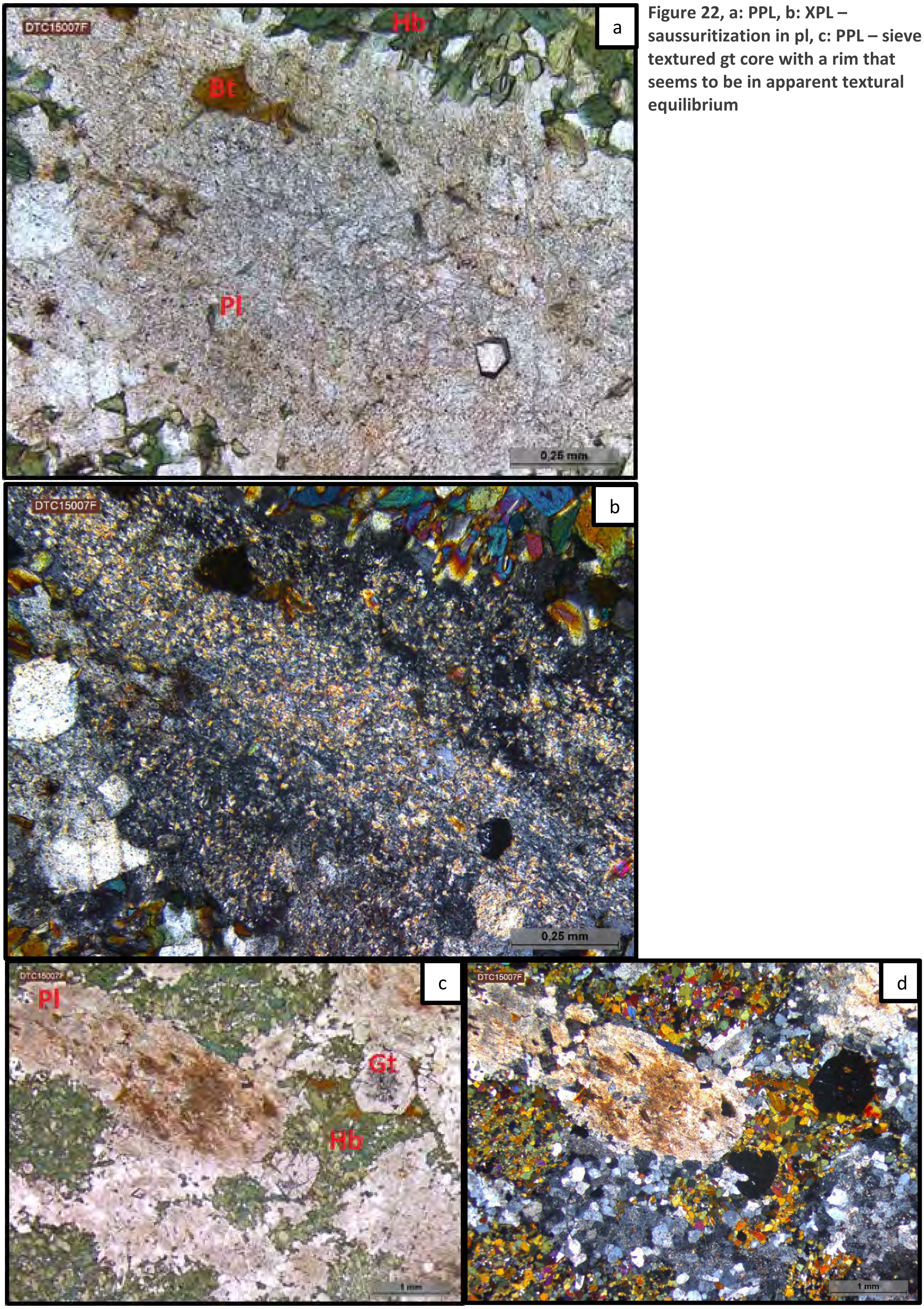

Figure 22, a: PPL, b: XPL – saussuritization in pl, c: PPL – sieve textured gt core with a rim that seems to be in apparent textural equilibrium

Metagabbro, type II - DTC15007G

Figure 23, Figure 24, a: hand sample, b: sawed sample (scale approx. 2.5 X 3.5 cm), c: scanned thin section in PPL (scale approx. 2.5 X 3.5 cm)

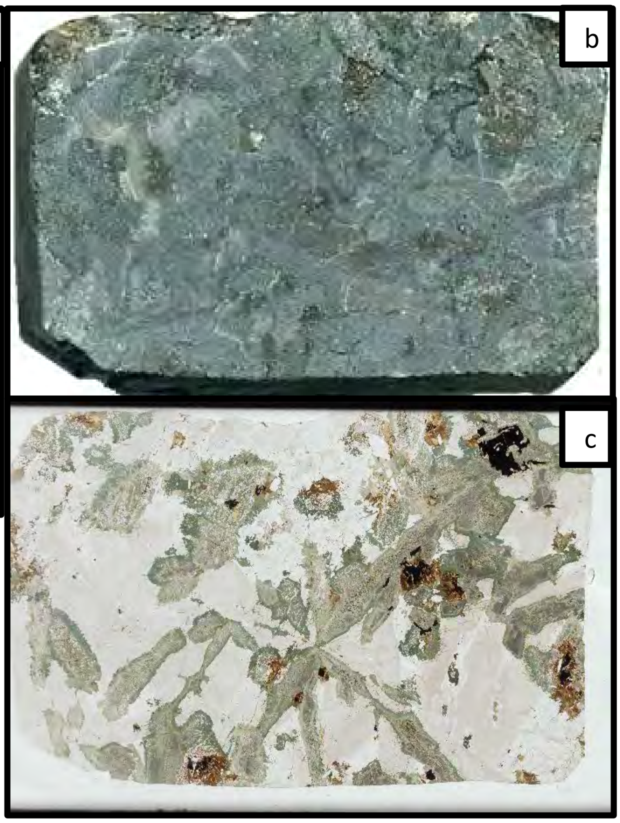

The main minerals are hornblende, plagioclase, pyroxene and biotite with accessory minerals garnet, quartz, apatite, calcite and titanite. There is about 30% dark phases in the sample.

The sample has a seriate texture with interlobate grain boundaries. Replacement textures are seen where pyroxene has recrystallized into hornblende at the rims. Dynamic recrystallization is coarse grained with medium deformation grade.

Very large plagioclase crystals with euhedral habit or as plagioclase laths are common. The plagioclase has a composition of anorthite$_{30}$, albite twinning is common and pericline twining is sparse. Myrmekitization between plagioclase and quartz crystals are sparse to fairly common in the sample. Augitic clinopyroxenes are bluish in colour and are found as long, large prismatic crystals where some are severely recrystallized into hornblende. Clinopyroxene is common in the sample. Hornblende is found with both green-brown and green-blue colour, occur as coronas around the pyroxenes and is common in the sample. Biotite has a brown-red colour, is found as individual grains or as aggregates and is fairly common in the sample. They often occur as corona like textures with a radiating appearance around the opaque minerals (figure 32a).

Garnet is sparse to fairly common in the sample. They have an anhedral habit, occur in aggregates and have a sieve texture and are commonly fractured. The opaque minerals are ilmenite and pyrite and have an anhedral habit. Ilmenite is often found in skeleton textures, where the opaque minerals occur together with biotite and calcite. Apatite is very common, has a large acicular or prismatic habit and a steel blue colour.

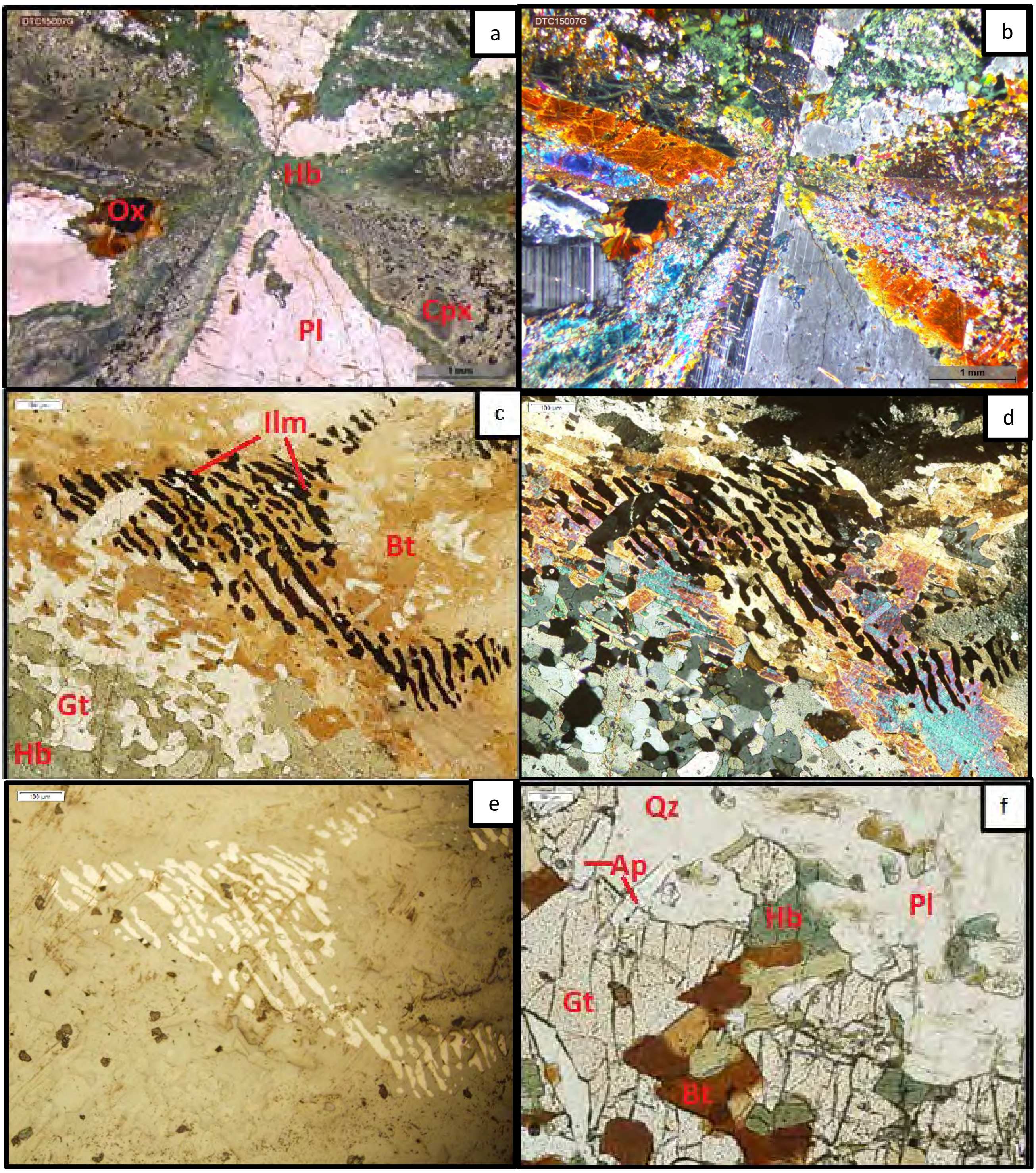

Figure 25, a: PPL, b: XPL, c: PPL – ilm skeleton surrounded by bt, d: XPL, e: RFL, f: PPL – gt, bt, hb, pl, qz and ap

Garnet-amphibolite, type III - DTC15007H

Figure 26, a: hand sample, b: sawed sample (scale approx. 2.5 X 3.5 cm), c: scanned thin section in PPL (scale approx. 2.5 X 3.5 cm)

The main minerals are hornblende, plagioclase, garnet and biotite with accessory minerals opaque minerals, apatite and quartz. There is about 35% dark phases in the sample.

The sample has a seriate texture with interlobate, occasionally polygonal, grain boundaries. Dynamic recrystallization is coarse grained with a medium to high deformation grade.

Plagioclase laths have a subhedral habit with a composition of anorthite$_{40\text{-}50}$. The laths are highly recrystallized, where several deformation events are visible as fractures in the plagioclase. Albite twinning with small narrow twins, pericline twins and Carlsbad twins are common. Inclusions are very common and are in some cases aligned along the pericline twinning. The plagioclase is fairly to severely saussuritized. Hornblende has a green-brown colour, occur in large domains of fine grained aggregates and is common in the sample. Biotite has a brown-red colour and occur in aggregates together with hornblende, the opaque minerals and occasionally garnet. Biotite is fairly common in the sample.

Garnets have a euhedral habit, they often occur in very large aggregates and as rims around the opaque minerals. They have a zoning with an inner rim that has a sieve texture and an outer rim that is in apparent textural equilibrium with the surrounding minerals. Garnet is common in the sample. The opaque minerals are ilmenite and pyrite. They have an anhedral habit, where ilmenite is occasionally found as skeleton textures. Ilmenite is more abundant than pyrite. The opaque minerals are found together with garnet, biotite and hornblende, where small pyrites often occur in the plagioclase. Apatite is found as large acicular crystals.

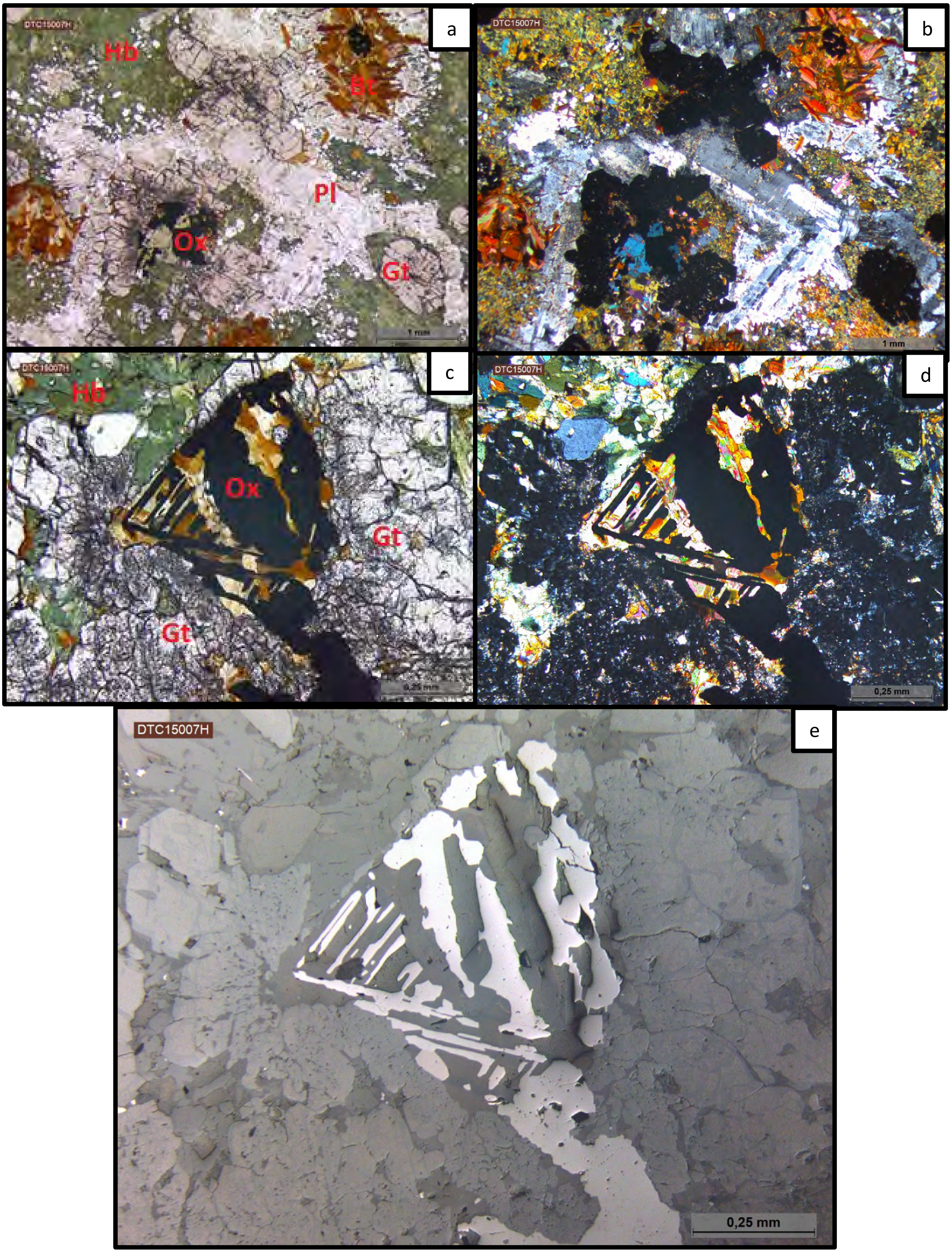

Figure 27, a: PPL – ox surrounded by bt or gt rims, b: XPL, c: PPL – ox skeleton surrounded by thick gt rim, d: XPL, e: RFL

Garnet-amphibolite, type IV - DTC15007I

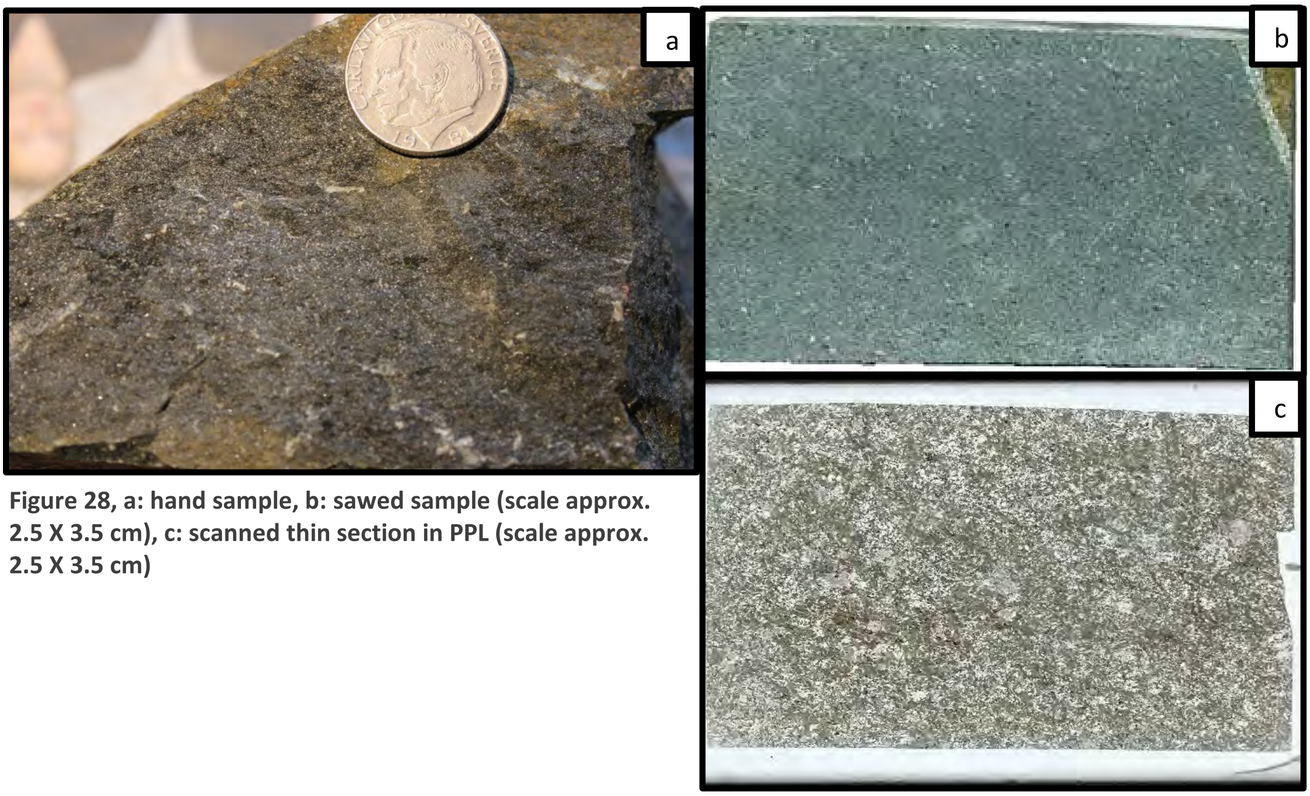

Figure 28, a: hand sample, b: sawed sample (scale approx. 2.5 X 3.5 cm), c: scanned thin section in PPL (scale approx. 2.5 X 3.5 cm)

The main minerals are hornblende, plagioclase, garnet, biotite and quartz with accessory minerals chlorite, apatite, amphibole and opaque minerals. There are more than 50% dark phases in the sample.

The sample has an equigranular texture with interlobate grain boundaries. Foliation is defined by aligned hornblende and biotite, where cleavage domains are parallel to somewhat anastomosing and have a smooth shape. Dynamic recrystallization is fine grained and clustered, with medium deformation grade.

Plagioclase has a subhedral to anhedral habit and a composition of anorthite$_{20\text{-}30}$. Pinning micro textures are common where surrounding minerals seems to take over the plagioclase crystals. Saussuritization is sparse in the plagioclase crystals. Hornblende has a green-brown colour, occur in aggregates and are common in the sample. Biotite has a brown-red colour, occur as individual crystals or aligned around domains of other minerals and is sparse to fairly common in the sample.

Garnet is found as individual crystals with anhedral habit, occasionally euhedral habit. The garnets have a sieve textured core with a rim that seem to be in apparent textural equilibration with the surrounding minerals. Pressure shadows and strain caps are seen where the garnets are syntectonic. Garnet is common in the sample. The opaque minerals consists of very small anhedral ilmenite and pyrite that are evenly distributed in the sample. The opaque minerals occasionally occur as small euhedral crystals.

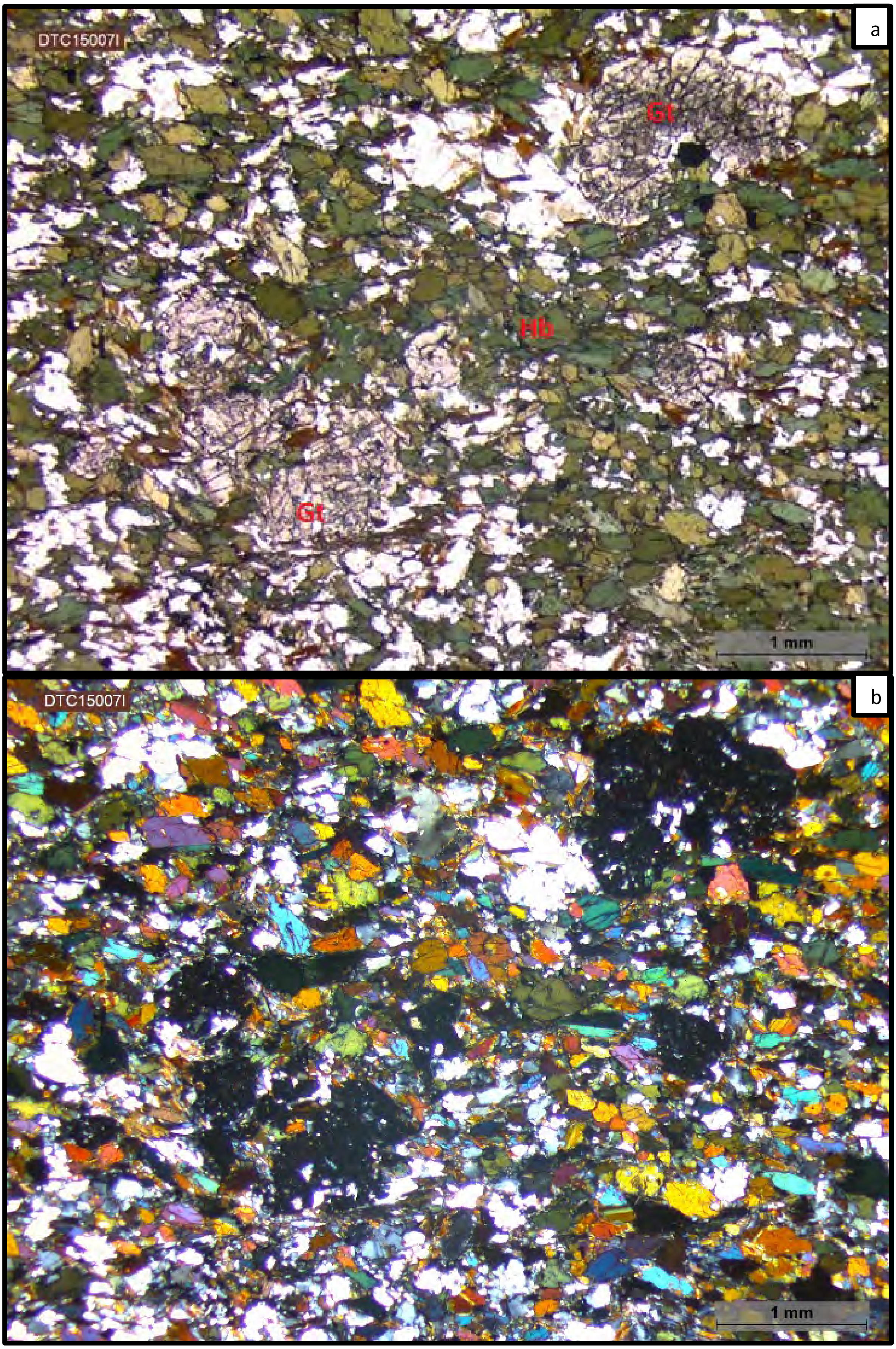

Figure 29, a: PPL – sieved textured gt, b: XPL

Garnet-amphibolite, type III - DTC15007J

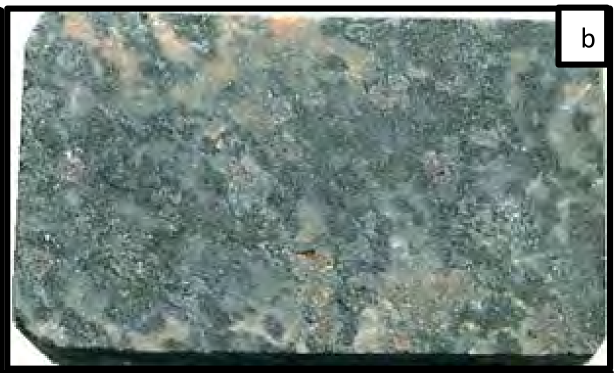

Figure 30, a: hand sample, b: sawed sample (scale approx. 2.5 X 3.5 cm), c: scanned thin section in PPL (scale approx. 2.5 X 3.5 cm)

The main minerals are hornblende, plagioclase, garnet and chlorite with accessory minerals opaque minerals, biotite, cordierite, sericite, calcite, apatite, titanite, zircon, quartz and epidote. There is about 30% dark phases in the sample.

The sample has a seriate texture with interlobate grain boundaries. Relict pyroxenes have been totally recrystallized into hornblende. The dynamic recrystallization is coarse grained with medium deformation grade.

Plagioclase occur as subhedral laths or anhedral crystals and has a composition of anorthite$_{30\text{-}40}$. They are severely sericitized and saussuritized. Thick albite twinning and narrow pericline twinning is common. Hornblende has a green-brown colour, is often found as recrystallized domains with no clear orientation and is common in the sample. Biotite has a brown-red colour, occur as individual crystals and is sparse in the sample.

Garnet has a euhedral habit, they are often found in aggregates and are common in the sample. The garnets are highly fractured. The opaque minerals are ilmenite and pyrite and have an anhedral habit. Ilmenite is more abundant with larger crystals than pyrite. The opaque minerals occur together with hornblende, chlorite and garnet. Occasionally domains with opaque minerals are found that are rimmed by chlorite or hornblende. Zircons are found as small prismatic crystals together with chlorite and titanite.

A large crack is seen through the sample. The crack is filled with calcite that has clear twinning (figure 38d), Berlin blue chlorite, acicular/elongated biotite and cordierite. The cordierite has a blue/grey colour with a very patchy undulose extinction (figure 38b). Chlorite is also found in domains with no clear orientation of the crystals.

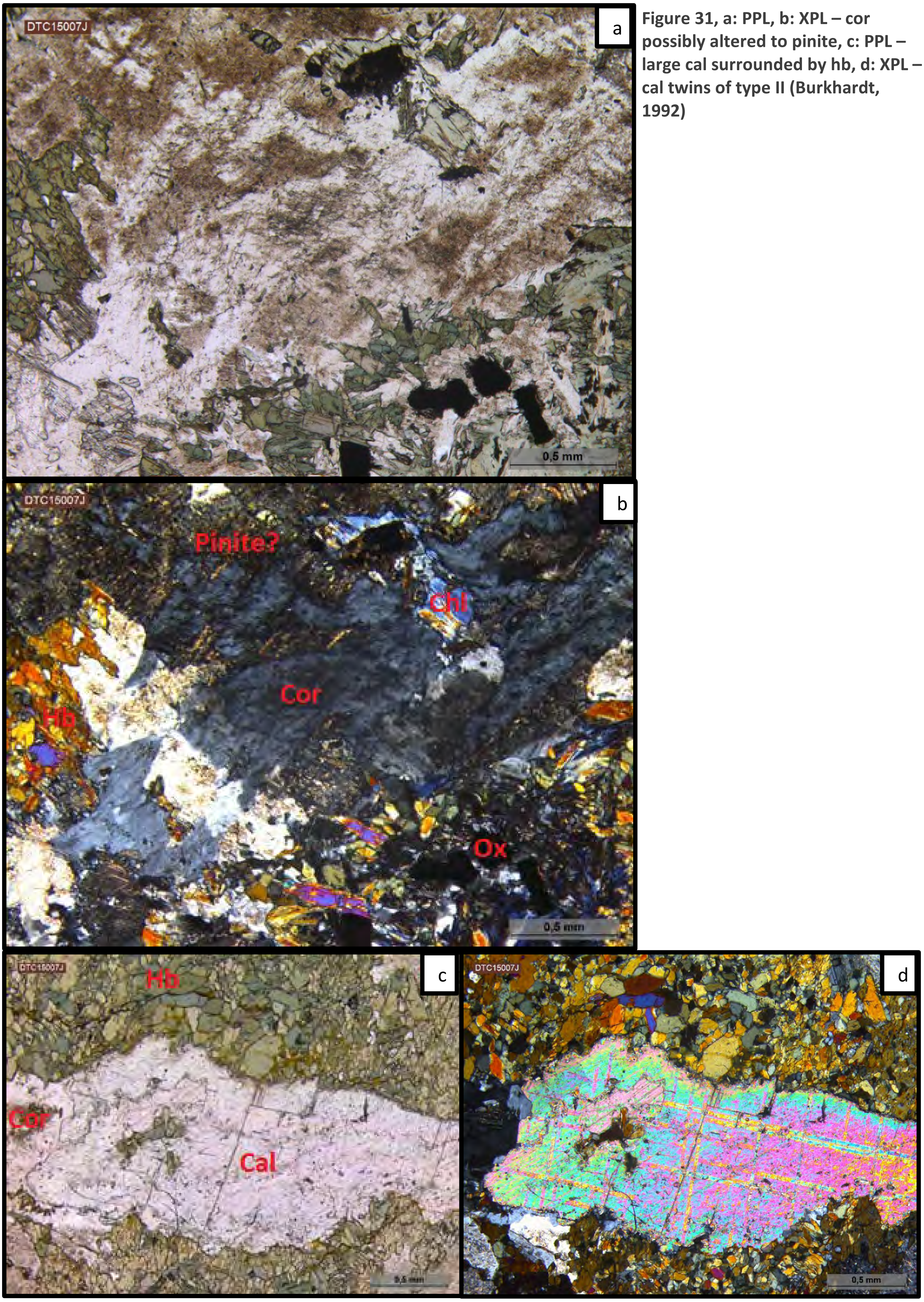

Figure 31, a: PPL, b: XPL – cor possibly altered to pinite, c: PPL – large cal surrounded by hb, d: XPL – cal twins of type II (Burkhardt, 1992)

Garnet-amphibolite, type III - DTC15007K

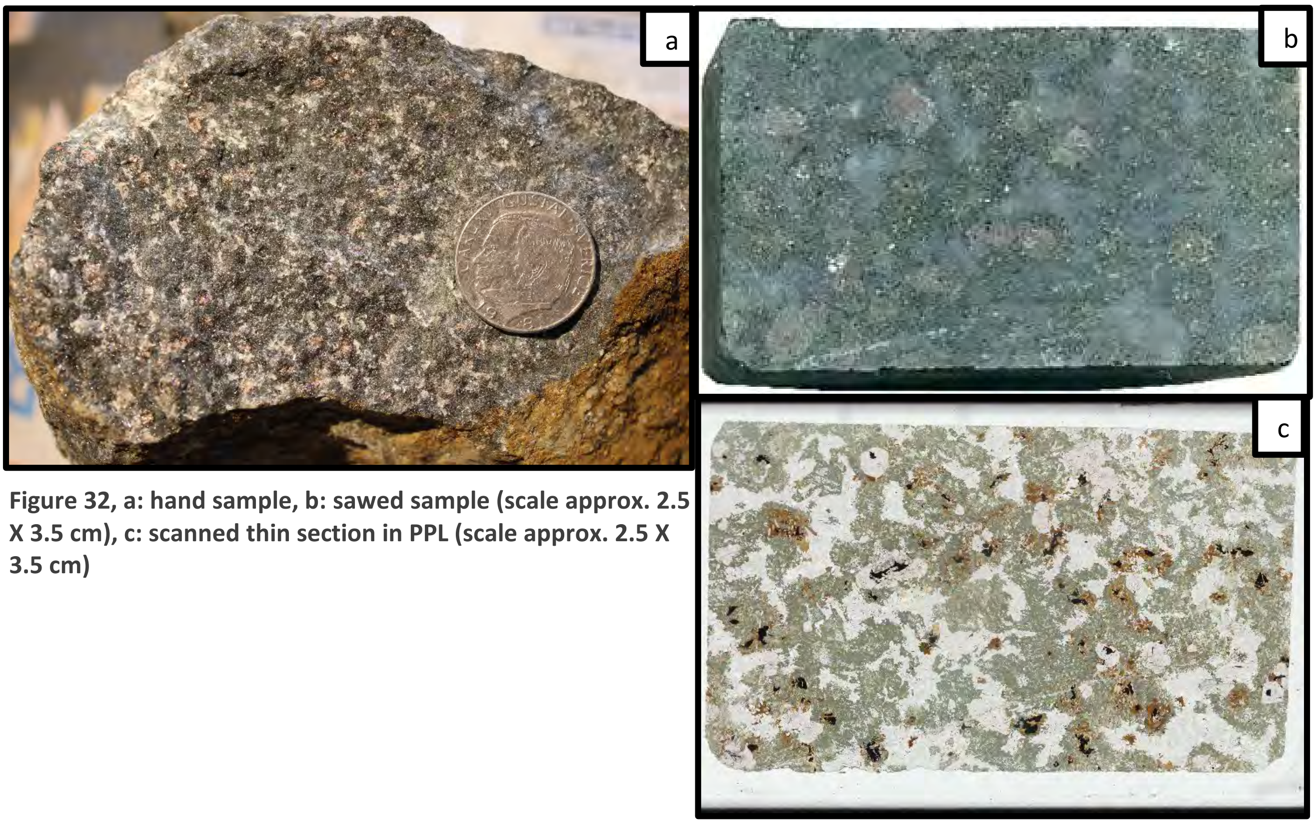

Figure 32, a: hand sample, b: sawed sample (scale approx. 2.5 X 3.5 cm), c: scanned thin section in PPL (scale approx. 2.5 X 3.5 cm)

The main minerals are hornblende, plagioclase, garnet, biotite, opaque minerals and quartz with accessory minerals calcite, apatite and titanite. There is about 45% dark phases in the sample.

The sample has a seriate texture with both interlobate and polygonal grain boundaries. The dynamic recrystallization is coarse grained with high deformation grade.

Plagioclase laths occur but are subhedral where most are badly affected at the edges by other minerals. The plagioclase has a composition of anorthite$_{30}$, concentric zoning, albite twinning and pericline twinning is common. Sericitization is fairly common. Hornblende has a green-brown colour and occur in large domains of fine to medium grained crystals. Hornblende also occur as rims around biotite, the opaque minerals and garnets where the rims have acicular crystals radiating outwards. Biotite has a brown-red colour, they occur in aggregates of acicular and anhedral crystals, often together with the opaque minerals, hornblende and garnets. Biotite is common in the sample.

Garnets are porphyroblastic and are occasionally fractured. They are fairly common to common in the sample. The opaque minerals are mostly ilmenite but small pyrite occur. Ilmenite has an anhedral habit and is found in skeleton textures. They occur together with biotite, hornblende and garnet. Calcite and titanite occur in thin crack veins as filling material.

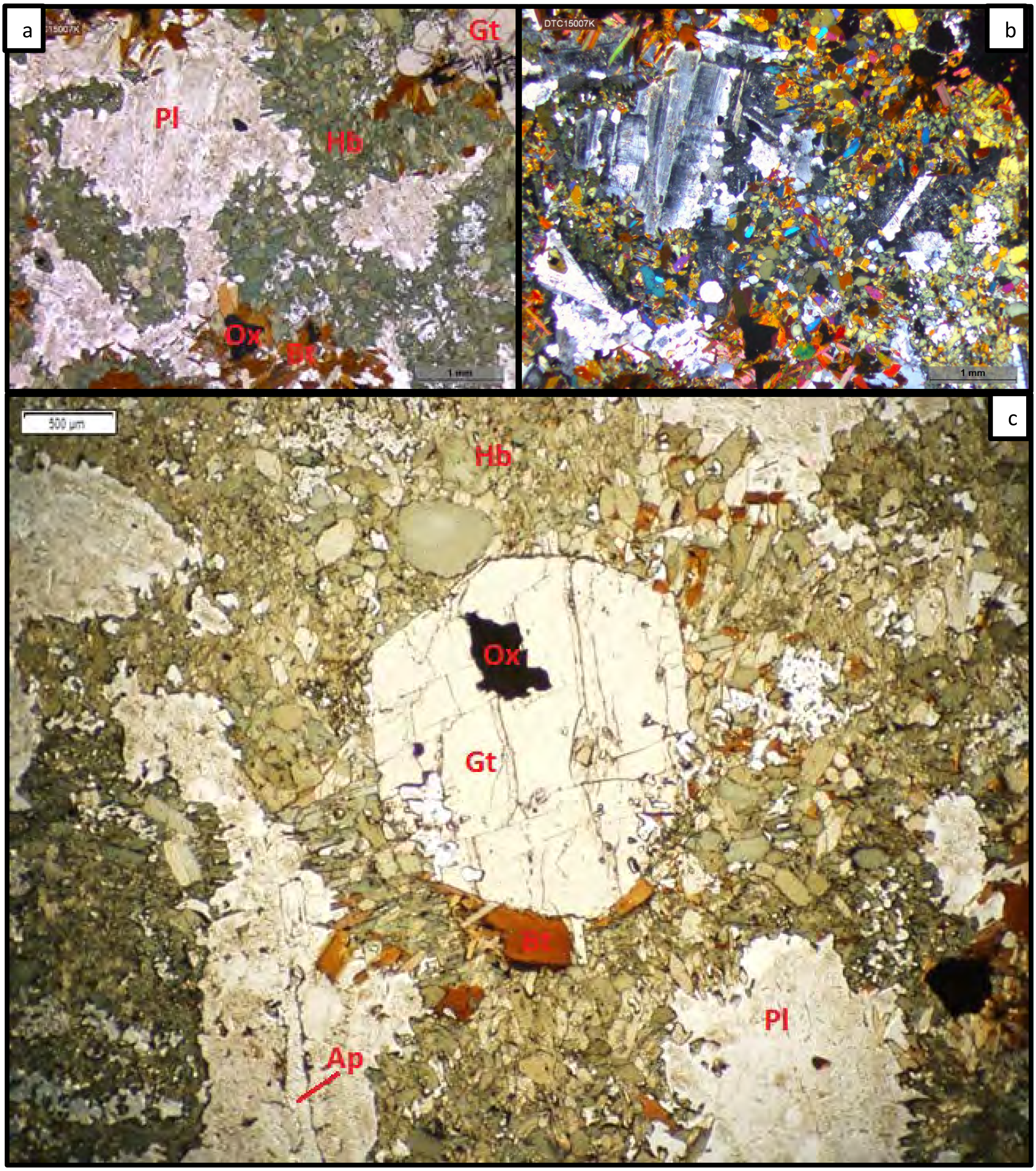

Figure 33, PPL - Pl domains surrounded by hb, ox commonly surrounded by bt, b: XPL, c: PPL – gt in apparent textural equilibrium surrounded by hb and bt

Gabbro, type I - DTC15007L

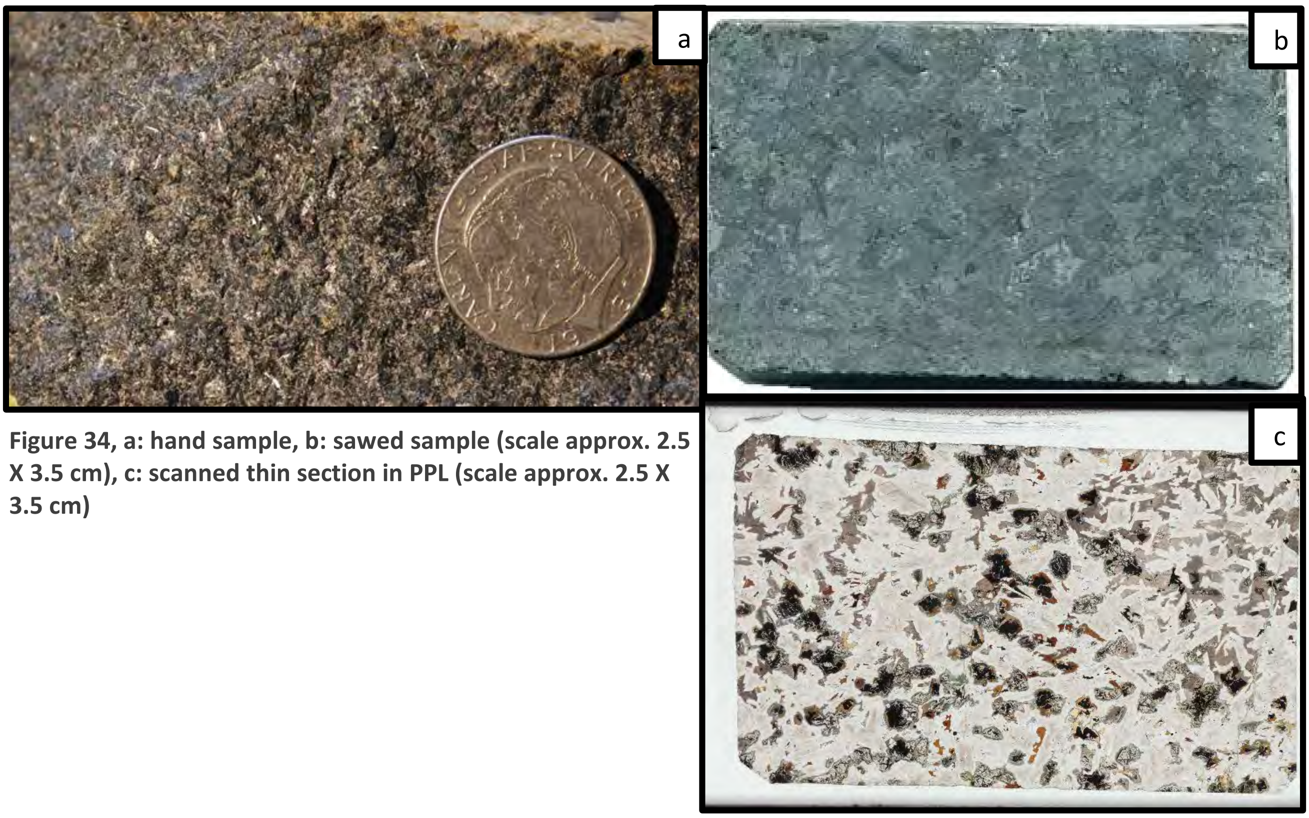

Figure 34, a: hand sample, b: sawed sample (scale approx. 2.5 X 3.5 cm), c: scanned thin section in PPL (scale approx. 2.5 X 3.5 cm)

The main minerals are plagioclase, pyroxene, olivine, opaque minerals, biotite and amphibole with accessory minerals apatite and titanite. There is about 25% dark phases in the sample.

The sample has a coronitic texture with polygonal grain boundaries. Clear magmatic texture, where olivine in contact with plagioclase has an inner rim of orthopyroxene and an outer rim of amphibole. The opaque minerals are rimmed by biotite and amphibole when in contact with plagioclase.

Well-developed plagioclase laths are common and have a composition of anorthite$_{40\text{-}50}$. Carlsbad twins, albite twins, pericline twins and concentric zoning is common. Magmatic orthopyroxenes have a brown colour with a purple tint, they are found as larger prismatic crystals where exsolution lamellae of augite along the {100} cleavage plane is common. Orthopyroxenes are common in the sample. Biotite has a brown-red colour and occur as large anhedral crystals, often as rims or in contact with the opaque minerals. Biotite is sparse to fairly common in the sample.

The opaque minerals are ilmenite, magnetite and pyrite. They occur as anhedral crystals in close contact with each other or as individual crystals.

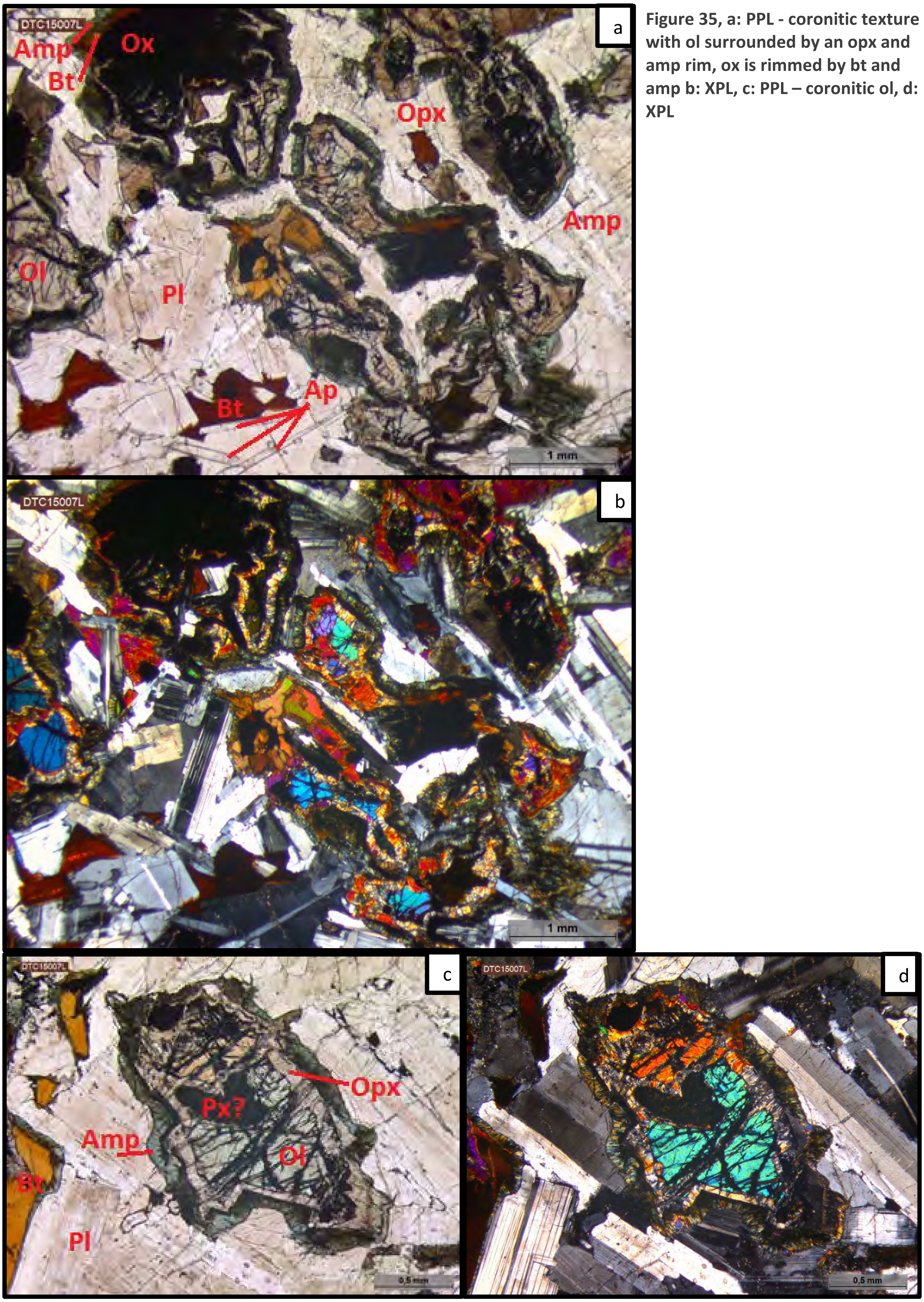

Figure 35, a: PPL - coronitic texture with ol surrounded by an opx and amp rim, ox is rimmed by bt and amp b: XPL, c: PPL – coronitic ol, d: XPL

Appendix C – SEM data

DTC15007L

Cpx-Opx Wood and Bonno (1973)

	Domain 1										
spec1	opx										
Element	Line	App. Conc	k ratio	Intensity corrn.	Weight%	Weight% sigma	Atomic%	Compound%	Formula	Number of ions	Standard
Mg	K_SERIES	8,31	0,05514	0,6879	12,09	0,04	11,37	20,04	MgO	1,14	mgo 16-Apr-2014 03:39 PM
Al	K_SERIES	0,4	0,0029	0,6783	0,59	0,02	0,5	1,12	Al2O3	0,05	al2o3 mac 16-Apr-2014 03:41 PM
Si	K_SERIES	19,78	0,14902	0,8215	24,08	0,05	19,61	51,5	SiO2	1,96	Wollastonite 16-Apr-2014 03:16 PM
Ca	K_SERIES	1,12	0,01004	0,9777	1,14	0,02	0,65	1,6	CaO	0,07	Wollastonite 16-Apr-2014 03:17 PM
Ti	K_SERIES	0,22	0,00222	0,8489	0,26	0,02	0,13	0,44	TiO2	0,01	Ti 16-Apr-2014 02:41 PM
Mn	K_SERIES	0,37	0,00371	0,8324	0,45	0,02	0,19	0,58	MnO	0,02	Mn 16-Apr-2014 02:52 PM
Fe	K_SERIES	17,35	0,15708	0,939	18,48	0,06	7,57	23,77	FeO	0,76	O5 olivine 7-May-2014 12:19 PM
O					41,96	0,07	59,99			6	
Totals					99,05						
									Cation sum	4	
spect2	cpx exsolution in opx										
Element	Line	App. Conc	k ratio	Intensity corrn.	Weight%	Weight% sigma	Atomic%	Compound%	Formula	Number of ions	Standard
Na	K_SERIES	0,23	0,00098	0,7715	0,3	0,02	0,29	0,4	Na2O	0,03	jadeite mac 16-Apr-2014 03:54 PM
Mg	K_SERIES	6,17	0,04089	0,7289	8,46	0,03	7,87	14,03	MgO	0,79	mgo 16-Apr-2014 03:39 PM
Al	K_SERIES	0,87	0,00625	0,7454	1,17	0,02	0,98	2,21	Al2O3	0,1	al2o3 mac 16-Apr-2014 03:41 PM
Si	K_SERIES	20,83	0,15696	0,8766	23,76	0,04	19,13	50,83	SiO2	1,92	Wollastonite 16-Apr-2014 03:16 PM
Ca	K_SERIES	13,91	0,12509	0,9794	14,2	0,04	8,01	19,87	CaO	0,8	Wollastonite 16-Apr-2014 03:17 PM
Ti	K_SERIES	0,36	0,00363	0,7989	0,45	0,02	0,21	0,76	TiO2	0,02	Ti 16-Apr-2014 02:41 PM
Mn	K_SERIES	0,18	0,00185	0,8105	0,23	0,02	0,09	0,29	MnO	0,01	Mn 16-Apr-2014 02:52 PM
Fe	K_SERIES	8,06	0,07294	0,9179	8,78	0,05	3,55	11,29	FeO	0,36	O5 olivine 7-May-2014 12:19 PM
O					42,33	0,07	59,85			6	
Totals					99,68						
									Cation sum	4,03	

spec1	opx	Domain 2									
Element	Line	App. Conc	k ratio	Intensity corrn.	Weight%	Weight% sigma	Atomic%	Compound%	Formula	Number of ions	Standard
Mg	K_SERIES	7,95	0,05271	0,6802	11,68	0,04	11,16	19,37	MgO	1,12	mgo 16-Apr-2014 03:39 PM
Al	K_SERIES	0,42	0,00299	0,6757	0,62	0,02	0,53	1,16	Al2O3	0,05	al2o3 mac 16-Apr-2014 03:41 PM
Si	K_SERIES	19,4	0,14622	0,819	23,7	0,05	19,6	50,69	SiO2	1,96	Wollastonite 16-Apr-2014 03:16 PM
Ca	K_SERIES	0,64	0,00577	0,9792	0,65	0,01	0,38	0,92	CaO	0,04	Wollastonite 16-Apr-2014 03:17 PM
Ti	K_SERIES	0,18	0,00175	0,8529	0,21	0,02	0,1	0,34	TiO2	0,01	Ti 16-Apr-2014 02:41 PM
Mn	K_SERIES	0,36	0,00361	0,8344	0,43	0,02	0,18	0,56	MnO	0,02	Mn 16-Apr-2014 02:52 PM
Fe	K_SERIES	18,26	0,1653	0,9411	19,4	0,06	8,07	24,96	FeO	0,81	O5 olivine 7-May-2014 12:19 PM
O					41,31	0,07	59,98			6	
Totals					98						
									Cation sum	4	

spec2	cpx										
Element	Line	App. Conc	k ratio	Intensity corrn.	Weight%	Weight% sigma	Atomic%	Compound%	Formula	Number of ions	Standard
Na	K_SERIES	0,23	0,00099	0,7772	0,3	0,02	0,3	0,4	Na2O	0,03	jadeite mac 16-Apr-2014 03:54 PM
Mg	K_SERIES	6,06	0,04022	0,7326	8,28	0,03	7,76	13,73	MgO	0,78	mgo 16-Apr-2014 03:39 PM
Al	K_SERIES	0,77	0,00554	0,7495	1,03	0,02	0,87	1,94	Al2O3	0,09	al2o3 mac 16-Apr-2014 03:41 PM
Si	K_SERIES	20,83	0,15699	0,881	23,65	0,04	19,19	50,59	SiO2	1,92	Wollastonite 16-Apr-2014 03:16 PM
Ca	K_SERIES	14,55	0,13085	0,98	14,85	0,04	8,44	20,78	CaO	0,85	Wollastonite 16-Apr-2014 03:17 PM
Sc	K_SERIES	0,17	0,00166	0,7877	0,21	0,04	0,11	0,32	Sc2O3	0,01	Sc 1-Jun-1999 12:00 AM
Ti	K_SERIES	0,33	0,00325	0,7959	0,41	0,02	0,19	0,68	TiO2	0,02	Ti 16-Apr-2014 02:41 PM
Mn	K_SERIES	0,16	0,00161	0,8089	0,2	0,02	0,08	0,26	MnO	0,01	Mn 16-Apr-2014 02:52 PM
Fe	K_SERIES	7,07	0,06401	0,9166	7,71	0,04	3,15	9,92	FeO	0,32	O5 olivine 7-May-2014 12:19 PM
I	L_SERIES	0,28	0,00284	0,7698	0,37	0,08	0,07	0		0,01	Not defined 1-Jun-1999 12:00 AM
Yb	L_SERIES	0,06	0,00039	0,9679	0,06	0,06	0,01	0,07	Yb2O3	0	YbGlass 19-Dec-2011 01:10 PM
O					42	0,08	59,83			5,99	
Totals					99,06						
									Cation sum	4,02	

spec1	opx	Domain 3									
Element	Line	App. Conc	k ratio	Intensity corrn.	Weight%	Weight% sigma	Atomic%	Compound%	Formula	Number of ions	Standard
Mg	K_SERIES	7,95	0,05271	0,6802	11,68	0,04	11,16	19,37	MgO	1,12	mgo 16-Apr-2014 03:39 PM
Al	K_SERIES	0,42	0,00299	0,6757	0,62	0,02	0,53	1,16	Al2O3	0,05	al2o3 mac 16-Apr-2014 03:41 PM
Si	K_SERIES	19,4	0,14622	0,819	23,7	0,05	19,6	50,69	SiO2	1,96	Wollastonite 16-Apr-2014 03:16 PM
Ca	K_SERIES	0,64	0,00577	0,9792	0,65	0,01	0,38	0,92	CaO	0,04	Wollastonite 16-Apr-2014 03:17 PM
Ti	K_SERIES	0,18	0,00175	0,8529	0,21	0,02	0,1	0,34	TiO2	0,01	Ti 16-Apr-2014 02:41 PM
Mn	K_SERIES	0,36	0,00361	0,8344	0,43	0,02	0,18	0,56	MnO	0,02	Mn 16-Apr-2014 02:52 PM
Fe	K_SERIES	18,26	0,1653	0,9411	19,4	0,06	8,07	24,96	FeO	0,81	O5 olivine 7-May-2014 12:19 PM
O					41,31	0,07	59,98			6	
Totals					98						
									Cation sum	4	

spec3	cpx										
Element	Line	App. Conc	k ratio	Intensity corrn.	Weight%	Weight% sigma	Atomic%	Compound%	Formula	Number of ions	Standard
Na	K_SERIES	0,22	0,00093	0,7705	0,28	0,02	0,28	0,38	Na2O	0,03	jadeite mac 16-Apr-2014 03:54 PM
Mg	K_SERIES	5,93	0,03931	0,7277	8,14	0,03	7,66	13,5	MgO	0,77	mgo 16-Apr-2014 03:39 PM
Al	K_SERIES	0,76	0,00547	0,7475	1,02	0,02	0,86	1,93	Al2O3	0,09	al2o3 mac 16-Apr-2014 03:41 PM
Si	K_SERIES	20,71	0,15603	0,8802	23,53	0,04	19,15	50,33	SiO2	1,92	Wollastonite 16-Apr-2014 03:16 PM
Ca	K_SERIES	14,43	0,1298	0,9811	14,71	0,04	8,39	20,59	CaO	0,84	Wollastonite 16-Apr-2014 03:17 PM
Sc	K_SERIES	0,17	0,0017	0,7891	0,21	0,04	0,11	0,33	Sc2O3	0,01	Sc 1-Jun-1999 12:00 AM
Ti	K_SERIES	0,33	0,0033	0,7973	0,41	0,02	0,2	0,69	TiO2	0,02	Ti 16-Apr-2014 02:41 PM
Mn	K_SERIES	0,18	0,0018	0,8096	0,22	0,02	0,09	0,29	MnO	0,01	Mn 16-Apr-2014 02:52 PM
Fe	K_SERIES	7,58	0,06864	0,9174	8,26	0,04	3,38	10,63	FeO	0,34	O5 olivine 7-May-2014 12:19 PM
I	L_SERIES	0,29	0,00288	0,7707	0,37	0,08	0,07	0		0,01	Not defined 1-Jun-1999 12:00 AM
Yb	L_SERIES	-0,02	-0,00016	0,9679	-0,02	0,06	0	-0,03	Yb2O3	0	YbGlass 19-Dec-2011 01:10 PM
O					41,86	0,08	59,81			5,99	
Totals					99,01						
									Cation sum	4,02	

cpx	spec1	Domain 4									
Element	Line	App. Conc	k ratio	Intensity corrn.	Weight%	Weight% sigma	Atomic%	Compound%	Formula	Number of ions	Standard
Na	K_SERIES	1,94	0,0083	0,753	2,57	0,03	2,6	3,46	Na2O	0,27	jadeite mac 16-Apr-2014 03:54 PM
Mg	K_SERIES	4,32	0,02866	0,6912	6,25	0,03	5,98	10,37	MgO	0,61	mgo 16-Apr-2014 03:39 PM
Al	K_SERIES	7,23	0,05192	0,7381	9,8	0,03	8,44	18,51	Al2O3	0,86	al2o3 mac 16-Apr-2014 03:41 PM
Si	K_SERIES	13,25	0,09988	0,783	16,93	0,04	14,02	36,21	SiO2	1,43	Wollastonite 16-Apr-2014 03:16 PM
Cl	K_SERIES	0,72	0,00508	1,0252	0,7	0,02	0,46	0		0,05	Tugtupite 10-Jan-2013 02:15 PM
K	K_SERIES	0,84	0,00672	1,0425	0,8	0,01	0,48	0,97	K2O	0,05	k-feldspar mac 16-Apr-2014 03:24 PM
Ca	K_SERIES	7,3	0,06568	0,9775	7,47	0,03	4,34	10,46	CaO	0,44	Wollastonite 16-Apr-2014 03:17 PM
Ti	K_SERIES	0,21	0,00206	0,8226	0,25	0,02	0,12	0,42	TiO2	0,01	Ti 16-Apr-2014 02:41 PM
Mn	K_SERIES	0,1	0,00102	0,8234	0,12	0,02	0,05	0,16	MnO	0,01	Mn 16-Apr-2014 02:52 PM
Fe	K_SERIES	11,9	0,10772	0,9309	12,78	0,05	5,32	16,44	FeO	0,54	O5 olivine 7-May-2014 12:19 PM
O					40,02	0,07	58,18			5,95	
Totals					97,7						
									Cation sum	4,23	

opx	spec1										
Element	Line	App. Conc	k ratio	Intensity corrn.	Weight%	Weight% sigma	Atomic%	Compound%	Formula	Number of ions	Standard
Mg	K_SERIES	6,92	0,04587	0,6555	10,55	0,04	10,1	17,49	MgO	1,01	mgo 16-Apr-2014 03:39 PM
Al	K_SERIES	0,26	0,00186	0,6717	0,39	0,02	0,33	0,73	Al2O3	0,03	al2o3 mac 16-Apr-2014 03:41 PM
Si	K_SERIES	19,5	0,14695	0,819	23,81	0,05	19,73	50,94	SiO2	1,97	Wollastonite 16-Apr-2014 03:16 PM
Ca	K_SERIES	0,73	0,00661	0,9842	0,75	0,01	0,43	1,04	CaO	0,04	Wollastonite 16-Apr-2014 03:17 PM
Ti	K_SERIES	0,08	0,00084	0,8585	0,1	0,01	0,05	0,16	TiO2	0	Ti 16-Apr-2014 02:41 PM
Mn	K_SERIES	0,38	0,00377	0,8377	0,45	0,02	0,19	0,58	MnO	0,02	Mn 16-Apr-2014 02:52 PM
Fe	K_SERIES	20,84	0,18868	0,9449	22,06	0,07	9,19	28,37	FeO	0,92	O5 olivine 7-May-2014 12:19 PM
O					41,23	0,07	59,97			6	
Totals					99,33						
									Cation sum	4	

Pl-Hb Holland and Blundy (1994)

spec1	Pl-core		D1								
Element	Line	App. Conc	k ratio	Intensity corrn.	Weight%	Weight% sigma	Atomic%	Compound%	Formula	Number of ions	Standard
Na	K_SERIES	3,42	0,01466	0,9086	3,76	0,03	3,49	5,07	Na2O	0,45	jadeite mac 16-Apr-2014 03:54 PM
Al	K_SERIES	13,35	0,0959	0,8945	14,93	0,04	11,8	28,21	Al2O3	1,54	al2o3 mac 16-Apr-2014 03:41 PM
Si	K_SERIES	20,62	0,1554	0,8308	24,82	0,05	18,85	53,1	SiO2	2,45	Wollastonite 16-Apr-2014 03:16 PM
K	K_SERIES	0,2	0,00161	1,0101	0,2	0,01	0,11	0,24	K2O	0,01	k-feldspar mac 16-Apr-2014 03:24 PM
Ca	K_SERIES	7,47	0,06715	0,9488	7,87	0,03	4,19	11,01	CaO	0,55	Wollastonite 16-Apr-2014 03:17 PM
Fe	K_SERIES	0,21	0,00194	0,9088	0,24	0,02	0,09	0,3	FeO	0,01	O5 olivine 7-May-2014 12:19 PM
O					46,12	0,07	61,47			8	
Totals					97,94						
									Cation sum	5,01	

10											
spec1	hb										
Element	Line	App. Conc	k ratio	Intensity corrn.	Weight%	Weight% sigma	Atomic%	Compound%	Formula	Number of ions	Standard
Na	K_SERIES	1,07	0,00459	0,7628	1,4	0,02	1,45	1,89	Na2O	0,57	jadeite mac 16-Apr-2014 03:54 PM
Mg	K_SERIES	4,09	0,02714	0,7089	5,77	0,03	5,64	9,57	MgO	2,21	mgo 16-Apr-2014 03:39 PM
Al	K_SERIES	7,53	0,05411	0,7548	9,98	0,04	8,8	18,86	Al2O3	3,44	al2o3 mac 16-Apr-2014 03:41 PM
Si	K_SERIES	13,49	0,10162	0,7906	17,06	0,04	14,44	36,49	SiO2	5,65	Wollastonite 16-Apr-2014 03:16 PM
Cl	K_SERIES	0,05	0,00037	1,0254	0,05	0,01	0,03	0		0,01	Tugtupite 10-Jan-2013 02:15 PM
K	K_SERIES	1,81	0,01452	1,0458	1,73	0,02	1,05	2,08	K2O	0,41	k-feldspar mac 16-Apr-2014 03:24 PM
Ca	K_SERIES	7,63	0,0686	0,9739	7,83	0,03	4,65	10,96	CaO	1,82	Wollastonite 16-Apr-2014 03:17 PM
Mn	K_SERIES	0,07	0,00072	0,8219	0,09	0,02	0,04	0,11	MnO	0,01	Mn 16-Apr-2014 02:52 PM
Fe	K_SERIES	11,21	0,10146	0,9294	12,06	0,05	5,13	15,51	FeO	2,01	O5 olivine 7-May-2014 12:19 PM
O					39,56	0,07	58,77			22,99	
Totals					95,53						
									Cation sum	16,11	

spec4 pl-rim D2

Element	Line	App. Conc	k ratio	Intensity corrn.	Weight%	Weight% sigma	Atomic%	Compound%	Formula	Number of ions	Standard
Na	K_SERIES	3,27	0,01403	0,9076	3,6	0,03	3,35	4,86	Na2O	0,44	jadeite mac 16-Apr-2014 03:54 PM
Al	K_SERIES	13,53	0,09715	0,8959	15,1	0,04	11,94	28,53	Al2O3	1,55	al2o3 mac 16-Apr-2014 03:41 PM
Si	K_SERIES	20,44	0,154	0,8301	24,62	0,05	18,7	52,66	SiO2	2,43	Wollastonite 16-Apr-2014 03:16 PM
K	K_SERIES	0,21	0,00171	1,0113	0,21	0,01	0,11	0,25	K2O	0,01	k-feldspar mac 16-Apr-2014 03:24 PM
Ca	K_SERIES	7,8	0,0701	0,9493	8,21	0,03	4,37	11,49	CaO	0,57	Wollastonite 16-Apr-2014 03:17 PM
Fe	K_SERIES	0,15	0,00135	0,9086	0,16	0,02	0,06	0,21	FeO	0,01	O5 olivine 7-May-2014 12:19 PM
O					46,1	0,07	61,47			8	
Totals					98,01						
									Cation sum	5,01	

spec1 hb

Element	Line	App. Conc	k ratio	Intensity corrn.	Weight%	Weight% sigma	Atomic%	Compound%	Formula	Number of ions	Standard
Na	K_SERIES	1,07	0,00459	0,7628	1,4	0,02	1,45	1,89	Na2O	0,57	jadeite mac 16-Apr-2014 03:54 PM
Mg	K_SERIES	4,09	0,02714	0,7089	5,77	0,03	5,64	9,57	MgO	2,21	mgo 16-Apr-2014 03:39 PM
Al	K_SERIES	7,53	0,05411	0,7548	9,98	0,04	8,8	18,86	Al2O3	3,44	al2o3 mac 16-Apr-2014 03:41 PM
Si	K_SERIES	13,49	0,10162	0,7906	17,06	0,04	14,44	36,49	SiO2	5,65	Wollastonite 16-Apr-2014 03:16 PM
Cl	K_SERIES	0,05	0,00037	1,0254	0,05	0,01	0,03	0		0,01	Tugtupite 10-Jan-2013 02:15 PM
K	K_SERIES	1,81	0,01452	1,0458	1,73	0,02	1,05	2,08	K2O	0,41	k-feldspar mac 16-Apr-2014 03:24 PM
Ca	K_SERIES	7,63	0,0686	0,9739	7,83	0,03	4,65	10,96	CaO	1,82	Wollastonite 16-Apr-2014 03:17 PM
Mn	K_SERIES	0,07	0,00072	0,8219	0,09	0,02	0,04	0,11	MnO	0,01	Mn 16-Apr-2014 02:52 PM
Fe	K_SERIES	11,21	0,10146	0,9294	12,06	0,05	5,13	15,51	FeO	2,01	O5 olivine 7-May-2014 12:19 PM
O					39,56	0,07	58,77			22,99	
Totals					95,53						
									Cation sum	16,11	

spec1	pl-c	D3									
Element	Line	App. Conc	k ratio	Intensity corrn.	Weight%	Weight% sigma	Atomic%	Compound%	Formula	Number of ions	Standard
Na	K_SERIES	2,59	0,01111	0,9173	2,83	0,02	2,81	3,81	Na2O	0,37	jadeite mac 16-Apr-2014 03:54 PM
Al	K_SERIES	13,29	0,09542	0,9047	14,69	0,04	12,43	27,75	Al2O3	1,62	al2o3 mac 16-Apr-2014 03:41 PM
Si	K_SERIES	18,55	0,13977	0,8291	22,37	0,05	18,2	47,86	SiO2	2,37	Wollastonite 16-Apr-2014 03:16 PM
K	K_SERIES	0,13	0,00105	1,0153	0,13	0,01	0,08	0,16	K2O	0,01	k-feldspar mac 16-Apr-2014 03:24 PM
Ca	K_SERIES	8,15	0,07326	0,9518	8,56	0,03	4,88	11,98	CaO	0,63	Wollastonite 16-Apr-2014 03:17 PM
Sc	K_SERIES	0,04	0,00044	0,7854	0,06	0,02	0,03	0,09	Sc2O3	0	Sc 1-Jun-1999 12:00 AM
Fe	K_SERIES	0,2	0,00179	0,9087	0,22	0,02	0,09	0,28	FeO	0,01	O5 olivine 7-May-2014 12:19 PM
O					43,07	0,07	61,49			8	
Totals					91,91						
									Cation sum	5,01	
spec1	hb										
Element	Line	App. Conc	k ratio	Intensity corrn.	Weight%	Weight% sigma	Atomic%	Compound%	Formula	Number of ions	Standard
Na	K_SERIES	1,07	0,00459	0,7628	1,4	0,02	1,45	1,89	Na2O	0,57	jadeite mac 16-Apr-2014 03:54 PM
Mg	K_SERIES	4,09	0,02714	0,7089	5,77	0,03	5,64	9,57	MgO	2,21	mgo 16-Apr-2014 03:39 PM
Al	K_SERIES	7,53	0,05411	0,7548	9,98	0,04	8,8	18,86	Al2O3	3,44	al2o3 mac 16-Apr-2014 03:41 PM
Si	K_SERIES	13,49	0,10162	0,7906	17,06	0,04	14,44	36,49	SiO2	5,65	Wollastonite 16-Apr-2014 03:16 PM
Cl	K_SERIES	0,05	0,00037	1,0254	0,05	0,01	0,03	0		0,01	Tugtupite 10-Jan-2013 02:15 PM
K	K_SERIES	1,81	0,01452	1,0458	1,73	0,02	1,05	2,08	K2O	0,41	k-feldspar mac 16-Apr-2014 03:24 PM
Ca	K_SERIES	7,63	0,0686	0,9739	7,83	0,03	4,65	10,96	CaO	1,82	Wollastonite 16-Apr-2014 03:17 PM
Mn	K_SERIES	0,07	0,00072	0,8219	0,09	0,02	0,04	0,11	MnO	0,01	Mn 16-Apr-2014 02:52 PM
Fe	K_SERIES	11,21	0,10146	0,9294	12,06	0,05	5,13	15,51	FeO	2,01	O5 olivine 7-May-2014 12:19 PM
O					39,56	0,07	58,77			22,99	
Totals					95,53						
									Cation sum	16,11	

spec2 pl-r D4

Element	Line	App. Conc	k ratio	Intensity corrn.	Weight%	Weight% sigma	Atomic%	Compound%	Formula	Number of ions	Standard
Na	K_SERIES	4,5	0,0193	0,9411	4,78	0,03	4,64	6,45	Na2O	0,6	jadeite mac 16-Apr-2014 03:54 PM
Al	K_SERIES	11,41	0,08195	0,8924	12,79	0,03	10,56	24,16	Al2O3	1,37	al2o3 mac 16-Apr-2014 03:41 PM
Si	K_SERIES	21,4	0,16129	0,8429	25,39	0,05	20,14	54,32	SiO2	2,62	Wollastonite 16-Apr-2014 03:16 PM
K	K_SERIES	0,15	0,0012	1,0013	0,15	0,01	0,08	0,18	K2O	0,01	k-feldspar mac 16-Apr-2014 03:24 PM
Ca	K_SERIES	4,97	0,0447	0,9448	5,26	0,03	2,92	7,36	CaO	0,38	Wollastonite 16-Apr-2014 03:17 PM
Ti	K_SERIES	0,04	0,00041	0,7953	0,05	0,01	0,02	0,09	TiO2	0	Ti 16-Apr-2014 02:41 PM
Fe	K_SERIES	0,1	0,00092	0,9097	0,11	0,02	0,04	0,14	FeO	0,01	O5 olivine 7-May-2014 12:19 PM
Sn	L_SERIES	0,12	0,00118	0,7364	0,16	0,05	0,03	0,2	SnO2	0	Sn 1-Jun-1999 12:00 AM
O					44,21	0,07	61,56			8	
Totals					92,9						
									Cation sum	5	

spec1 hb

Element	Line	App. Conc	k ratio	Intensity corrn.	Weight%	Weight% sigma	Atomic%	Compound%	Formula	Number of ions	Standard
Na	K_SERIES	1,07	0,00459	0,7628	1,4	0,02	1,45	1,89	Na2O	0,57	jadeite mac 16-Apr-2014 03:54 PM
Mg	K_SERIES	4,09	0,02714	0,7089	5,77	0,03	5,64	9,57	MgO	2,21	mgo 16-Apr-2014 03:39 PM
Al	K_SERIES	7,53	0,05411	0,7548	9,98	0,04	8,8	18,86	Al2O3	3,44	al2o3 mac 16-Apr-2014 03:41 PM
Si	K_SERIES	13,49	0,10162	0,7906	17,06	0,04	14,44	36,49	SiO2	5,65	Wollastonite 16-Apr-2014 03:16 PM
Cl	K_SERIES	0,05	0,00037	1,0254	0,05	0,01	0,03	0		0,01	Tugtupite 10-Jan-2013 02:15 PM
K	K_SERIES	1,81	0,01452	1,0458	1,73	0,02	1,05	2,08	K2O	0,41	k-feldspar mac 16-Apr-2014 03:24 PM
Ca	K_SERIES	7,63	0,0686	0,9739	7,83	0,03	4,65	10,96	CaO	1,82	Wollastonite 16-Apr-2014 03:17 PM
Mn	K_SERIES	0,07	0,00072	0,8219	0,09	0,02	0,04	0,11	MnO	0,01	Mn 16-Apr-2014 02:52 PM
Fe	K_SERIES	11,21	0,10146	0,9294	12,06	0,05	5,13	15,51	FeO	2,01	O5 olivine 7-May-2014 12:19 PM
O					39,56	0,07	58,77			22,99	
Totals					95,53						
									Cation sum	16,11	

DTC15007I

	Domain 1										
spec1	gt-rim										
Element	Line	App. Conc	k ratio	Intensity corrn.	Weight%	Weight% sigma	Atomic%	Compound%	Formula	Number of ions	Standard
Mg	K_SERIES	1,3	0,00864	0,6419	2,03	0,02	1,97	3,37	MgO	0,39	mgo 16-Apr-2014 03:39 PM
Al	K_SERIES	8,41	0,06039	0,745	11,29	0,04	9,86	21,33	Al2O3	1,98	al2o3 mac 16-Apr-2014 03:41 PM
Si	K_SERIES	13,79	0,10389	0,7811	17,65	0,04	14,82	37,77	SiO2	2,97	Wollastonite 16-Apr-2014 03:16 PM
Ca	K_SERIES	6,13	0,05512	0,9985	6,14	0,03	3,61	8,59	CaO	0,72	Wollastonite 16-Apr-2014 03:17 PM
Mn	K_SERIES	1,5	0,01501	0,8385	1,79	0,03	0,77	2,31	MnO	0,15	Mn 16-Apr-2014 02:52 PM
Fe	K_SERIES	20,33	0,18408	0,9471	21,47	0,07	9,06	27,62	FeO	1,82	O5 olivine 7-May-2014 12:19 PM
Co	K_SERIES	0,05	0,00054	0,839	0,06	0,03	0,03	0,08	CoO	0,01	Co metal uncoated 16-Apr-2014 02:16 PM
O					40,63	0,08	59,88			12	
Totals					101,06						
									Cation sum	8,04	

spec4	gt-core										
Element	Line	App. Conc	k ratio	Intensity corrn.	Weight%	Weight% sigma	Atomic%	Compound%	Formula	Number of ions	Standard
Mg	K_SERIES	1,31	0,00869	0,6369	2,06	0,02	2	3,41	MgO	0,4	mgo 16-Apr-2014 03:39 PM
Al	K_SERIES	8,3	0,05964	0,7402	11,22	0,04	9,82	21,2	Al2O3	1,97	al2o3 mac 16-Apr-2014 03:41 PM
Si	K_SERIES	13,68	0,10311	0,7787	17,57	0,04	14,78	37,59	SiO2	2,96	Wollastonite 16-Apr-2014 03:16 PM
Ca	K_SERIES	5,5	0,04949	0,9999	5,5	0,03	3,24	7,7	CaO	0,65	Wollastonite 16-Apr-2014 03:17 PM
Mn	K_SERIES	1,66	0,0166	0,8403	1,97	0,03	0,85	2,55	MnO	0,17	Mn 16-Apr-2014 02:52 PM
Fe	K_SERIES	21,01	0,19023	0,949	22,14	0,07	9,37	28,48	FeO	1,88	O5 olivine 7-May-2014 12:19 PM
Co	K_SERIES	0,06	0,00059	0,8405	0,07	0,03	0,03	0,09	CoO	0,01	Co metal uncoated 16-Apr-2014 02:16 PM
Sb	L_SERIES	0,19	0,00193	0,7802	0,25	0,07	0,05	0,3	Sb2O3	0,01	Sb 1-Jun-1999 12:00 AM
O					40,53	0,08	59,86			12	
Totals					101,32						
									Cation sum	8,05	

spec1	bt-c										
Element	Line	App. Conc	k ratio	Intensity corrn.	Weight%	Weight% sigma	Atomic%	Compound%	Formula	Number of ions	Standard
Na	K_SERIES	0,11	0,00049	0,7148	0,16	0,02	0,17	0,22	Na2O	0,03	jadeite mac 16-Apr-2014 03:54 PM
Mg	K_SERIES	4,61	0,03057	0,6893	6,69	0,03	6,69	11,09	MgO	1,26	mgo 16-Apr-2014 03:39 PM
Al	K_SERIES	5,59	0,04016	0,7327	7,63	0,04	6,88	14,42	Al2O3	1,29	al2o3 mac 16-Apr-2014 03:41 PM
Si	K_SERIES	13,51	0,10178	0,8004	16,88	0,04	14,62	36,1	SiO2	2,74	Wollastonite 16-Apr-2014 03:16 PM
Cl	K_SERIES	0,35	0,0025	1,0397	0,34	0,01	0,23	0		0,04	Tugtupite 10-Jan-2013 02:15 PM
K	K_SERIES	8,18	0,06568	1,0477	7,8	0,03	4,86	9,4	K2O	0,91	k-feldspar mac 16-Apr-2014 03:24 PM
Ti	K_SERIES	2,43	0,02432	0,8372	2,9	0,02	1,48	4,85	TiO2	0,28	Ti 16-Apr-2014 02:41 PM
Fe	K_SERIES	14,39	0,13023	0,9375	15,34	0,06	6,68	19,74	FeO	1,25	O5 olivine 7-May-2014 12:19 PM
Yb	L_SERIES	0,02	0,00013	0,9753	0,02	0,06	0	0,02	Yb2O3	0	YbGlass 19-Dec-2011 01:10 PM
O					38,41	0,08	58,39			10,96	
Totals					96,17						
									Cation sum	7,76	

spec2	bt-r										
Element	Line	App. Conc	k ratio	Intensity corrn.	Weight%	Weight% sigma	Atomic%	Compound%	Formula	Number of ions	Standard
Na	K_SERIES	0,13	0,00054	0,7098	0,18	0,02	0,19	0,24	Na2O	0,04	jadeite mac 16-Apr-2014 03:54 PM
Mg	K_SERIES	4,42	0,02933	0,6851	6,46	0,03	6,62	10,7	MgO	1,24	mgo 16-Apr-2014 03:39 PM
Al	K_SERIES	5,66	0,04066	0,7304	7,75	0,03	7,16	14,65	Al2O3	1,35	al2o3 mac 16-Apr-2014 03:41 PM
Si	K_SERIES	12,94	0,09753	0,796	16,26	0,04	14,43	34,79	SiO2	2,71	Wollastonite 16-Apr-2014 03:16 PM
Cl	K_SERIES	0,39	0,00276	1,0393	0,37	0,01	0,26	0		0,05	Tugtupite 10-Jan-2013 02:15 PM
K	K_SERIES	7,82	0,0628	1,0475	7,46	0,03	4,76	8,99	K2O	0,89	k-feldspar mac 16-Apr-2014 03:24 PM
Ti	K_SERIES	2,03	0,02029	0,8388	2,42	0,02	1,26	4,03	TiO2	0,24	Ti 16-Apr-2014 02:41 PM
Mn	K_SERIES	0,1	0,00105	0,8302	0,13	0,02	0,06	0,16	MnO	0,01	Mn 16-Apr-2014 02:52 PM
Fe	K_SERIES	14,71	0,1332	0,9389	15,67	0,06	6,99	20,16	FeO	1,31	O5 olivine 7-May-2014 12:19 PM
O					37,4	0,07	58,27			10,95	
Totals					94,1						
									Cation sum	7,79	

spec1 pl-core

Element	Line	App. Conc	k ratio	Intensity corrn.	Weight%	Weight% sigma	Atomic%	Compound%	Formula	Number of ions	Standard
Na	K_SERIES	5,6	0,024	0,9379	5,97	0,03	5,41	8,05	Na2O	0,7	jadeite mac 16-Apr-2014 03:54 PM
Al	K_SERIES	11,31	0,08122	0,8832	12,8	0,04	9,88	24,19	Al2O3	1,28	al2o3 mac 16-Apr-2014 03:41 PM
Si	K_SERIES	23,8	0,17931	0,8454	28,14	0,05	20,86	60,21	SiO2	2,71	Wollastonite 16-Apr-2014 03:16 PM
K	K_SERIES	0,09	0,00073	0,9953	0,09	0,01	0,05	0,11	K2O	0,01	k-feldspar mac 16-Apr-2014 03:24 PM
Ca	K_SERIES	4,02	0,03616	0,9416	4,27	0,02	2,22	5,98	CaO	0,29	Wollastonite 16-Apr-2014 03:17 PM
Fe	K_SERIES	0,12	0,00112	0,9097	0,14	0,02	0,05	0,17	FeO	0,01	O5 olivine 7-May-2014 12:19 PM
O					47,29	0,07	61,54			8	
Totals					98,71						
									Cation sum	5	

spec2 pl-rim

Element	Line	App. Conc	k ratio	Intensity corrn.	Weight%	Weight% sigma	Atomic%	Compound%	Formula	Number of ions	Standard
Na	K_SERIES	5,09	0,02181	0,9309	5,46	0,03	4,94	7,37	Na2O	0,64	jadeite mac 16-Apr-2014 03:54 PM
Al	K_SERIES	11,86	0,08521	0,8859	13,39	0,04	10,32	25,3	Al2O3	1,34	al2o3 mac 16-Apr-2014 03:41 PM
Si	K_SERIES	23,22	0,175	0,842	27,58	0,05	20,42	59	SiO2	2,65	Wollastonite 16-Apr-2014 03:16 PM
K	K_SERIES	0,07	0,00053	0,9985	0,07	0,01	0,04	0,08	K2O	0	k-feldspar mac 16-Apr-2014 03:24 PM
Ca	K_SERIES	4,82	0,04334	0,9434	5,11	0,02	2,65	7,15	CaO	0,34	Wollastonite 16-Apr-2014 03:17 PM
Fe	K_SERIES	0,2	0,00177	0,9096	0,22	0,02	0,08	0,28	FeO	0,01	O5 olivine 7-May-2014 12:19 PM
O					47,35	0,07	61,55			8	
Totals					99,18						
									Cation sum	5	

spec1 hb-core

Element	Line	App. Conc	k ratio	Intensity corrn.	Weight%	Weight% sigma	Atomic%	Compound%	Formula	Number of ions	Standard
Na	K_SERIES	0,89	0,00382	0,7236	1,23	0,02	1,26	1,66	Na2O	0,49	jadeite mac 16-Apr-2014 03:54 PM
Mg	K_SERIES	3,55	0,02354	0,6844	5,19	0,03	5,02	8,6	MgO	1,94	mgo 16-Apr-2014 03:39 PM
Al	K_SERIES	5,55	0,03983	0,7457	7,44	0,03	6,48	14,05	Al2O3	2,51	al2o3 mac 16-Apr-2014 03:41 PM
Si	K_SERIES	15,54	0,11708	0,8127	19,12	0,04	16,01	40,9	SiO2	6,19	Wollastonite 16-Apr-2014 03:16 PM
Cl	K_SERIES	0,45	0,00317	1,0293	0,43	0,01	0,29	0		0,11	Tugtupite 10-Jan-2013 02:15 PM
K	K_SERIES	0,99	0,00795	1,0485	0,94	0,01	0,57	1,14	K2O	0,22	k-feldspar mac 16-Apr-2014 03:24 PM

Ca	K_SERIES	8,07	0,07255	0,9813	8,22	0,03	4,82	11,5	CaO	1,86	Wollastonite 16-Apr-2014 03:17 PM
Sc	K_SERIES	0,06	0,00064	0,8159	0,08	0,02	0,04	0,12	Sc2O3	0,02	Sc 1-Jun-1999 12:00 AM
Ti	K_SERIES	0,56	0,0056	0,823	0,68	0,02	0,33	1,13	TiO2	0,13	Ti 16-Apr-2014 02:41 PM
Mn	K_SERIES	0,13	0,00128	0,8235	0,16	0,02	0,07	0,2	MnO	0,03	Mn 16-Apr-2014 02:52 PM
Fe	K_SERIES	13,1	0,11856	0,9314	14,06	0,06	5,92	18,09	FeO	2,29	O5 olivine 7-May-2014 12:19 PM
O					40,28	0,07	59,2			22,89	
Totals					97,83						
									Cation sum	15,66	

spec2 hb-rim

Element	Line	App. Conc	k ratio	Intensity corrn.	Weight%	Weight% sigma	Atomic%	Compound%	Formula	Number of ions	Standard
Na	K_SERIES	0,8	0,00341	0,7139	1,11	0,02	1,15	1,5	Na2O	0,44	jadeite mac 16-Apr-2014 03:54 PM
Mg	K_SERIES	3,38	0,02241	0,6781	4,98	0,03	4,84	8,26	MgO	1,87	mgo 16-Apr-2014 03:39 PM
Al	K_SERIES	5,25	0,0377	0,7431	7,07	0,03	6,19	13,35	Al2O3	2,39	al2o3 mac 16-Apr-2014 03:41 PM
Si	K_SERIES	15,68	0,11814	0,8146	19,25	0,04	16,2	41,17	SiO2	6,26	Wollastonite 16-Apr-2014 03:16 PM
Cl	K_SERIES	0,48	0,00344	1,0302	0,47	0,01	0,31	0		0,12	Tugtupite 10-Jan-2013 02:15 PM
K	K_SERIES	0,88	0,00706	1,0496	0,84	0,01	0,51	1,01	K2O	0,2	k-feldspar mac 16-Apr-2014 03:24 PM
Ca	K_SERIES	8,18	0,07353	0,9828	8,32	0,03	4,91	11,64	CaO	1,9	Wollastonite 16-Apr-2014 03:17 PM
Ti	K_SERIES	0,46	0,00462	0,8249	0,56	0,02	0,28	0,93	TiO2	0,11	Ti 16-Apr-2014 02:41 PM
Mn	K_SERIES	0,11	0,00113	0,8247	0,14	0,02	0,06	0,18	MnO	0,02	Mn 16-Apr-2014 02:52 PM
Fe	K_SERIES	14	0,12673	0,9328	15,01	0,06	6,35	19,31	FeO	2,45	O5 olivine 7-May-2014 12:19 PM
O					40,08	0,07	59,21			22,88	
Totals					97,82						
									Cation sum	15,64	

Domain 2

spec1	gt										
Element	Line	App. Conc	k ratio	Intensity corrn.	Weight%	Weight% sigma	Atomic%	Compound%	Formula	Number of ions	Standard
Mg	K_SERIES	1,19	0,0079	0,6401	1,86	0,02	1,81	3,09	MgO	0,36	mgo 16-Apr-2014 03:39 PM
Al	K_SERIES	8,38	0,0602	0,7451	11,25	0,04	9,86	21,25	Al2O3	1,98	al2o3 mac 16-Apr-2014 03:41 PM
Si	K_SERIES	13,75	0,10361	0,7816	17,59	0,04	14,81	37,64	SiO2	2,97	Wollastonite 16-Apr-2014 03:16 PM
Ca	K_SERIES	6,21	0,05588	0,9992	6,22	0,03	3,67	8,7	CaO	0,74	Wollastonite 16-Apr-2014 03:17 PM
Mn	K_SERIES	1,67	0,01668	0,839	1,99	0,03	0,86	2,57	MnO	0,17	Mn 16-Apr-2014 02:52 PM
Fe	K_SERIES	20,33	0,18403	0,9475	21,45	0,07	9,08	27,6	FeO	1,82	O5 olivine 7-May-2014 12:19 PM
Co	K_SERIES	0,09	0,00092	0,8391	0,11	0,03	0,04	0,14	CoO	0,01	Co metal uncoated 16-Apr-2014 02:16 PM
O					40,51	0,08	59,87			12	
Totals					100,98						
									Cation sum	8,04	

spec1	hb										
Element	Line	App. Conc	k ratio	Intensity corrn.	Weight%	Weight% sigma	Atomic%	Compound%	Formula	Number of ions	Standard
Na	K_SERIES	0,89	0,00383	0,7298	1,22	0,02	1,24	1,65	Na2O	0,48	jadeite mac 16-Apr-2014 03:54 PM
Mg	K_SERIES	3,73	0,02475	0,6893	5,42	0,03	5,21	8,98	MgO	2,01	mgo 16-Apr-2014 03:39 PM
Al	K_SERIES	5,56	0,03997	0,7472	7,45	0,03	6,45	14,07	Al2O3	2,49	al2o3 mac 16-Apr-2014 03:41 PM
Si	K_SERIES	15,72	0,11844	0,8136	19,32	0,04	16,07	41,33	SiO2	6,21	Wollastonite 16-Apr-2014 03:16 PM
Cl	K_SERIES	0,45	0,0032	1,0282	0,44	0,01	0,29	0		0,11	Tugtupite 10-Jan-2013 02:15 PM
K	K_SERIES	1,01	0,0081	1,0474	0,96	0,01	0,58	1,16	K2O	0,22	k-feldspar mac 16-Apr-2014 03:24 PM
Ca	K_SERIES	8,17	0,07349	0,9798	8,34	0,03	4,86	11,67	CaO	1,88	Wollastonite 16-Apr-2014 03:17 PM
Ti	K_SERIES	0,6	0,00598	0,8216	0,73	0,02	0,36	1,21	TiO2	0,14	Ti 16-Apr-2014 02:41 PM
Mn	K_SERIES	0,12	0,00117	0,8225	0,14	0,02	0,06	0,18	MnO	0,02	Mn 16-Apr-2014 02:52 PM
Fe	K_SERIES	12,57	0,11378	0,9303	13,51	0,05	5,65	17,38	FeO	2,18	O5 olivine 7-May-2014 12:19 PM
O					40,55	0,07	59,23			22,89	
Totals					98,08						
									Cation sum	15,64	

spec2	bt										
Element	Line	App. Conc	k ratio	Intensity corrn.	Weight%	Weight% sigma	Atomic%	Compound%	Formula	Number of ions	Standard
Na	K_SERIES	0,08	0,00033	0,7201	0,11	0,02	0,11	0,15	Na2O	0,02	jadeite mac 16-Apr-2014 03:54 PM
Mg	K_SERIES	4,94	0,03277	0,694	7,12	0,03	7,14	11,8	MgO	1,34	mgo 16-Apr-2014 03:39 PM
Al	K_SERIES	5,86	0,0421	0,7306	8,02	0,03	7,26	15,16	Al2O3	1,36	al2o3 mac 16-Apr-2014 03:41 PM
Si	K_SERIES	13,21	0,09955	0,794	16,64	0,04	14,45	35,6	SiO2	2,71	Wollastonite 16-Apr-2014 03:16 PM
Cl	K_SERIES	0,37	0,00263	1,0358	0,36	0,01	0,25	0		0,05	Tugtupite 10-Jan-2013 02:15 PM
K	K_SERIES	7,51	0,0603	1,0448	7,19	0,03	4,48	8,66	K2O	0,84	k-feldspar mac 16-Apr-2014 03:24 PM
Ti	K_SERIES	2,12	0,02124	0,8373	2,54	0,02	1,29	4,23	TiO2	0,24	Ti 16-Apr-2014 02:41 PM
Mn	K_SERIES	0,05	0,00052	0,8288	0,06	0,02	0,03	0,08	MnO	0,01	Mn 16-Apr-2014 02:52 PM
Fe	K_SERIES	14,09	0,12755	0,9372	15,03	0,06	6,57	19,34	FeO	1,23	O5 olivine 7-May-2014 12:19 PM
O					38,3	0,07	58,41			10,95	
Totals					95,37						
									Cation sum	7,75	

spec3	pl										
Element	Line	App. Conc	k ratio	Intensity corrn.	Weight%	Weight% sigma	Atomic%	Compound%	Formula	Number of ions	Standard
Na	K_SERIES	5,13	0,02199	0,9318	5,51	0,03	4,96	7,42	Na2O	0,64	jadeite mac 16-Apr-2014 03:54 PM
Al	K_SERIES	11,78	0,08463	0,8861	13,3	0,04	10,22	25,13	Al2O3	1,33	al2o3 mac 16-Apr-2014 03:41 PM
Si	K_SERIES	23,46	0,1768	0,8434	27,82	0,05	20,53	59,51	SiO2	2,67	Wollastonite 16-Apr-2014 03:16 PM
K	K_SERIES	0,07	0,00054	0,9981	0,07	0,01	0,04	0,08	K2O	0	k-feldspar mac 16-Apr-2014 03:24 PM
Ca	K_SERIES	4,77	0,04288	0,9431	5,06	0,02	2,61	7,07	CaO	0,34	Wollastonite 16-Apr-2014 03:17 PM
Fe	K_SERIES	0,16	0,00144	0,9095	0,18	0,02	0,07	0,23	FeO	0,01	O5 olivine 7-May-2014 12:19 PM
O					47,52	0,07	61,57			8	
Totals					99,44						
									Cation sum	4,99	

Domain 3

spec1 gt

Element	Line	App. Conc	k ratio	Intensity corrn.	Weight%	Weight% sigma	Atomic%	Compound%	Formula	Number of ions	Standard
Mg	K_SERIES	1,37	0,00911	0,6373	2,15	0,02	2,1	3,57	MgO	0,42	mgo 16-Apr-2014 03:39 PM
Al	K_SERIES	8,28	0,05947	0,7395	11,2	0,04	9,84	21,16	Al2O3	1,97	al2o3 mac 16-Apr-2014 03:41 PM
Si	K_SERIES	13,69	0,10317	0,7775	17,61	0,04	14,87	37,67	SiO2	2,98	Wollastonite 16-Apr-2014 03:16 PM
Ca	K_SERIES	5,02	0,04516	0,999	5,03	0,02	2,97	7,03	CaO	0,6	Wollastonite 16-Apr-2014 03:17 PM
Mn	K_SERIES	1,59	0,01593	0,8405	1,9	0,03	0,82	2,45	MnO	0,16	Mn 16-Apr-2014 02:52 PM
Fe	K_SERIES	21,26	0,19244	0,9493	22,39	0,07	9,51	28,81	FeO	1,9	O5 olivine 7-May-2014 12:19 PM
O					40,41	0,07	59,89			12	
Totals					100,69						
									Cation sum	8,04	

spec2 hb

Element	Line	App. Conc	k ratio	Intensity corrn.	Weight%	Weight% sigma	Atomic%	Compound%	Formula	Number of ions	Standard
Na	K_SERIES	0,83	0,00356	0,7238	1,15	0,02	1,16	1,55	Na2O	0,45	jadeite mac 16-Apr-2014 03:54 PM
Mg	K_SERIES	3,73	0,02472	0,6855	5,44	0,03	5,2	9,02	MgO	2,01	mgo 16-Apr-2014 03:39 PM
Al	K_SERIES	5,28	0,03793	0,7445	7,09	0,03	6,11	13,4	Al2O3	2,36	al2o3 mac 16-Apr-2014 03:41 PM
Si	K_SERIES	16,12	0,12148	0,8158	19,76	0,04	16,35	42,28	SiO2	6,31	Wollastonite 16-Apr-2014 03:16 PM
Cl	K_SERIES	0,43	0,00307	1,0278	0,42	0,01	0,28	0		0,11	Tugtupite 10-Jan-2013 02:15 PM
K	K_SERIES	0,87	0,00702	1,0475	0,83	0,01	0,5	1,01	K2O	0,19	k-feldspar mac 16-Apr-2014 03:24 PM
Ca	K_SERIES	8,26	0,07432	0,9808	8,43	0,03	4,88	11,79	CaO	1,89	Wollastonite 16-Apr-2014 03:17 PM
Ti	K_SERIES	0,45	0,00449	0,8227	0,55	0,02	0,26	0,91	TiO2	0,1	Ti 16-Apr-2014 02:41 PM
Mn	K_SERIES	0,12	0,00123	0,8233	0,15	0,02	0,06	0,19	MnO	0,02	Mn 16-Apr-2014 02:52 PM
Fe	K_SERIES	13,26	0,12003	0,9311	14,24	0,06	5,92	18,32	FeO	2,29	O5 olivine 7-May-2014 12:19 PM
O					40,82	0,07	59,28			22,89	
Totals					98,88						
									Cation sum	15,62	

spec4 bt

Element	Line	App. Conc	k ratio	Intensity corrn.	Weight%	Weight% sigma	Atomic%	Compound%	Formula	Number of ions	Standard
Na	K_SERIES	0,1	0,00041	0,7231	0,13	0,02	0,14	0,18	Na2O	0,03	jadeite mac 16-Apr-2014 03:54 PM
Mg	K_SERIES	4,91	0,03257	0,6962	7,05	0,03	6,99	11,69	MgO	1,31	mgo 16-Apr-2014 03:39 PM
Al	K_SERIES	5,84	0,04197	0,7341	7,96	0,03	7,11	15,04	Al2O3	1,33	al2o3 mac 16-Apr-2014 03:41 PM
Si	K_SERIES	13,59	0,10242	0,7984	17,02	0,04	14,6	36,42	SiO2	2,74	Wollastonite 16-Apr-2014 03:16 PM
Cl	K_SERIES	0,42	0,00295	1,0372	0,4	0,01	0,27	0		0,05	Tugtupite 10-Jan-2013 02:15 PM
K	K_SERIES	8,17	0,06563	1,045	7,82	0,03	4,82	9,42	K2O	0,9	k-feldspar mac 16-Apr-2014 03:24 PM
Ti	K_SERIES	2,17	0,02175	0,8353	2,6	0,02	1,31	4,34	TiO2	0,25	Ti 16-Apr-2014 02:41 PM
Fe	K_SERIES	13,92	0,12599	0,9364	14,86	0,06	6,41	19,12	FeO	1,2	O5 olivine 7-May-2014 12:19 PM
O					38,76	0,07	58,36			10,95	
Totals					96,62						
									Cation sum	7,76	

25

spec1 pl

Element	Line	App. Conc	k ratio	Intensity corrn.	Weight%	Weight% sigma	Atomic%	Compound%	Formula	Number of ions	Standard
Na	K_SERIES	5,68	0,02435	0,9359	6,07	0,03	5,42	8,18	Na2O	0,71	jadeite mac 16-Apr-2014 03:54 PM
Al	K_SERIES	11,38	0,08173	0,8819	12,9	0,04	9,83	24,38	Al2O3	1,28	al2o3 mac 16-Apr-2014 03:41 PM
Si	K_SERIES	24,14	0,18192	0,8457	28,55	0,05	20,88	61,07	SiO2	2,71	Wollastonite 16-Apr-2014 03:16 PM
K	K_SERIES	0,12	0,00099	0,9957	0,12	0,01	0,06	0,15	K2O	0,01	k-feldspar mac 16-Apr-2014 03:24 PM
Ca	K_SERIES	4,02	0,03617	0,942	4,27	0,03	2,19	5,97	CaO	0,28	Wollastonite 16-Apr-2014 03:17 PM
Fe	K_SERIES	0,14	0,00126	0,91	0,15	0,02	0,06	0,2	FeO	0,01	O5 olivine 7-May-2014 12:19 PM
Sb	L_SERIES	0,14	0,00138	0,7355	0,19	0,06	0,03	0,22	Sb2O3	0	Sb 1-Jun-1999 12:00 AM
O					47,92	0,07	61,53			8	
Totals					100,17						
									Cation sum	5	

DTC15002D

Domain
1

spec1 gt-rim

Element	Line	App. Conc	k ratio	Intensity corrn.	Weight%	Weight% sigma	Atomic%	Compound%	Formula	Number of ions	Standard
Mg	K_SERIES	1,8	0,01196	0,6431	2,8	0,02	2,72	4,65	MgO	0,54	mgo 16-Apr-2014 03:39 PM
Al	K_SERIES	8,35	0,06	0,7376	11,33	0,04	9,89	21,4	Al2O3	1,98	al2o3 mac 16-Apr-2014 03:41 PM
Si	K_SERIES	13,77	0,10374	0,7743	17,78	0,04	14,92	38,04	SiO2	2,99	Wollastonite 16-Apr-2014 03:16 PM
Ca	K_SERIES	4,37	0,03928	0,9961	4,38	0,02	2,58	6,14	CaO	0,52	Wollastonite 16-Apr-2014 03:17 PM
Mn	K_SERIES	1,07	0,01073	0,8399	1,28	0,03	0,55	1,65	MnO	0,11	Mn 16-Apr-2014 02:52 PM
Fe	K_SERIES	21,18	0,19174	0,9483	22,33	0,07	9,42	28,73	FeO	1,89	O5 olivine 7-May-2014 12:19 PM
O					40,7	0,07	59,93			12	
Totals					100,61						
									Cation sum	8,02	

spec5 gt-core

Element	Line	App. Conc	k ratio	Intensity corrn.	Weight%	Weight% sigma	Atomic%	Compound%	Formula	Number of ions	Standard
Mg	K_SERIES	1,78	0,0118	0,6421	2,77	0,02	2,73	4,6	MgO	0,55	mgo 16-Apr-2014 03:39 PM
Al	K_SERIES	8,17	0,05867	0,7366	11,09	0,04	9,84	20,95	Al2O3	1,97	al2o3 mac 16-Apr-2014 03:41 PM
Si	K_SERIES	13,56	0,10222	0,7743	17,52	0,04	14,93	37,48	SiO2	2,99	Wollastonite 16-Apr-2014 03:16 PM
Ca	K_SERIES	4,16	0,03744	0,9966	4,18	0,02	2,49	5,85	CaO	0,5	Wollastonite 16-Apr-2014 03:17 PM
Mn	K_SERIES	1,36	0,01357	0,8404	1,61	0,03	0,7	2,09	MnO	0,14	Mn 16-Apr-2014 02:52 PM
Fe	K_SERIES	20,78	0,18816	0,9488	21,9	0,07	9,39	28,18	FeO	1,88	O5 olivine 7-May-2014 12:19 PM
O					40,06	0,07	59,92			12	
Totals					99,14						
									Cation sum	8,03	

spec10 pl

Element	Line	App. Conc	k ratio	Intensity corrn.	Weight%	Weight% sigma	Atomic%	Compound%	Formula	Number of ions	Standard
Na	K_SERIES	5,54	0,02374	0,938	5,9	0,03	5,34	7,96	Na2O	0,69	jadeite mac 16-Apr-2014 03:54 PM
Al	K_SERIES	11,4	0,08188	0,8841	12,9	0,03	9,94	24,37	Al2O3	1,29	al2o3 mac 16-Apr-2014 03:41 PM
Si	K_SERIES	23,8	0,17938	0,8451	28,17	0,05	20,85	60,25	SiO2	2,71	Wollastonite 16-Apr-2014 03:16 PM
K	K_SERIES	0,05	0,00044	0,9952	0,05	0,01	0,03	0,07	K2O	0	k-feldspar mac 16-Apr-2014 03:24 PM
Ca	K_SERIES	4,06	0,0365	0,9417	4,31	0,02	2,24	6,03	CaO	0,29	Wollastonite 16-Apr-2014 03:17 PM
Fe	K_SERIES	0,1	0,00093	0,9096	0,11	0,02	0,04	0,15	FeO	0,01	O5 olivine 7-May-2014 12:19 PM
O					47,38	0,07	61,57			8	
Totals					98,82						
									Cation sum	4,99	

spec11 bt

Element	Line	App. Conc	k ratio	Intensity corrn.	Weight%	Weight% sigma	Atomic%	Compound%	Formula	Number of ions	Standard
Mg	K_SERIES	5,41	0,03587	0,7098	7,62	0,03	7,83	12,63	MgO	1,47	mgo 16-Apr-2014 03:39 PM
Al	K_SERIES	5,69	0,04084	0,7338	7,75	0,03	7,18	14,64	Al2O3	1,35	al2o3 mac 16-Apr-2014 03:41 PM
Si	K_SERIES	13,11	0,09877	0,7957	16,47	0,04	14,66	35,24	SiO2	2,75	Wollastonite 16-Apr-2014 03:16 PM
Cl	K_SERIES	0,17	0,00121	1,0322	0,17	0,01	0,12	0		0,02	Tugtupite 10-Jan-2013 02:15 PM
K	K_SERIES	7,66	0,06155	1,0418	7,35	0,03	4,7	8,86	K2O	0,88	k-feldspar mac 16-Apr-2014 03:24 PM
Ca	K_SERIES	0,05	0,00045	0,9512	0,05	0,01	0,03	0,07	CaO	0,01	Wollastonite 16-Apr-2014 03:17 PM
Ti	K_SERIES	1,87	0,01875	0,8322	2,25	0,02	1,18	3,76	TiO2	0,22	Ti 16-Apr-2014 02:41 PM
Mn	K_SERIES	0,02	0,00018	0,8261	0,02	0,02	0,01	0,03	MnO	0	Mn 16-Apr-2014 02:52 PM
Fe	K_SERIES	12,14	0,10988	0,9342	12,99	0,05	5,81	16,71	FeO	1,09	O5 olivine 7-May-2014 12:19 PM
O					37,43	0,07	58,48			10,98	
Totals					92,12						
									Cation sum	7,77	

spect12	hb										
Element	Line	App. Conc	k ratio	Intensity corrn.	Weight%	Weight% sigma	Atomic%	Compound%	Formula	Number of ions	Standard
Na	K_SERIES	1	0,0043	0,7383	1,36	0,02	1,39	1,83	Na2O	0,54	jadeite mac 16-Apr-2014 03:54 PM
Mg	K_SERIES	4,15	0,0275	0,6939	5,98	0,03	5,78	9,91	MgO	2,24	mgo 16-Apr-2014 03:39 PM
Al	K_SERIES	5,31	0,0381	0,7435	7,14	0,03	6,22	13,48	Al2O3	2,41	al2o3 mac 16-Apr-2014 03:41 PM
Si	K_SERIES	15,69	0,11823	0,8124	19,31	0,04	16,18	41,32	SiO2	6,26	Wollastonite 16-Apr-2014 03:16 PM
Cl	K_SERIES	0,2	0,0014	1,0248	0,19	0,01	0,13	0		0,05	Tugtupite 10-Jan-2013 02:15 PM
K	K_SERIES	0,75	0,00603	1,046	0,72	0,01	0,43	0,86	K2O	0,17	k-feldspar mac 16-Apr-2014 03:24 PM
Ca	K_SERIES	8,06	0,07245	0,9795	8,23	0,03	4,83	11,51	CaO	1,87	Wollastonite 16-Apr-2014 03:17 PM
Ti	K_SERIES	0,59	0,00587	0,8205	0,72	0,02	0,35	1,19	TiO2	0,14	Ti 16-Apr-2014 02:41 PM
Cr	K_SERIES	-0,01	-0,00007	0,8566	-0,01	0,02	0	-0,01	Cr2O3	0	Cr 16-Apr-2014 02:47 PM
Mn	K_SERIES	0,05	0,00054	0,8214	0,07	0,02	0,03	0,09	MnO	0,01	Mn 16-Apr-2014 02:52 PM
Fe	K_SERIES	11,83	0,10712	0,929	12,74	0,05	5,37	16,39	FeO	2,08	O5 olivine 7-May-2014 12:19 PM
O					40,33	0,07	59,3			22,95	
Totals					96,76						
									Cation sum	15,7	

	Domain 2										
spec1	gt-core										
Element	Line	App. Conc	k ratio	Intensity corrn.	Weight%	Weight% sigma	Atomic%	Compound%	Formula	Number of ions	Standard
Mg	K_SERIES	2	0,01327	0,6426	3,11	0,03	2,99	5,16	MgO	0,6	mgo 16-Apr-2014 03:39 PM
Al	K_SERIES	8,42	0,06044	0,7342	11,46	0,04	9,9	21,66	Al2O3	1,98	al2o3 mac 16-Apr-2014 03:41 PM
Si	K_SERIES	13,8	0,10398	0,7716	17,88	0,04	14,85	38,26	SiO2	2,97	Wollastonite 16-Apr-2014 03:16 PM
Ca	K_SERIES	3,86	0,03473	0,9961	3,88	0,02	2,26	5,43	CaO	0,45	Wollastonite 16-Apr-2014 03:17 PM
Mn	K_SERIES	1,33	0,01329	0,841	1,58	0,03	0,67	2,04	MnO	0,13	Mn 16-Apr-2014 02:52 PM
Fe	K_SERIES	21,38	0,19354	0,9492	22,52	0,07	9,4	28,98	FeO	1,88	O5 olivine 7-May-2014 12:19 PM
Co	K_SERIES	0,07	0,00069	0,8407	0,08	0,03	0,03	0,1	CoO	0,01	Co metal uncoated 16-Apr-2014 02:16 PM
O					41,1	0,08	59,9			12	
Totals					101,63						
									Cation sum	8,03	

spec2 gt-rim

Element	Line	App. Conc	k ratio	Intensity corrn.	Weight%	Weight% sigma	Atomic%	Compound%	Formula	Number of ions	Standard
Mg	K_SERIES	2,05	0,0136	0,6478	3,17	0,03	3,02	5,25	MgO	0,61	mgo 16-Apr-2014 03:39 PM
Al	K_SERIES	8,47	0,0608	0,7382	11,47	0,04	9,87	21,67	Al2O3	1,98	al2o3 mac 16-Apr-2014 03:41 PM
Si	K_SERIES	13,93	0,10493	0,7743	17,99	0,04	14,87	38,48	SiO2	2,98	Wollastonite 16-Apr-2014 03:16 PM
Ca	K_SERIES	4,61	0,04147	0,9949	4,64	0,02	2,69	6,49	CaO	0,54	Wollastonite 16-Apr-2014 03:17 PM
Mn	K_SERIES	1,05	0,01048	0,8389	1,25	0,03	0,53	1,61	MnO	0,11	Mn 16-Apr-2014 02:52 PM
Fe	K_SERIES	20,69	0,1873	0,9471	21,84	0,07	9,09	28,1	FeO	1,82	O5 olivine 7-May-2014 12:19 PM
Co	K_SERIES	0,05	0,0005	0,8394	0,06	0,03	0,02	0,08	CoO	0	Co metal uncoated 16-Apr-2014 02:16 PM
O					41,26	0,08	59,91			12	
Totals					101,67						
									Cation sum	8,03	

spec3 bt

Element	Line	App. Conc	k ratio	Intensity corrn.	Weight%	Weight% sigma	Atomic%	Compound%	Formula	Number of ions	Standard
Na	K_SERIES	0,12	0,00049	0,742	0,16	0,02	0,17	0,21	Na2O	0,03	jadeite mac 16-Apr-2014 03:54 PM
Mg	K_SERIES	5,49	0,0364	0,7105	7,73	0,03	7,88	12,81	MgO	1,48	mgo 16-Apr-2014 03:39 PM
Al	K_SERIES	5,91	0,04248	0,7335	8,06	0,03	7,41	15,24	Al2O3	1,39	al2o3 mac 16-Apr-2014 03:41 PM
Si	K_SERIES	12,99	0,09787	0,7927	16,38	0,04	14,46	35,05	SiO2	2,72	Wollastonite 16-Apr-2014 03:16 PM
Cl	K_SERIES	0,13	0,0009	1,0318	0,12	0,01	0,09	0		0,02	Tugtupite 10-Jan-2013 02:15 PM
K	K_SERIES	7,8	0,06263	1,0416	7,48	0,03	4,75	9,02	K2O	0,89	k-feldspar mac 16-Apr-2014 03:24 PM
Ti	K_SERIES	1,83	0,01827	0,8318	2,2	0,02	1,14	3,66	TiO2	0,21	Ti 16-Apr-2014 02:41 PM
Fe	K_SERIES	12,07	0,10931	0,934	12,93	0,05	5,74	16,63	FeO	1,08	O5 olivine 7-May-2014 12:19 PM
O					37,68	0,07	58,38			10,98	
Totals					92,74						
									Cation sum	7,81	

spec4	hb										
Element	Line	App. Conc	k ratio	Intensity corrn.	Weight%	Weight% sigma	Atomic%	Compound%	Formula	Number of ions	Standard
Na	K_SERIES	1,15	0,00492	0,7474	1,54	0,03	1,55	2,07	Na2O	0,6	jadeite mac 16-Apr-2014 03:54 PM
Mg	K_SERIES	4,34	0,0288	0,6988	6,21	0,03	5,93	10,3	MgO	2,3	mgo 16-Apr-2014 03:39 PM
Al	K_SERIES	5,64	0,04052	0,7451	7,57	0,03	6,51	14,31	Al2O3	2,53	al2o3 mac 16-Apr-2014 03:41 PM
Si	K_SERIES	15,71	0,11835	0,8095	19,4	0,04	16,03	41,51	SiO2	6,21	Wollastonite 16-Apr-2014 03:16 PM
Cl	K_SERIES	0,14	0,001	1,0229	0,14	0,01	0,09	0		0,03	Tugtupite 10-Jan-2013 02:15 PM
K	K_SERIES	0,77	0,00619	1,0445	0,74	0,01	0,44	0,89	K2O	0,17	k-feldspar mac 16-Apr-2014 03:24 PM
Ca	K_SERIES	8,12	0,07299	0,9779	8,3	0,03	4,81	11,61	CaO	1,86	Wollastonite 16-Apr-2014 03:17 PM
Ti	K_SERIES	0,49	0,00494	0,819	0,6	0,02	0,29	1,01	TiO2	0,11	Ti 16-Apr-2014 02:41 PM
Mn	K_SERIES	0,06	0,00058	0,8206	0,07	0,02	0,03	0,09	MnO	0,01	Mn 16-Apr-2014 02:52 PM
Fe	K_SERIES	11,3	0,10232	0,928	12,18	0,05	5,06	15,67	FeO	1,96	O5 olivine 7-May-2014 12:19 PM
O					40,84	0,07	59,25			22,97	
Totals					97,6						
									Cation sum	15,76	

spec5	pl										
Element	Line	App. Conc	k ratio	Intensity corrn.	Weight%	Weight% sigma	Atomic%	Compound%	Formula	Number of ions	Standard
Na	K_SERIES	5,71	0,02447	0,9394	6,08	0,03	5,49	8,19	Na2O	0,71	jadeite mac 16-Apr-2014 03:54 PM
Al	K_SERIES	11,14	0,08001	0,8827	12,62	0,03	9,72	23,85	Al2O3	1,26	al2o3 mac 16-Apr-2014 03:41 PM
Si	K_SERIES	24,08	0,18147	0,847	28,43	0,05	21,04	60,82	SiO2	2,73	Wollastonite 16-Apr-2014 03:16 PM
K	K_SERIES	0,07	0,00056	0,9941	0,07	0,01	0,04	0,08	K2O	0	k-feldspar mac 16-Apr-2014 03:24 PM
Ca	K_SERIES	3,77	0,03391	0,9411	4,01	0,02	2,08	5,61	CaO	0,27	Wollastonite 16-Apr-2014 03:17 PM
Fe	K_SERIES	0,13	0,00117	0,9097	0,14	0,02	0,05	0,18	FeO	0,01	O5 olivine 7-May-2014 12:19 PM
O					47,39	0,07	61,57			8	
Totals					98,73						
									Cation sum	4,99	

Domain 3

spec1 gt-core

Element	Line	App. Conc	k ratio	Intensity corrn.	Weight%	Weight% sigma	Atomic%	Compound%	Formula	Number of ions	Standard
Mg	K_SERIES	1,6	0,01061	0,6397	2,5	0,02	2,41	4,15	MgO	0,48	mgo 16-Apr-2014 03:39 PM
Al	K_SERIES	8,38	0,06022	0,7381	11,36	0,04	9,88	21,47	Al2O3	1,98	al2o3 mac 16-Apr-2014 03:41 PM
Si	K_SERIES	13,78	0,10387	0,7756	17,77	0,04	14,85	38,02	SiO2	2,97	Wollastonite 16-Apr-2014 03:16 PM
Ca	K_SERIES	4,66	0,04189	0,998	4,67	0,02	2,73	6,53	CaO	0,55	Wollastonite 16-Apr-2014 03:17 PM
Mn	K_SERIES	1,7	0,01703	0,8406	2,03	0,03	0,86	2,62	MnO	0,17	Mn 16-Apr-2014 02:52 PM
Fe	K_SERIES	21,17	0,19166	0,9492	22,3	0,07	9,37	28,69	FeO	1,88	O5 olivine 7-May-2014 12:19 PM
O					40,84	0,07	59,89			12	
Totals					101,47						
									Cation sum	8,04	

spec2 gt-rim

Element	Line	App. Conc	k ratio	Intensity corrn.	Weight%	Weight% sigma	Atomic%	Compound%	Formula	Number of ions	Standard
Mg	K_SERIES	1,81	0,012	0,6417	2,82	0,03	2,78	4,68	MgO	0,56	mgo 16-Apr-2014 03:39 PM
Al	K_SERIES	8,09	0,05809	0,7357	10,99	0,04	9,78	20,77	Al2O3	1,96	al2o3 mac 16-Apr-2014 03:41 PM
Si	K_SERIES	13,43	0,10123	0,7744	17,35	0,04	14,82	37,11	SiO2	2,97	Wollastonite 16-Apr-2014 03:16 PM
Ca	K_SERIES	4,57	0,04108	0,9968	4,58	0,02	2,74	6,41	CaO	0,55	Wollastonite 16-Apr-2014 03:17 PM
Mn	K_SERIES	0,94	0,00942	0,84	1,12	0,02	0,49	1,45	MnO	0,1	Mn 16-Apr-2014 02:52 PM
Fe	K_SERIES	21,01	0,19016	0,9484	22,15	0,07	9,51	28,49	FeO	1,91	O5 olivine 7-May-2014 12:19 PM
Co	K_SERIES	0,05	0,00045	0,8407	0,05	0,03	0,02	0,07	CoO	0	Co metal uncoated 16-Apr-2014 02:16 PM
O					39,92	0,08	59,85			12	
Totals					98,98						
									Cation sum	8,05	

spec3 hb

Element	Line	App. Conc	k ratio	Intensity corrn.	Weight%	Weight% sigma	Atomic%	Compound%	Formula	Number of ions	Standard
Na	K_SERIES	1,03	0,00442	0,7374	1,4	0,03	1,44	1,89	Na2O	0,56	jadeite mac 16-Apr-2014 03:54 PM
Mg	K_SERIES	4,31	0,02856	0,6925	6,22	0,03	6,05	10,31	MgO	2,34	mgo 16-Apr-2014 03:39 PM
Al	K_SERIES	5,13	0,03687	0,7393	6,95	0,03	6,09	13,12	Al2O3	2,36	al2o3 mac 16-Apr-2014 03:41 PM
Si	K_SERIES	15,63	0,11777	0,8104	19,29	0,04	16,25	41,26	SiO2	6,29	Wollastonite 16-Apr-2014 03:16 PM
Cl	K_SERIES	0,16	0,00115	1,0228	0,16	0,01	0,11	0		0,04	Tugtupite 10-Jan-2013 02:15 PM
K	K_SERIES	0,79	0,00635	1,0443	0,76	0,01	0,46	0,91	K2O	0,18	k-feldspar mac 16-Apr-2014 03:24 PM
Ca	K_SERIES	7,32	0,06584	0,979	7,48	0,03	4,42	10,46	CaO	1,71	Wollastonite 16-Apr-2014 03:17 PM
Ti	K_SERIES	0,59	0,00592	0,8227	0,72	0,02	0,36	1,2	TiO2	0,14	Ti 16-Apr-2014 02:41 PM
Mn	K_SERIES	0,08	0,00076	0,8223	0,09	0,02	0,04	0,12	MnO	0,02	Mn 16-Apr-2014 02:52 PM
Fe	K_SERIES	12,06	0,10917	0,9298	12,97	0,05	5,49	16,68	FeO	2,13	O5 olivine 7-May-2014 12:19 PM
O					40,09	0,07	59,3			22,96	
Totals					96,11						
									Cation sum	15,72	

spec4 bt

Element	Line	App. Conc	k ratio	Intensity corrn.	Weight%	Weight% sigma	Atomic%	Compound%	Formula	Number of ions	Standard
Na	K_SERIES	0,13	0,00054	0,7309	0,17	0,02	0,18	0,23	Na2O	0,03	jadeite mac 16-Apr-2014 03:54 PM
Mg	K_SERIES	5,21	0,03459	0,7017	7,43	0,03	7,55	12,32	MgO	1,42	mgo 16-Apr-2014 03:39 PM
Al	K_SERIES	5,68	0,04077	0,7314	7,76	0,03	7,1	14,67	Al2O3	1,34	al2o3 mac 16-Apr-2014 03:41 PM
Si	K_SERIES	13,18	0,09934	0,7954	16,57	0,04	14,57	35,46	SiO2	2,74	Wollastonite 16-Apr-2014 03:16 PM
Cl	K_SERIES	0,17	0,0012	1,0342	0,16	0,01	0,11	0		0,02	Tugtupite 10-Jan-2013 02:15 PM
K	K_SERIES	7,87	0,06318	1,0437	7,54	0,03	4,76	9,08	K2O	0,9	k-feldspar mac 16-Apr-2014 03:24 PM
Ti	K_SERIES	1,95	0,01947	0,8341	2,33	0,02	1,2	3,89	TiO2	0,23	Ti 16-Apr-2014 02:41 PM
Fe	K_SERIES	13,01	0,11777	0,9354	13,91	0,05	6,15	17,89	FeO	1,16	O5 olivine 7-May-2014 12:19 PM
O					37,82	0,07	58,37			10,98	
Totals					93,7						
									Cation sum	7,81	

spec5 pl

Element	Line	App. Conc	k ratio	Intensity corrn.	Weight%	Weight% sigma	Atomic%	Compound%	Formula	Number of ions	Standard
Na	K_SERIES	5,98	0,02563	0,9422	6,35	0,03	5,69	8,55	Na2O	0,74	jadeite mac 16-Apr-2014 03:54 PM
Al	K_SERIES	11,02	0,07913	0,8814	12,5	0,03	9,55	23,62	Al2O3	1,24	al2o3 mac 16-Apr-2014 03:41 PM
Si	K_SERIES	24,51	0,18472	0,8481	28,9	0,05	21,22	61,83	SiO2	2,76	Wollastonite 16-Apr-2014 03:16 PM
K	K_SERIES	0,09	0,0007	0,9927	0,09	0,01	0,05	0,11	K2O	0,01	k-feldspar mac 16-Apr-2014 03:24 PM
Ca	K_SERIES	3,41	0,0307	0,9403	3,63	0,02	1,87	5,08	CaO	0,24	Wollastonite 16-Apr-2014 03:17 PM
Fe	K_SERIES	0,13	0,00118	0,9099	0,14	0,02	0,05	0,18	FeO	0,01	O5 olivine 7-May-2014 12:19 PM
O					47,76	0,07	61,56			8	
Totals					99,37						
									Cation sum	4,99	

Appendix D – garnet profiles

DTC15002D

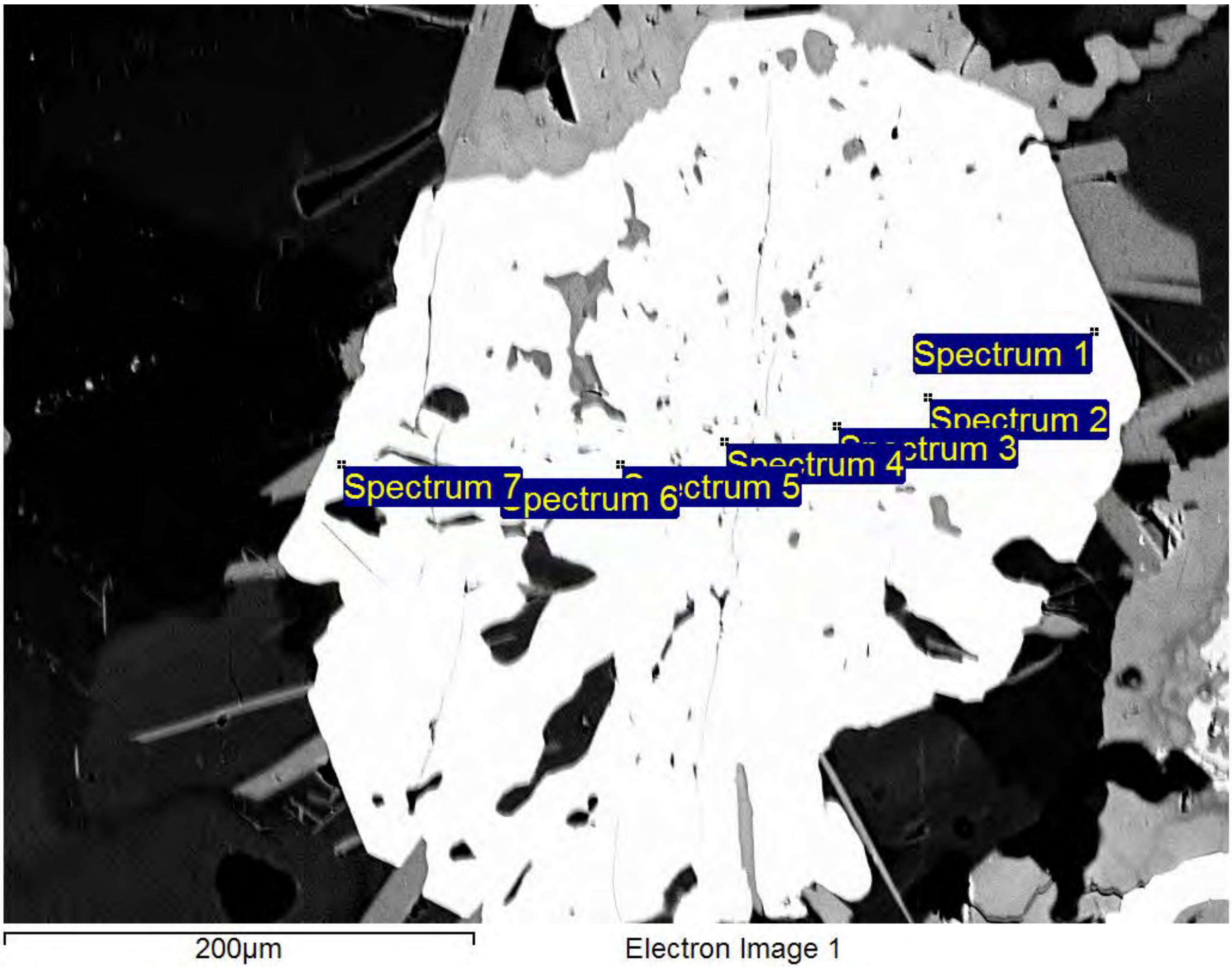

Figure 1, SEM - garnet analyse in DTC15002

Table 1

	DTC15001 - metagabbro						
	spec1	spec2	spec3	spec4	spec5	spec6	spec7
SiO2	38.04	37.91	37.96	36.87	37.99	38.05	37.72
Al2O3	21.41	21.36	21.41	22.45	21.37	21.4	21.2
FeO	26.23	24.84	24.95	25.05	24.9	24.52	26.21
MgO	5.80	6.63	6.47	6.52	6.57	6.43	5.50
MnO	1.30	0.92	0.99	1.02	0.94	0.95	1.19
CaO	6.62	7.11	7.14	6.89	7.11	7.58	6.82
Total	**99.4**	**98.77**	**98.92**	**98.8**	**98.88**	**98.93**	**98.64**
Si	17.78	17.72	17.75	17.23	17.76	17.79	17.63
Al	11.33	11.3	11.33	11.88	11.31	11.33	11.22
Fe	20.39	19.31	19.4	19.47	19.36	19.06	20.38
Mg	3.50	4.00	3.9	3.93	3.96	3.88	3.32
Mn	1.01	0.71	0.76	0.79	0.73	0.73	0.92
Ca	4.73	5.08	5.10	4.92	5.08	5.42	4.88
O	40.66	40.64	40.68	40.56	40.69	40.73	40.31

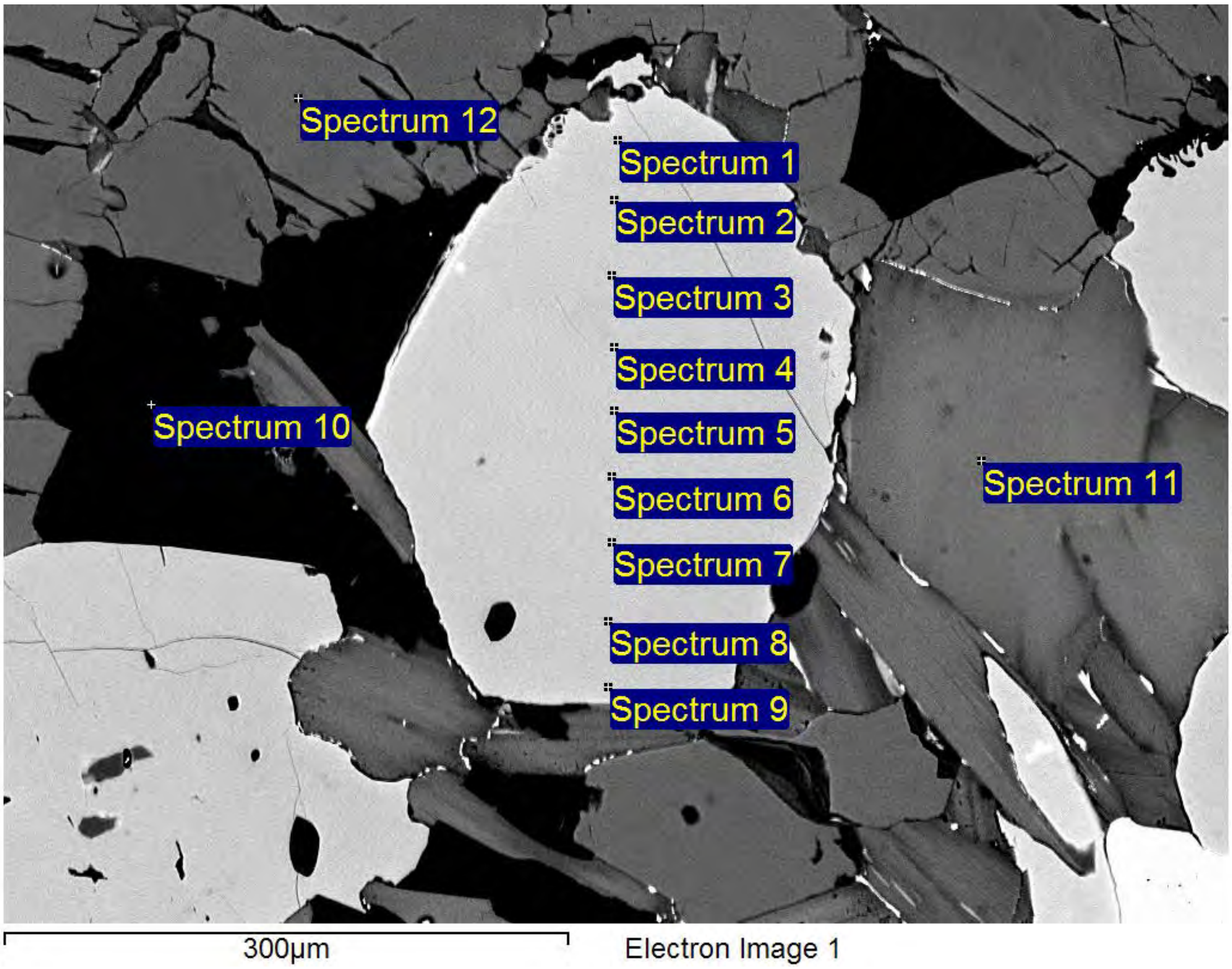

Figure 2, SEM - garnet analyse in DTC15002D

Table 2

	DTC15002D - garnet-amphibolite								
	spec1	spec2	spec3	spec4	spec5	spec6	spec7	spec8	spec9
SiO2	38.04	37.79	37.63	37.5	37.48	37.25	36.91	36.59	35.18
Al2O3	21.4	21.27	21.14	21.15	20.95	20.79	20.87	20.61	19.77
FeO	28.73	28.42	28.32	28.2	28.18	28.14	28.05	28.06	28.06
MgO	4.65	4.73	4.65	4.64	4.60	4.55	4.54	4.54	3.99
MnO	1.65	1.78	1.88	1.99	2.09	1.93	1.83	1.66	1.52
CaO	6.14	6.04	6.06	6.01	5.85	6.1	6.1	6.14	6.31
Total	**100.61**	**100.03**	**99.68**	**99.49**	**99.15**	**98.76**	**98.3**	**97.6**	**94.83**
Si	17.78	17.67	17.59	17.53	17.52	17.41	17.25	17.1	16.44
Al	11.33	11.26	11.19	11.19	11.09	11.00	11.05	10.91	10.46
Fe	22.33	22.09	22.01	21.92	21.9	21.87	21.81	21.81	21.81
Mg	2.80	2.86	2.80	2.80	2.77	2.74	2.74	2.74	2.41
Mn	1.28	1.38	1.46	1.54	1.61	1.49	1.42	1.29	1.17
Ca	4.38	4.31	4.33	4.29	4.18	4.36	4.36	4.39	4.51
O	40.7	40.47	40.3	40.21	40.06	39.87	39.68	39.36	38.01

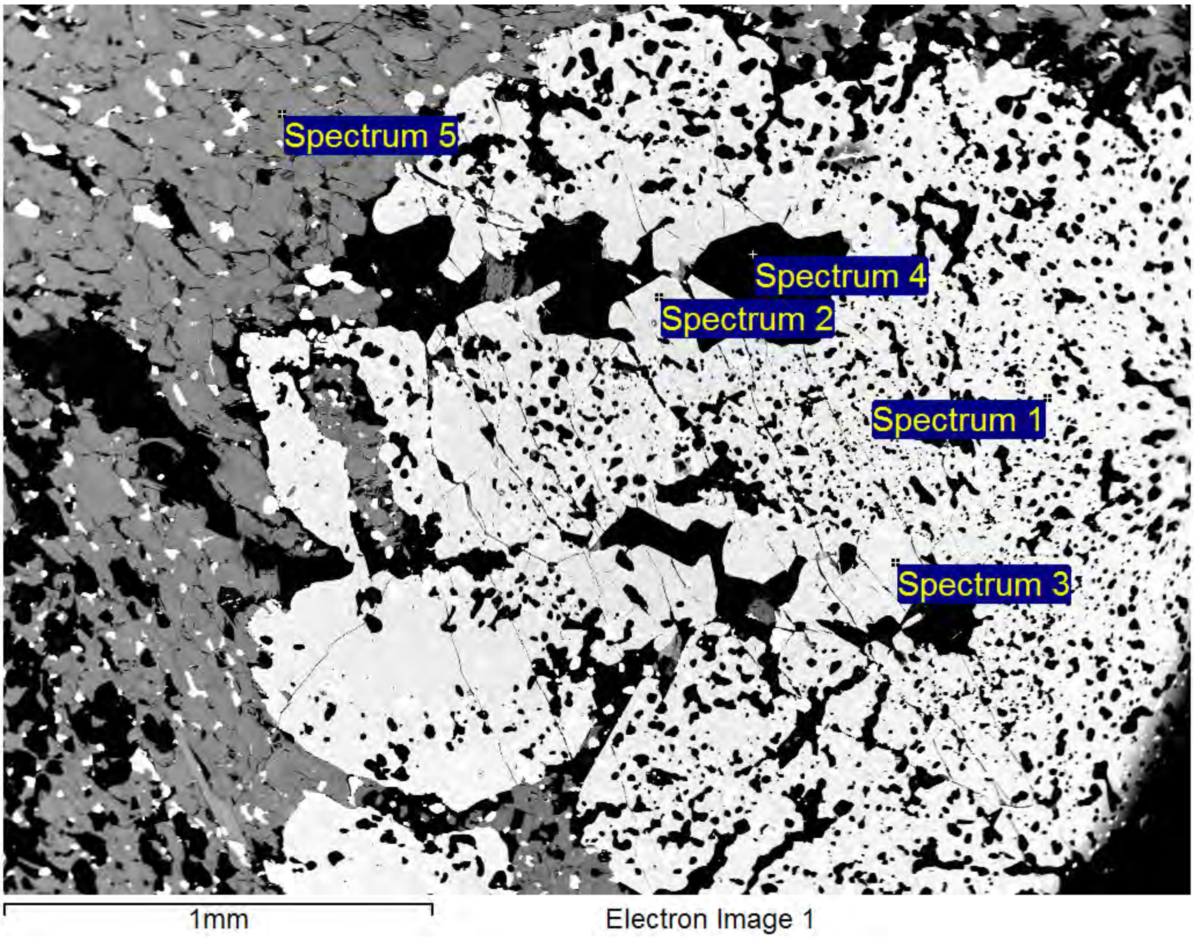

Figure 3, SEM - garnet analyse in DTC15002D in the diabase intrusion

Table 3

	DTC15002D – diabase intrusion in garnet-amphibolite				
	Gt	Gt	Gt	Pl	Hb
	spec1	spec2	spec3	spec4	spec5
SiO2	30.49	37.95	32.22	58.48	36.07
Al2O3	17.03	21.43	18.04	25.46	10.88
FeO	24.1	28.63	25.26	0.13	15.48
MgO	3.26	4.19	3.33	0.02	8.09
MnO	1.65	1.17	1.75	0.01	0.10
CaO	5.25	7.09	5.48	7.42	9.66
Na2O	n.d	n.d	n.d	7.14	1.66
K2O	n.d	n.d	n.d	0.16	0.81
TiO2	n.d	n.d	n.d	0.01	1.19
Total	**81.78**	**100.46**	**86.08**	**98.83**	**83.94**
Si	14.25	17.74	15.06	27.34	16.86
Al	9.01	11.34	9.55	13.48	5.76
Fe	18.74	22.26	19.63	0.1	12.03
Mg	1.97	2.53	2.01	0.01	4.88
Mn	1.28	0.90	1.35	0.01	0.08
Ca	3.75	5.07	3.92	5.3	6.91
Na	n.d	n.d	n.d	5.3	1.23
K	n.d	n.d	n.d	0.13	0.67
Ti	n.d	n.d	n.d	0.01	0.71
O	32.78	40.63	34.55	47.16	34.81

DTC15007I

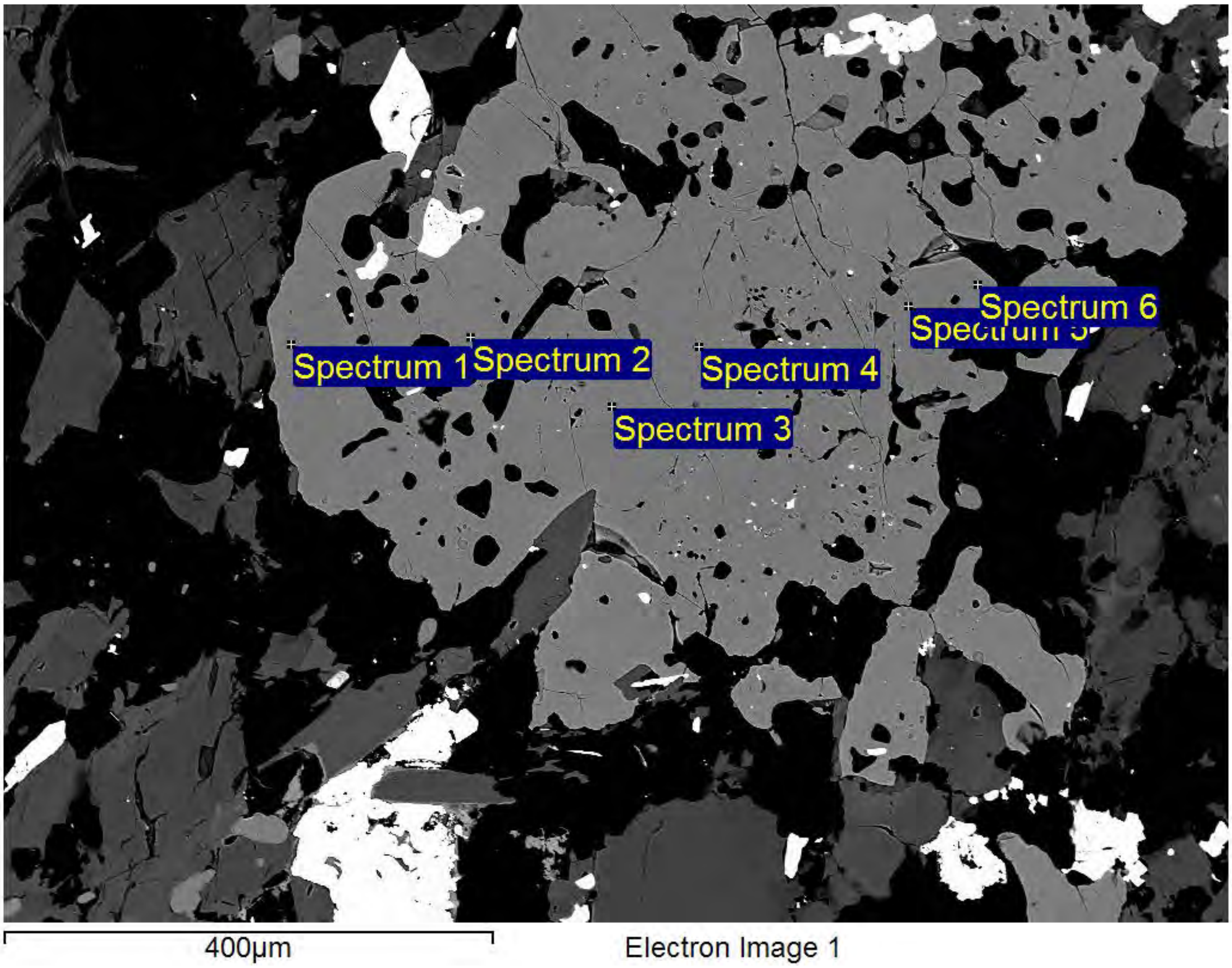

Figure 4, SEM - garnet analyse in DTCC15007I

Table 4

	DTC15007I - garnet-amphibolite					
	spec1	spec2	spec3	spec4	spec5	spec6
SiO2	37.77	36.69	37.51	37.59	38.00	38.26
Al2O3	21.33	20.93	21.25	21.20	21.33	21.48
FeO	27.62	29.43	28.93	28.48	29.05	28.74
MgO	3.37	3.87	3.59	3.41	3.83	3.48
MnO	2.31	2.43	2.39	2.55	2.49	2.58
CaO	8.59	6.54	7.10	7.70	6.78	7.27
Total	**100.99**	**99.89**	**100.77**	**100.93**	**101.48**	**101.81**
Si	17.65	17.15	17.53	17.57	17.76	17.89
Al	11.29	11.08	11.25	11.22	11.29	11.37
Fe	21.47	22.88	22.49	22.14	22.58	22.34
Mg	2.03	2.34	2.16	2.06	2.31	2.10
Mn	1.79	1.88	1.85	1.97	1.93	2.00
Ca	6.14	4.67	5.08	5.50	4.84	5.19
O	40.63	39.90	40.48	40.53	40.79	40.94

Appendix E: THERMOCALC output and PT-estimates

DTC15007I

DTC15007I, domain 1 (garnet core)

Activities and their uncertainties

	phl	ann	east	py	gr	alm	an
a	0.0560	0.0640	0.00940	0.00540	0.0126	0.170	0.380
sd(a)/a	0.34963	0.32400	0.48930	0.61191	0.52988	0.17905	0.11532

	tr	fact	ts	q	H2O
a	0.0157	0.00190	0.00130	1.00	1.00
sd(a)/a	0.45906	0.76556	0.84615	0	

Independent set of reactions

1) 2py + 4gr + 3ts + 12q = 12an + 3tr

2) 21an + 6tr = 10py + 11gr + 27q + 6H2O

3) 21an + 6fact = 11gr + 10alm + 27q + 6H2O

4) 5phl + 3fact = 5ann + 3tr

5) 3east + py + 2gr + 6q = 3phl + 6an

Calculations for the independent set of reactions (for x(H2O) = 1.0)

	P(T)	sd(P)	a	sd(a)	b	c	ln_K	sd(ln_K)
1	8.7	1.40	-23.14	6.48	-0.38390	21.360	23.802	4.031
2	10.5	1.35	541.26	4.63	0.43622	-49.741	-55.084	9.212
3	8.2	1.10	-25.05	11.26	0.60180	-54.015	-7.920	8.009
4	5.6	38.33	-60.17	6.73	0.01524	-0.701	7.003	3.585
5	8.4	1.57	-0.48	1.59	-0.21480	10.648	13.518	2.287

Diagnostics, hat < 0.42, e* < 2.5, fit < 1.61

	P	sd(P)	T	sd(T)	cor	fit	e*	hat
phl	10.25	1.59	823	111	0.620	0.25	-0.26	0.01
ann	10.25	1.59	815	111	0.600	0.23	0.26	0.03
east	10.21	1.59	818	116	0.596	0.30	-0.04	0.12
py	9.91	2.02	790	166	0.785	0.27	0.17	0.62
gr	10.28	2.49	820	113	0.555	0.30	-0.02	0.65
alm	10.23	1.60	817	112	0.579	0.29	-0.08	0.05
an	10.18	1.73	820	111	0.511	0.30	-0.03	0.15
tr	10.26	1.68	822	115	0.649	0.29	0.07	0.07
fact	10.17	1.60	823	112	0.583	0.28	-0.18	0.09
ts	10.27	1.61	829	119	0.624	0.27	0.22	0.18
q	10.21	1.59	819	111	0.616	0.30	0	0
H2O	10.21	1.59	819	111	0.616	0.30	0	0

T = 819¡C, sd = 111,

P = 10.2 kbars, sd = 1.6, cor = 0.616, sigf

DTC15007I, domain 1 (garnet rim)

Activities and their uncertainties

	phl	ann	east	py	gr	alm	an
a	0.0540	0.0710	0.0138	0.00550	0.0170	0.160	0.450
sd(a)/a	0.35355	0.30897	0.46731	0.61031	0.49667	0.18806	0.09075

	tr	fact	ts	q	H2O
a	0.0151	0.00270	0.00150	1.00	1.00
sd(a)/a	0.46177	0.72164	0.80000	0	

Independent set of reactions

1) 2py + 4gr + 3ts + 12q = 12an + 3tr

2) 21an + 6tr = 10py + 11gr + 27q + 6H2O

3) 21an + 6fact = 11gr + 10alm + 27q + 6H2O

4) 5phl + 3fact = 5ann + 3tr

5) 3east + py + 2gr + 6q = 3phl + 6an

Calculations for the independent set of reactions (for x(H2O) = 1.0)

	P(T)	sd(P)	a	sd(a)	b	c	ln_K	sd(ln_K)
1	9.0	1.44	0.35	6.48	-0.39707	20.711	24.042	3.782
2	10.5	1.39	482.15	4.63	0.48401	-49.000	-54.907	8.855
3	8.3	1.10	-79.19	11.26	0.64279	-53.208	-10.890	7.468
4	5.7	39.16	-60.14	6.73	0.01524	-0.703	6.525	3.481
5	9.5	1.63	11.53	1.59	-0.22155	10.316	12.654	2.179

Diagnostics, hat < 0.42, e* < 2.5, fit < 1.61

	P	sd(P)	T	sd(T)	cor	fit	e*	hat
phl	10.15	1.51	833	111	0.636	0.36	-0.55	0.02
ann	10.10	1.51	821	110	0.617	0.48	0.20	0.03
east	10.08	1.50	839	114	0.609	0.43	0.43	0.12
py	9.51	1.94	768	164	0.797	0.43	0.32	0.62
gr	10.23	2.36	826	112	0.563	0.50	-0.05	0.66
alm	10.13	1.52	818	111	0.591	0.47	-0.19	0.06
an	9.99	1.60	825	110	0.553	0.50	-0.08	0.11
tr	10.10	1.60	825	113	0.662	0.50	0.04	0.07
fact	10.10	1.52	821	111	0.600	0.49	0.16	0.09
ts	10.12	1.53	834	119	0.638	0.49	0.22	0.19
q	10.06	1.50	824	110	0.632	0.51	0	0
H2O	10.06	1.50	824	110	0.632	0.51	0	0

T = 824¡C, sd = 110,

P = 10.1 kbars, sd = 1.5, cor = 0.632, sigf

DTC15007I domain 2 (average core and rim)

Activities and their uncertainties

	phl	ann	east	py	gr	alm	an
a	0.0600	0.0460	0.0180	0.00470	0.0180	0.160	0.460
sd(a)/a	0.34206	0.37060	0.44980	0.62374	0.49008	0.18806	0.08748

	tr	fact	ts	q	H2O
a	0.0210	0.00170	0.00130	1.00	1.00
sd(a)/a	0.43870	0.77909	0.84615	0	

Independent set of reactions

1) 2py + 4gr + 3ts + 12q = 12an + 3tr

2) 21an + 6tr = 10py + 11gr + 27q + 6H2O

3) 21an + 6fact = 11gr + 10alm + 27q + 6H2O

4) 3east + py + 2gr + 6q = 3phl + 6an

5) 3east + 2gr + alm + 6q = 2phl + ann + 6an

Calculations for the independent set of reactions (for x(H2O) = 1.0)

	P(T)	sd(P)	a	sd(a)	b	c	ln_K	sd(ln_K)
1	8.0	1.34	-23.14	6.48	-0.38390	21.360	25.818	3.831
2	10.0	1.29	541.26	4.63	0.43622	-49.741	-58.307	8.847
3	8.2	1.04	-25.05	11.26	0.60180	-54.015	-7.947	7.604
4	9.2	1.45	-0.48	1.59	-0.21480	10.648	12.348	2.121
5	8.5	1.29	44.12	1.84	-0.22832	10.935	8.554	1.923

Diagnostics, hat < 0.42, e* < 2.5, fit < 1.61

	P	sd(P)	T	sd(T)	cor	fit	e*	hat
phl	9.95	1.42	766	100	0.651	0.49	-0.37	0.02
ann	9.87	1.42	761	99	0.628	0.54	-0.11	0.04
east	9.92	1.41	782	104	0.624	0.39	0.61	0.14
py	9.82	1.85	754	147	0.810	0.55	0.04	0.62
gr	9.87	2.18	760	101	0.569	0.55	0.00	0.64
alm	9.89	1.42	759	100	0.609	0.55	-0.02	0.05
an	9.88	1.49	760	99	0.572	0.55	-0.01	0.11
tr	10.03	1.50	767	102	0.676	0.52	0.19	0.07
fact	9.92	1.42	757	100	0.614	0.54	0.17	0.10
ts	9.76	1.43	738	106	0.651	0.45	-0.53	0.18
q	9.88	1.41	760	99	0.646	0.55	0	0
H2O	9.88	1.41	760	99	0.646	0.55	0	0

T = 760¡C, sd = 99,

P = 9.9 kbars, sd = 1.4, cor = 0.646, sigfit = 0.55

DTC15007I, domain 3 (average core and rim)

Activities and their uncertainties

	phl	ann	east	py	gr	alm	an
a	0.0620	0.0540	0.0190	0.00610	0.0101	0.190	0.390
sd(a)/a	0.33840	0.34822	0.44599	0.60116	0.55297	0.16265	0.11163

	tr	fact	ts	q	H2O
a	0.0250	0.00230	0.00160	1.00	1.00
sd(a)/a	0.42526	0.74191	0.81250	0	

Independent set of reactions

1) 2py + 4gr + 3ts + 12q = 12an + 3tr

2) 21an + 6tr = 10py + 11gr + 27q + 6H2O

3) 21an + 6fact = 11gr + 10alm + 27q + 6H2O

4) 3east + py + 2gr + 6q = 3phl + 6an

5) 3east + 2gr + alm + 6q = 2phl + ann + 6an

Calculations for the independent set of reactions (for x(H2O) = 1.0)

	P(T)	sd(P)	a	sd(a)	b	c	ln_K	sd(ln_K)
1	8.1	1.38	-23.14	6.48	-0.38390	21.360	25.527	3.962
2	9.8	1.35	541.26	4.63	0.43622	-49.741	-59.635	9.227
3	7.8	1.10	-25.05	11.26	0.60180	-54.015	-10.932	8.059
4	9.3	1.51	-0.48	1.59	-0.21480	10.648	12.188	2.203
5	8.5	1.35	44.12	1.84	-0.22832	10.935	8.611	2.017

Diagnostics, hat < 0.42, e* < 2.5, fit < 1.61

	P	sd(P)	T	sd(T)	cor	fit	e*	hat
phl	9.54	1.46	758	94	0.595	0.51	-0.60	0.02
ann	9.45	1.46	749	94	0.574	0.64	0.01	0.03
east	9.48	1.45	774	98	0.569	0.42	0.77	0.12
py	9.09	1.81	714	140	0.762	0.61	0.23	0.61
gr	9.57	2.34	750	96	0.545	0.64	-0.04	0.68
alm	9.48	1.46	746	94	0.560	0.63	-0.12	0.04
an	9.37	1.58	750	94	0.487	0.64	-0.08	0.14
tr	9.54	1.53	754	97	0.624	0.63	0.13	0.06
fact	9.51	1.46	743	94	0.559	0.61	0.32	0.08
ts	9.40	1.46	740	101	0.595	0.63	-0.24	0.18
q	9.45	1.45	749	93	0.590	0.64	0	0
H2O	9.45	1.45	749	93	0.590	0.64	0	0

T = 749¡C, sd = 93,

P = 9.4 kbars, sd = 1.4, cor = 0.590, sigfit = 0.64

DTC15007I Fe^{3+} corrected

DTC15007I, domain 1 (garnet core)

Activities and their uncertainties

	phl	ann	east	py	gr	alm	an
a	0.0430	0.0620	0.0131	0.00720	0.0135	0.170	0.480
sd(a)/a	0.37696	0.32856	0.47051	0.58598	0.52243	0.17905	0.08112

	tr	fact	ts	q	H2O
a	0.0387	0.00220 0	.000900	1.00	1.00
sd(a)/a	0.38718	0.74746	1.22222	0	

Independent set of reactions

1) 2py + 4gr + 3ts + 12q = 12an + 3tr

2) 21an + 6tr = 10py + 11gr + 27q + 6H2O

3) 21an + 6fact = 11gr + 10alm + 27q + 6H2O

4) 5phl + 3fact = 5ann + 3tr

5) 3east + py + 2gr + 6q = 3phl + 6an

Calculations for the independent set of reactions (for x(H2O) = 1.0)

	P(T)	sd(P)	a	sd(a)	b	c	ln_K	sd(ln_K)
1	7.0	1.75	0.35	6.48 -	0.39707	20.711	29.563	4.635
2	9.4	1.37	482.15	4.63	0.48401	-49.000	-61.766	8.698
3	8.0	1.13	-79.19	11.26	0.64279	-53.208	-12.946	7.697
4	48.3	39.93	-60.14	6.73	0.01524	-0.703	10.431	3.554
5	9.5	1.66	11.53	1.59 -	0.22155	10.316	12.706	2.223

Diagnostics, hat < 0.42, e* < 2.5, fit < 1.61

	P	sd(P)	T	sd(T)	cor	fit	e*	hat
phl	9.14	1.42	821	109	0.567	0.71	-1.15	0.01
ann	9.08	1.42	791	109	0.539	0.92	0.56	0.04
east	8.99	1.42	831	115	0.531	0.92	0.63	0.15
py	8.43	1.82	742	168	0.763	0.97	0.33	0.65
gr	9.04	2.33	805	111	0.498	1.01	-0.02	0.70
alm	9.02	1.43	799	111	0.514	1.00	-0.12	0.06
an	8.97	1.52	805	109	0.507	1.01	-0.02	0.08
tr	9.38	1.51	831	114	0.611	0.91	0.49	0.07
fact	8.91	1.43	816	110	0.526	0.96	-0.46	0.10
ts	8.93	1.42	787	112	0.561	0.95	-0.60	0.11
q	8.99	1.43	804	109	0.563	1.01	0	0
H2O	8.99	1.43	804	109	0.563	1.01	0	0

T = 804¡C, sd = 109,

P = 9.0 kbars, sd = 1.4, cor = 0.563, sigfi = 1.01

DTC15007I, domain 1 (garnet rim)

Activities and their uncertainties

	phl	ann	east	py	gr	alm	an
a	0.0540	0.0710	0.0138	0.00550	0.0170	0.160	0.450
sd(a)/a	0.35355	0.30897	0.46731	0.61031	0.49667	0.18806	0.09075

	tr	fact	ts	q	H2O
a	0.0150	0.00270	0.00150	1.00	1.00
sd(a)/a	0.46194	0.72164	0.80000	0	

Independent set of reactions

1) 2py + 4gr + 3ts + 12q = 12an + 3tr

2) 21an + 6tr = 10py + 11gr + 27q + 6H2O

3) 21an + 6fact = 11gr + 10alm + 27q + 6H2O

4) 5phl + 3fact = 5ann + 3tr

5) 3east + py + 2gr + 6q = 3phl + 6an

Calculations for the independent set of reactions (for x(H2O) = 1.0)

	P(T)	sd(P)	a	sd(a)	b	c	ln_K	sd(ln_K)
1	8.6	1.32	-23.14	6.48	-0.38390	21.360	24.034	3.782
2	10.5	1.30	541.26	4.63	0.43622	-49.741	-54.891	8.855
3	7.8	1.02	-25.05	11.26	0.60180	-54.015	-10.890	7.468
4	0.60	37.29	-60.17	6.73	0.01524	-0.701	6.517	3.481
5	9.0	1.49	-0.48	1.59	-0.21480	10.648	12.654	2.179

Diagnostics, hat < 0.42, e* < 2.5, fit < 1.61

	P	sd(P)	T	sd(T)	cor	fit	e*	hat
phl	10.15	1.51	833	110	0.640	0.36	-0.55	0.02
ann	10.10	1.51	821	110	0.622	0.48	0.20	0.03
east	10.08	1.51	839	114	0.614	0.43	0.43	0.13
py	9.51	1.94	768	164	0.799	0.43	0.32	0.62
gr	10.23	2.36	826	112	0.566	0.50	-0.05	0.66
alm	10.13	1.52	818	111	0.595	0.47	-0.19	0.06
an	9.99	1.60	825	110	0.557	0.50	-0.08	0.11
tr	10.10	1.60	825	113	0.666	0.50	0.04	0.07
fact	10.10	1.52	821	111	0.604	0.49	0.16	0.09
ts	10.12	1.53	834	119	0.643	0.49	0.22	0.19
q	10.07	1.51	824	109	0.636	0.51	0	0
H2O	10.07	1.51	824	109	0.636	0.51	0	0

T = 824¡C, sd = 109,

P = 10.1 kbars, sd = 1.5, cor = 0.636, sigfit = 0.51

DTC15007I domain 2 (average core and rim)

Activities and their uncertainties

	phl	ann	east	py	gr	alm	an
a	0.0600	0.0460	0.0180	0.00470	0.0180	0.160	0.460
sd(a)/a	0.34206	0.37060	0.44980	0.62374	0.49008	0.18806	0.08748

	tr	fact	ts	q	H2O
a	0.0209	0.00170	0.00130	1.00	1.00
sd(a)/a	0.43906	0.77909	0.84615	0	

Independent set of reactions

1) 2py + 4gr + 3ts + 12q = 12an + 3tr

2) 21an + 6tr = 10py + 11gr + 27q + 6H2O

3) 21an + 6fact = 11gr + 10alm + 27q + 6H2O

4) 3east + py + 2gr + 6q = 3phl + 6an

5) 3east + 2gr + alm + 6q = 2phl + ann + 6an

Calculations for the independent set of reactions (for x(H2O) = 1.0)

	P(T)	sd(P)	a	sd(a)	b	c	ln_K	sd(ln_K)
1	8.0	1.34	-23.14	6.48	-0.38390	21.360	25.804	3.831
2	10.0	1.29	541.26	4.63	0.43622	-49.741	-58.278	8.848
3	8.2	1.04	-25.05	11.26	0.60180	-54.015	-7.947	7.604
4	9.2	1.45	-0.48	1.59	-0.21480	10.648	12.348	2.121
5	8.5	1.29	44.12	1.84	-0.22832	10.935	8.554	1.923

Diagnostics, hat < 0.42, e* < 2.5, fit < 1.61

	P	sd(P)	T	sd(T)	cor	fit	e*	hat
phl	9.95	1.42	767	100	0.651	0.49	-0.36	0.02
ann	9.87	1.42	762	99	0.629	0.54	-0.11	0.04
east	9.92	1.41	782	104	0.624	0.39	0.61	0.14
py	9.82	1.85	754	147	0.810	0.54	0.04	0.62
gr	9.88	2.18	760	101	0.569	0.55	0.00	0.64
alm	9.89	1.42	760	100	0.609	0.55	-0.02	0.05
an	9.88	1.49	760	99	0.572	0.55	-0.01	0.11
tr	10.03	1.50	767	102	0.676	0.52	0.19	0.07
fact	9.92	1.42	757	100	0.614	0.53	0.17	0.10
ts	9.77	1.43	739	107	0.651	0.45	-0.53	0.18
q	9.89	1.41	760	99	0.646	0.55	0	0
H2O	9.89	1.41	760	99	0.646	0.55	0	0

T = 760¡C, sd = 99,

P = 9.9 kbars, sd = 1.4, cor = 0.646, sigfit = 0.55

DTC15007I domain 3 (average core and rim)

Activities and their uncertainties

	phl	ann	east	py	gr	alm	an
a	0.0620	0.0540	0.0190	0.00620	0.0101	0.190	0.390
sd(a)/a	0.33840	0.34822	0.44599	0.59970	0.55297	0.16265	0.11163

	tr	fact	ts	q	H2O
a	0.0250	0.00230	0.00160	1.00	1.00
sd(a)/a	0.42526	0.74191	0.81250	0	

Independent set of reactions

1) 2py + 4gr + 3ts + 12q = 12an + 3tr

2) 21an + 6tr = 10py + 11gr + 27q + 6H2O

3) 21an + 6fact = 11gr + 10alm + 27q + 6H2O

4) 3east + py + 2gr + 6q = 3phl + 6an

5) 3east + 2gr + alm + 6q = 2phl + ann + 6an

Calculations for the independent set of reactions (for x(H2O) = 1.0)

	P(T)	sd(P)	a	sd(a)	b	c	ln_K	sd(ln_K)
1	8.1	1.38	-23.14	6.48 -	0.38390	21.360	25.495	3.962
2	9.9	1.35	541.26	4.63	0.43622	-49.741	-59.472	9.218
3	7.8	1.10	-25.05	11.26	0.60180	-54.015	-10.932	8.059
4	9.4	1.51	-0.48	1.59 -	0.21480	10.648	12.172	2.203
5	8.5	1.35	44.12	1.84 -	0.22832	10.935	8.611	2.017

Diagnostics, hat < 0.42, e* < 2.5, fit < 1.61

	P	sd(P)	T	sd(T)	cor	fit	e*	hat
phl	9.56	1.46	760	95	0.595	0.52	-0.61	0.02
ann	9.47	1.46	751	94	0.574	0.65	0.02	0.03
east	9.50	1.45	776	98	0.569	0.42	0.78	0.12
py	9.10	1.82	716	140	0.762	0.62	0.24	0.61
gr	9.60	2.35	752	96	0.545	0.64	-0.04	0.68
alm	9.51	1.46	748	95	0.560	0.64	-0.13	0.04
an	9.39	1.58	752	94	0.487	0.64	-0.08	0.14
tr	9.56	1.53	756	97	0.624	0.64	0.13	0.06
fact	9.53	1.46	745	95	0.559	0.61	0.32	0.08
ts	9.42	1.47	742	101	0.595	0.63	-0.23	0.18
q	9.47	1.45	751	94	0.590	0.65	0	0
H2O	9.47	1.45	751	94	0.590	0.65	0	0

T = 751¡C, sd = 94,

P = 9.5 kbars, sd = 1.5, cor = 0.590, sigfit = 0.65

Summary DTC15007I

	DTC15007I domain 1			
	Fe3+ uncorrected		Fe3+ corrected	
All reactions	core	rim	core	rim
P kbar	10.2	10.1	10.2	10.1
P (sd)	1.6	1.5	1.6	1.5
T °C	818	824	819	824
T (sd)	111	109	111	109

	DTC15007I domain 2	
	Fe3+ uncorrected	Fe3+ corrected
All reactions		
P kbar	9.9	9.9
P (sd)	1.4	1.4
T °C	760	760
T (sd)	99	99

	DTC15007I domain 3	
	Fe3+ uncorrected	Fe3+ corrected
All reactions		
P kbar	9.4	9.5
P (sd)	1.4	1.5
T °C	749	751
T (sd)	93	94

	DTC15007I Average PT			
	Fe3+ uncorrected		Fe3+ corrected	
	core	rim	core	rim
P kbar	9.8	9.8	9.9	9.8
P (sd)	1.5	1.4	1.5	1.5
T °C	776	778	777	778
T (sd)	101	100	101	101

DTC15002D

DTC15002D, domain 1 (garnet core)

Activities and their uncertainties

	phl	ann	east	py	gr	alm	an
a	0.0880	0.0380	0.0280	0.0115	0.00700	0.190	0.410
sd(a)/a	0.29682	0.39657	0.41600	0.53956	0.58861	0.16265	0.10443

	tr	fact	ts	q	H2O
a	0.0387	0.00100	0.00110	1.00	1.00
sd(a)/a	0.38715	0.84108	1.36364	0	

Independent set of reactions

1) 2py + 4gr + 3ts + 12q = 12an + 3tr

2) 21an + 6tr = 10py + 11gr + 27q + 6H2O

3) 21an + 6fact = 11gr + 10alm + 27q + 6H2O

4) 5phl + 3fact = 5ann + 3tr

5) 3east + py + 2gr + 6q = 3phl + 6an

Calculations for the independent set of reactions (for x(H2O) = 1.0)

	P(T)	sd(P)	a	sd(a)	b	c	ln_K	sd(ln_K)
1	7.0	1.77	-23.14	6.48	-0.38390	21.360	28.761	5.134
2	9.6	1.32	541.26	4.63	0.43622	-49.741	-60.999	9.013
3	7.8	1.18	-25.05	11.26	0.60180	-54.015	-11.018	8.651
4	3.2	39.70	-60.17	6.73	0.01524	-0.701	6.769	3.722
5	9.2	1.44	-0.48	1.59	-0.21480	10.648	12.475	2.102

Diagnostics, hat < 0.42, e* < 2.5, fit < 1.61

	P	sd(P)	T	sd(T)	cor	fit	e*	hat
phl	9.40	1.45	755	93	0.539	0.67	-0.61	0.02
ann	9.34	1.45	745	94	0.508	0.78	0.05	0.06
east	9.37	1.45	780	99	0.505	0.58	0.79	0.18
py	9.05	1.80	718	139	0.733	0.77	0.18	0.60
gr	9.41	2.41	747	94	0.498	0.78	-0.02	0.71
alm	9.35	1.45	743	94	0.502	0.78	-0.09	0.04
an	9.28	1.57	747	92	0.457	0.78	-0.05	0.11
tr	9.53	1.54	759	98	0.592	0.75	0.24	0.08
fact	9.36	1.45	742	94	0.502	0.77	0.21	0.10
ts	9.26	1.45	728	95	0.534	0.65	-0.81	0.09
q	9.33	1.45	746	92	0.536	0.78	0	0
H2O	9.33	1.45	746	92	0.536	0.78	0	0

T = 746¡C, sd = 92,

P = 9.3 kbars, sd = 1.4, cor = 0.536, sigfit = 0.78

DTC15002D, domain 2 (garnet core)

Activities and their uncertainties

	phl	ann	east	py	gr	alm	an
a	0.0890	0.0360	0.0330	0.0146	0.00580	0.190	0.380
sd(a)/a	0.29541	0.40378	0.40181	0.51383	0.60565	0.16265	0.11532

	tr	fact	ts	q	H2O
a	0.0417 0	.000660	0.000900	1.00	1.00
sd(a)/a	0.37997	0.88668	1.77778	0	

Independent set of reactions

1) 2py + 4gr + 3ts + 12q = 12an + 3tr

2) 21an + 6tr = 10py + 11gr + 27q + 6H2O

3) 21an + 6fact = 11gr + 10alm + 27q + 6H2O

4) 5phl + 3fact = 5ann + 3tr

5) 3east + py + 2gr + 6q = 3phl + 6an

Calculations for the independent set of reactions (for x(H2O) = 1.0)

	P(T)	sd(P)	a	sd(a)	b	c	ln_K	sd(ln_K)
1	7.3	2.32	0.35	6.48	-0.39707	20.711	28.950	6.212
2	9.8	1.42	482.15	4.63	0.48401	-49.000	-59.533	9.047
3	8.5	1.32	-79.19	11.26	0.64279	-53.208	-8.997	9.011
4	20.8	42.81	-60.14	6.73	0.01524	-0.703	7.912	3.825
5	10.2	1.58	11.53	1.59	-0.22155	10.316	11.697	2.109

Diagnostics, hat < 0.42, e* < 2.5, fit < 1.61

	P	sd(P)	T	sd(T)	cor	fit	e*	hat
phl	9.62	1.46	746	89	0.520	0.73	-0.87	0.02
ann	9.56	1.46	725	91	0.486	0.90	0.29	0.08
east	9.58	1.45	773	96	0.485	0.71	0.89	0.19
py	9.03	1.80	685	134	0.720	0.89	0.31	0.58
gr	9.70	2.44	735	91	0.486	0.93	-0.05	0.71
alm	9.56	1.46	727	91	0.483	0.91	-0.17	0.04
an	9.43	1.60	734	88	0.431	0.92	-0.09	0.13
tr	9.78	1.55	749	95	0.580	0.89	0.30	0.08
fact	9.55	1.46	729	90	0.484	0.92	0.17	0.10
ts	9.48	1.46	720	90	0.516	0.82	-0.81	0.06
q	9.53	1.45	733	88	0.517	0.93	0	0
H2O	9.53	1.45	733	88	0.517	0.93	0	0

T = 733¡C, sd = 88,

P = 9.5 kbars, sd = 1.5, cor = 0.517, sigfit = 0.93

DTC15002D, domain 3 (garnet core)

Activities and their uncertainties

	phl	ann	east	py	gr	alm	an
a	0.0760	0.0460	0.0220	0.00900	0.00880	0.180	0.350
sd(a)/a	0.31478	0.37060	0.43521	0.56453	0.56674	0.17060	0.12675

	tr	fact	ts	q
a	0.0450 0	.000580	0.00140	1.00
sd(a)/a	0.37244	0.90033	1.35714	0

Independent set of reactions

1) 2py + 4gr + 3ts + 12q = 12an + 3tr

2) 21an + 6tr = 10py + 11gr + 27q + 6H2O

3) 21an + 6fact = 11gr + 10alm + 27q + 6H2O

4) 3east + py + 2gr + 6q = 3phl + 6an

5) 3east + 2gr + alm + 6q = 2phl + ann + 6an

Calculations for the independent set of reactions (for x(H2O) = 1.0)

	P(T)	sd(P)	a	sd(a)	b	c	ln_K	sd(ln_K)
1	7.9	1.78	-23.14	6.48	-0.38390	21.360	26.166	5.153
2	10.0	1.33	541.26	4.63	0.43622	-49.741	-58.516	9.100
3	8.9	1.21	-25.05	11.26	0.60180	-54.015	-2.450	8.834
4	9.8	1.50	-0.48	1.59	-0.21480	10.648	11.597	2.186
5	8.8	1.36	44.12	1.84	-0.22832	10.935	8.099	2.032

Diagnostics, hat < 0.42, e* < 2.5, fit < 1.61

	P	sd(P)	T	sd(T)	cor	fit	e*	hat
phl	9.90	1.43	727	90	0.564	0.64	-0.83	0.02
ann	9.85	1.43	703	91	0.530	0.74	0.54	0.06
east	9.82	1.43	737	97	0.535	0.77	0.51	0.17
py	9.33	1.81	675	136	0.754	0.81	0.27	0.61
gr	9.82	2.30	716	91	0.506	0.84	-0.01	0.66
alm	9.79	1.43	712	91	0.523	0.84	-0.10	0.04
an	9.75	1.59	716	90	0.451	0.84	-0.02	0.16
tr	10.10	1.52	735	94	0.608	0.76	0.41	0.07
fact	9.71	1.43	725	91	0.528	0.79	-0.48	0.09
ts	9.71	1.43	703	92	0.560	0.78	-0.59	0.09
q	9.77	1.43	715	89	0.558	0.84	0	0
H2O	9.77	1.43	715	89	0.558	0.84	0	0

T = 715¡C, sd = 89,

P = 9.8 kbars, sd = 1.4, cor = 0.558, sigfit = 0.84

DTC15002D, domain 1 (garnet rim)

Activities and their uncertainties

	phl	ann	east	py	gr	alm	an
a	0.0880	0.0380	0.0280	0.0117	0.00790	0.200	0.400
sd(a)/a	0.29682	0.39657	0.41600	0.53775	0.57721	0.15515	0.10800

	tr	fact	ts	q	H2O
a	0.0375	0.00100	0.00110	1.00	1.00
sd(a)/a	0.39012	0.84108	1.36364	0	

Independent set of reactions

1) 2py + 4gr + 3ts + 12q = 12an + 3tr

2) 21an + 6tr = 10py + 11gr + 27q + 6H2O

3) 21an + 6fact = 11gr + 10alm + 27q + 6H2O

4) 5phl + 3fact = 5ann + 3tr

5) 3east + py + 2gr + 6q = 3phl + 6an

Calculations for the independent set of reactions (for x(H2O) = 1.0)

	P(T)	sd(P)	a	sd(a)	b	c	ln_K	sd(ln_K)
1	7.3	1.77	-23.14	6.48	-0.38390	21.360	27.852	5.126
2	10.0	1.31	541.26	4.63	0.43622	-49.741	-58.789	8.936
3	8.1	1.17	-25.05	11.26	0.60180	-54.015	-8.656	8.563
4	2.2	39.73	-60.17	6.73	0.01524	-0.701	6.674	3.724
5	9.4	1.44	-0.48	1.59	-0.21480	10.648	12.068	2.096

Diagnostics, hat < 0.42, e* < 2.5, fit < 1.61

	P	sd(P)	T	sd(T)	cor	fit	e*	hat
phl	9.80	1.46	757	93	0.559	0.66	-0.57	0.02
ann	9.73	1.46	747	94	0.529	0.76	0.03	0.07
east	9.77	1.46	781	99	0.529	0.58	0.77	0.17
py	9.46	1.84	723	140	0.749	0.75	0.16	0.60
gr	9.79	2.39	749	94	0.508	0.76	-0.02	0.70
alm	9.74	1.46	745	94	0.525	0.76	-0.08	0.04
an	9.67	1.59	748	92	0.472	0.76	-0.05	0.12
tr	9.92	1.55	760	98	0.611	0.74	0.23	0.08
fact	9.75	1.46	743	94	0.522	0.75	0.22	0.10
ts	9.64	1.46	730	95	0.555	0.63	-0.81	0.09
q	9.72	1.45	748	92	0.556	0.77	0	0
H2O	9.72	1.45	748	92	0.556	0.77	0	0

T = 748¡C, sd = 92,

P = 9.7 kbars, sd = 1.5, cor = 0.556, sigfit = 0.77

DTC15002D, domain 2 (garnet rim)

Activities and their uncertainties

	phl	ann	east	py	gr	alm	an
a	0.0910	0.0370	0.0320	0.0158	0.00930	0.170	0.370
sd(a)/a	0.29261	0.40013	0.40454	0.50500	0.56127	0.17905	0.11907

	tr	fact	ts	q	H2O
a	0.0365	0.000650	0.00100	1.00	1.00
sd(a)/a	0.39264	0.88830	1.60000	0	

Independent set of reactions

1) 2py + 4gr + 3ts + 12q = 12an + 3tr

2) 21an + 6tr = 10py + 11gr + 27q + 6H2O

3) 21an + 6fact = 11gr + 10alm + 27q + 6H2O

4) 5phl + 3fact = 5ann + 3tr

5) 3east + py + 2gr + 6q = 3phl + 6an

Calculations for the independent set of reactions (for x(H2O) = 1.0)

	P(T)	sd(P)	a	sd(a)	b	c	ln_K	sd(ln_K)
1	8.4	2.14	0.35	6.48	-0.39707	20.711	25.867	5.703
2	10.9	1.36	482.15	4.63	0.48401	-49.000	-52.191	8.685
3	9.2	1.27	-79.19	11.26	0.64279	-53.208	-4.264	8.717
4	17.2	42.81	-60.14	6.73	0.01524	-0.703	7.585	3.825
5	11.0	1.54	11.53	1.59	-0.22155	10.316	10.673	2.066

Diagnostics, hat < 0.42, e* < 2.5, fit < 1.61

	P	sd(P)	T	sd(T)	cor	fit	e*	hat
phl	10.88	1.52	791	96	0.575	0.70	-0.86	0.01
ann	10.79	1.52	770	99	0.545	0.88	0.28	0.08
east	10.87	1.52	821	104	0.549	0.67	0.91	0.18
py	10.19	1.96	727	145	0.767	0.86	0.31	0.58
gr	10.93	2.45	780	98	0.516	0.90	-0.05	0.67
alm	10.80	1.52	770	99	0.535	0.89	-0.19	0.05
an	10.65	1.68	779	96	0.475	0.90	-0.10	0.15
tr	11.06	1.64	796	103	0.632	0.86	0.30	0.09
fact	10.79	1.52	774	98	0.541	0.90	0.19	0.10
ts	10.70	1.52	764	98	0.573	0.82	-0.71	0.07
q	10.77	1.52	778	96	0.572	0.90	0	0
H2O	10.77	1.52	778	96	0.572	0.90	0	0

T = 778¡C, sd = 96,

P = 10.8 kbars, sd = 1.5, cor = 0.572, sigfit = 0.90

DTC15002D, domain 3 (garnet rim)

Activities and their uncertainties

	phl	ann	east	py	gr	alm	an
a	0.0790	0.0470	0.0210	0.0126	0.00860	0.180	0.330
sd(a)/a	0.31012	0.36762	0.43870	0.52988	0.56899	0.17060	0.13467

	tr	fact	ts	q
a	0.0374	0.000560	0.00150	1.00
sd(a)/a	0.39037	0.90400	1.26667	0

Independent set of reactions

1) 2py + 4gr + 3ts + 12q = 12an + 3tr

2) 21an + 6tr = 10py + 11gr + 27q + 6H2O

3) 21an + 6fact = 11gr + 10alm + 27q + 6H2O

4) 3east + py + 2gr + 6q = 3phl + 6an

5) 3east + 2gr + alm + 6q = 2phl + ann + 6an

Calculations for the independent set of reactions (for x(H2O) = 1.0)

	P(T)	sd(P)	a	sd(a)	b	c	ln_K	sd(ln_K)
1	8.6	1.72	-23.14	6.48	-0.38390	21.360	24.117	4.973
2	10.8	1.31	541.26	4.63	0.43622	-49.741	-53.058	8.985
3	9.1	1.22	-25.05	11.26	0.60180	-54.015	-1.257	8.916
4	10.0	1.51	-0.48	1.59	-0.21480	10.648	11.209	2.197
5	8.9	1.38	44.12	1.84	-0.22832	10.935	8.030	2.056

Diagnostics, hat < 0.42, e* < 2.5, fit < 1.61

	P	sd(P)	T	sd(T)	cor	fit	e*	hat
phl	10.78	1.56	786	97	0.573	0.57	-0.84	0.01
ann	10.71	1.56	760	99	0.543	0.68	0.57	0.06
east	10.70	1.56	798	105	0.549	0.72	0.51	0.17
py	10.10	1.98	726	147	0.762	0.75	0.30	0.60
gr	10.74	2.49	776	99	0.519	0.79	-0.03	0.65
alm	10.67	1.56	770	100	0.535	0.79	-0.13	0.05
an	10.59	1.74	776	97	0.454	0.79	-0.05	0.18
tr	11.00	1.66	795	103	0.620	0.72	0.39	0.07
fact	10.60	1.56	785	99	0.540	0.75	-0.42	0.10
ts	10.60	1.56	767	101	0.573	0.77	-0.35	0.10
q	10.65	1.55	775	97	0.569	0.80	0	0
H2O	10.65	1.55	775	97	0.569	0.80	0	0

T = 775¡C, sd = 97,

P = 10.6 kbars, sd = 1.6, cor = 0.569, sigfit = 0.80

DTC15002D Fe^{3+} corrected

DTC15002D, domain 1 (garnet core)

Activities and their uncertainties

	phl	ann	east	py	gr	alm	an
a	0.0880	0.0380	0.0280	0.0116	0.00690	0.190	0.410
sd(a)/a	0.29682	0.39657	0.41600	0.53865	0.58994	0.16265	0.10443

	tr	fact	ts	q	H2O
a	0.0385	0.00100	0.00110	1.00	1.00
sd(a)/a	0.38764	0.84108	1.36364	0	

Independent set of reactions

1) 2py + 4gr + 3ts + 12q = 12an + 3tr

2) 21an + 6tr = 10py + 11gr + 27q + 6H2O

3) 21an + 6fact = 11gr + 10alm + 27q + 6H2O

4) 5phl + 3fact = 5ann + 3tr

5) 3east + py + 2gr + 6q = 3phl + 6an

Calculations for the independent set of reactions (for x(H2O) = 1.0)

	P(T)	sd(P)	a	sd(a)	b	c	ln_K	sd(ln_K)
1	7.0	1.77	-23.14	6.48 -	0.38390	21.360	28.785	5.137
2	9.6	1.32	541.26	4.63	0.43622	-49.741	-61.040	9.019
3	7.8	1.18	-25.05	11.26	0.60180	-54.015	-11.176	8.662
4	3.1	39.71	-60.17	6.73	0.01524	-0.701	6.753	3.722
5	9.1	1.44	-0.48	1.59 -	0.21480	10.648	12.495	2.104

Diagnostics, hat < 0.42, e* < 2.5, fit < 1.61

	P	sd(P)	T	sd(T)	cor	fit	e*	hat
phl	9.39	1.45	757	93	0.538	0.67	-0.61	0.02
ann	9.33	1.45	746	94	0.507	0.78	0.06	0.06
east	9.35	1.45	781	99	0.504	0.58	0.79	0.18
py	9.04	1.81	719	140	0.732	0.77	0.18	0.60
gr	9.40	2.42	748	94	0.497	0.78	-0.02	0.71
alm	9.34	1.45	744	94	0.500	0.78	-0.09	0.04
an	9.27	1.57	748	92	0.456	0.78	-0.05	0.11
tr	9.52	1.54	760	98	0.591	0.75	0.24	0.08
fact	9.35	1.45	743	94	0.501	0.77	0.21	0.10
ts	9.25	1.45	730	95	0.533	0.65	-0.80	0.09
q	9.32	1.45	747	92	0.535	0.78	0	0
H2O	9.32	1.45	747	92	0.535	0.78	0	0

T = 747¡C, sd = 92,

P = 9.3 kbars, sd = 1.4, cor = 0.535, sigfit = 0.78

DTC15002D, domain 2 (garnet core)

Activities and their uncertainties

	phl	ann	east	py	gr	alm	an
a	0.0890	0.0360	0.0330	0.0146	0.00580	0.190	0.380
sd(a)/a	0.29541	0.40378	0.40181	0.51383	0.60565	0.16265	0.11532

	tr	fact	ts	q	H2O
a	0.0422	0.000660	0.000900	1.00	1.00
sd(a)/a	0.37881	0.88668	1.77778	0	

Independent set of reactions

1) 2py + 4gr + 3ts + 12q = 12an + 3tr

2) 21an + 6tr = 10py + 11gr + 27q + 6H2O

3) 21an + 6fact = 11gr + 10alm + 27q + 6H2O

4) 5phl + 3fact = 5ann + 3tr

5) 3east + py + 2gr + 6q = 3phl + 6an

Calculations for the independent set of reactions (for x(H2O) = 1.0)

	P(T)	sd(P)	a	sd(a)	b	c	ln_K	sd(ln_K)
1	7.2	2.32	0.35	6.48	-0.39707	20.711	28.985	6.211
2	9.8	1.42	482.15	4.63	0.48401	-49.000	-59.605	9.045
3	8.5	1.32	-79.19	11.26	0.64279	-53.208	-8.997	9.011
4	21.2	42.80	-60.14	6.73	0.01524	-0.703	7.948	3.824
5	10.2	1.58	11.53	1.59	-0.22155	10.316	11.697	2.109

Diagnostics, hat < 0.42, e* < 2.5, fit < 1.61

	P	sd(P)	T	sd(T)	cor	fit	e*	hat
phl	9.61	1.45	745	89	0.519	0.73	-0.87	0.02
ann	9.55	1.45	724	91	0.485	0.91	0.29	0.08
east	9.57	1.45	772	96	0.484	0.71	0.89	0.19
py	9.02	1.80	684	134	0.720	0.89	0.31	0.58
gr	9.69	2.43	734	90	0.485	0.93	-0.05	0.71
alm	9.55	1.46	726	91	0.482	0.92	-0.17	0.04
an	9.42	1.60	733	88	0.430	0.93	-0.09	0.13
tr	9.77	1.55	748	95	0.579	0.89	0.30	0.08
fact	9.54	1.46	729	90	0.484	0.92	0.17	0.10
ts	9.47	1.45	719	90	0.515	0.83	-0.82	0.06
q	9.52	1.45	732	88	0.516	0.93	0	0
H2O	9.52	1.45	732	88	0.516	0.93	0	0

T = 732¡C, sd = 88,

P = 9.5 kbars, sd = 1.5, cor = 0.516, sigfit = 0.93

DTC15002D, domain 3 (garnet core)

Activities and their uncertainties

	phl	ann	east	py	gr	alm	an
a	0.0770	0.0460	0.0220	0.00910	0.00870	0.180	0.350
sd(a)/a	0.31321	0.37060	0.43521	0.56343	0.56786	0.17060	0.12675

	tr	fact	ts	q	H20
a	0.0447	0.000580	0.00140	1.00	1.00
sd(a)/a	0.37311	0.90033	1.35714	0	0

Independent set of reactions

1) 2py + 4gr + 3ts + 12q = 12an + 3tr

2) 21an + 6tr = 10py + 11gr + 27q + 6H2O

3) 21an + 6fact = 11gr + 10alm + 27q + 6H2O

4) 3east + py + 2gr + 6q = 3phl + 6an

5) 3east + 2gr + alm + 6q = 2phl + ann + 6an

Calculations for the independent set of reactions (for x(H2O) = 1.0)

	P(T)	sd(P)	a	sd(a)	b	c	ln_K s	d(ln_K)
1	7.9	1.78	-23.14	6.48	-0.38390	21.360	26.169	5.155
2	10.0	1.33	541.26	4.63	0.43622	-49.741	-58.491	9.103
3	8.9	1.21	-25.05	11.26	0.60180	-54.015	-2.576	8.843
4	9.7	1.50	-0.48	1.59	-0.21480	10.648	11.648	2.185
5	8.8	1.36	44.12	1.84	-0.22832	10.935	8.148	2.033

Diagnostics, hat < 0.42, e* < 2.5, fit < 1.61

	P	sd(P)	T	sd(T)	cor	fit	e*	hat
phl	9.91	1.44	729	90	0.563	0.63	-0.81	0.02
ann	9.85	1.43	705	91	0.529	0.73	0.54	0.06
east	9.82	1.43	739	97	0.534	0.76	0.50	0.17
py	9.34	1.82	678	136	0.754	0.80	0.26	0.61
gr	9.82	2.31	718	91	0.505	0.83	-0.01	0.66
alm	9.80	1.44	714	92	0.522	0.82	-0.10	0.04
an	9.75	1.59	718	90	0.451	0.83	-0.02	0.16
tr	10.10	1.52	736	94	0.607	0.75	0.40	0.07
fact	9.72	1.43	727	91	0.527	0.78	-0.48	0.09
ts	9.71	1.44	705	92	0.559	0.77	-0.58	0.09
q	9.78	1.43	717	89	0.558	0.83	0	0
H2O	9.78	1.43	717	89	0.558	0.83	0	0

T = 717¡C, sd = 89,

P = 9.8 kbars, sd = 1.4, cor = 0.558, sigfit = 0.83

DTC15002D, domain 1 (garnet rim)

Activities and their uncertainties

	phl	ann	east	py	gr	alm	an
a	0.0880	0.0380	0.0280	0.0117	0.00800	0.200	0.410
sd(a)/a	0.29682	0.39657	0.41600	0.53775	0.57600	0.15515	0.10443

	tr	fact	ts	q	H2O
a	0.0385	0.00100	0.00110	1.00	1.00
sd(a)/a	0.38764	0.84108	1.36364	0	

Independent set of reactions

1) 2py + 4gr + 3ts + 12q = 12an + 3tr

2) 21an + 6tr = 10py + 11gr + 27q + 6H2O

3) 21an + 6fact = 11gr + 10alm + 27q + 6H2O

4) 5phl + 3fact = 5ann + 3tr

5) 3east + py + 2gr + 6q = 3phl + 6an

Calculations for the independent set of reactions (for x(H2O) = 1.0)

	P(T)	sd(P)	a	sd(a)	b	c	ln_K	sd(ln_K)
1	7.2	1.76	-23.14	6.48 -	0.38390	21.360	28.176	5.111
2	9.9	1.30	541.26	4.63	0.43622	-49.741	-59.327	8.904
3	8.0	1.17	-25.05	11.26	0.60180	-54.015	-9.036	8.534
4	3.1	39.71	-60.17	6.73	0.01524	-0.701	6.753	3.722
5	9.3	1.43	-0.48	1.59 -	0.21480	10.648	12.191	2.088

Diagnostics, hat < 0.42, e* < 2.5, fit < 1.61

	P	sd(P)	T	sd(T)	cor	fit	e*	hat
phl	9.71	1.45	756	93	0.557	0.67	-0.57	0.02
ann	9.64	1.45	747	94	0.526	0.77	0.04	0.07
east	9.68	1.44	780	99	0.525	0.59	0.76	0.17
py	9.38	1.82	723	140	0.748	0.76	0.15	0.60
gr	9.69	2.38	748	94	0.506	0.77	-0.02	0.70
alm	9.65	1.45	745	94	0.522	0.76	-0.07	0.04
an	9.60	1.57	748	92	0.474	0.77	-0.04	0.11
tr	9.84	1.54	760	98	0.609	0.74	0.24	0.08
fact	9.66	1.45	744	94	0.520	0.76	0.19	0.10
ts	9.56	1.45	729	95	0.553	0.63	-0.84	0.09
q	9.64	1.44	748	92	0.554	0.77	0	0
H2O	9.64	1.44	748	92	0.554	0.77	0	0

T = 748¡C, sd = 92,

P = 9.6 kbars, sd = 1.4, cor = 0.554, sigfit = 0.77

DTC15002D, domain 2 (garnet rim)

Activities and their uncertainties

	phl	ann	east	py	gr	alm	an
a	0.0770	0.0340	0.0420	0.0192	0.0107	0.160	0.450
sd(a)/a	0.31321	0.41133	0.37927	0.48254	0.54706	0.18806	0.09075

	tr	fact	ts	q	H2O
		.000740			
a	0.0826 0	0	.000600	1.00	1.00
sd(a)/a	0.30468	0.87438	2.66667	0	

Independent set of reactions

1) 2py + 4gr + 3ts + 12q = 12an + 3tr

2) 21an + 6tr = 10py + 11gr + 27q + 6H2O

3) 21an + 6fact = 11gr + 10alm + 27q + 6H2O

4) 5phl + 3fact = 5ann + 3tr

5) 3east + py + 2gr + 6q = 3phl + 6an

Calculations for the independent set of reactions (for x(H2O) = 1.0)

	P(T)	sd(P)	a	sd(a)	b	c	ln_K	sd(ln_K)
1	6.4	3.15	0.35	6.48 -	0.39707	20.711	31.248	8.470
2	10.1	1.28	482.15	4.63	0.48401	-49.000	-57.710	8.153
3	8.6	1.23	-79.19	11.26	0.64279	-53.208	-8.217	8.420
4	44.2	42.48	-60.14	6.73	0.01524	-0.703	10.058	3.795
5	11.4	1.48	11.53	1.59 -	0.22155	10.316	10.055	1.976

Diagnostics, hat < 0.42, e* < 2.5, fit < 1.61

	P	sd(P)	T	sd(T)	cor	fit	e*	hat
phl	9.84	1.36	745	87	0.520	1.05	-1.62	0.03
ann	9.75	1.81	699	119	0.481	1.40	0.71	0.09
east	9.75	1.52	780	107	0.481	1.17	1.31	0.21
py	8.71	2.29	630	173	0.738	1.38	0.60	0.58
gr	9.98	3.19	721	124	0.471	1.48	-0.10	0.71
alm	9.74	1.85	701	123	0.470	1.43	-0.41	0.07
an	9.54	2.06	720	121	0.453	1.47	-0.15	0.09
tr	9.95	1.98	737	126	0.575	1.44	0.36	0.07
fact	9.70	1.91	713	125	0.485	1.47	0.24	0.11
ts	9.65	1.81	709	116	0.516	1.40	-0.94	0.03
q	9.68	1.91	718	121	0.517	1.48	0	0
H2O	9.68	1.91	718	121	0.517	1.48	0	0

T = 718¡C, sd = 121,

P = 9.7 kbars, sd = 1.9, cor = 0.517, sigfit = 1.48

DTC15002D, domain 3 (garnet rim)

Activities and their uncertainties

	phl	ann	east	py	gr	alm	an
a	0.0790	0.0470	0.0210	0.0126	0.00860	0.170	0.330
sd(a)/a	0.31012	0.36762	0.43870	0.52988	0.56899	0.17905	0.13467

	tr	fact	ts	q	H2O
a	0.0368	0.000550	0.00150	1.00	1.00
sd(a)/a	0.39188	0.90587	1.26667	0	

Independent set of reactions

1) 2py + 4gr + 3ts + 12q = 12an + 3tr

2) 21an + 6tr = 10py + 11gr + 27q + 6H2O

3) 21an + 6fact = 11gr + 10alm + 27q + 6H2O

4) 3east + py + 2gr + 6q = 3phl + 6an

5) 3east + 2gr + alm + 6q = 2phl + ann + 6an

Calculations for the independent set of reactions (for x(H2O) = 1.0)

	P(T)	sd(P)	a	sd(a)	b	c	ln_K	sd(ln_K)
1	8.6	1.72	-23.14	6.48	-0.38390	21.360	24.068	4.974
2	10.8	1.31	541.26	4.63	0.43622	-49.741	-52.961	8.988
3	9.0	1.22	-25.05	11.26	0.60180	-54.015	-1.720	8.940
4	10.0	1.51	-0.48	1.59	-0.21480	10.648	11.209	2.197
5	8.8	1.38	44.12	1.84	-0.22832	10.935	8.087	2.057

Diagnostics, hat < 0.42, e* < 2.5, fit < 1.61

	P	sd(P)	T	sd(T)	cor	fit	e*	hat
phl	10.78	1.57	792	99	0.572	0.57	-0.87	0.01
ann	10.71	1.56	765	100	0.541	0.69	0.59	0.06
east	10.70	1.56	805	106	0.547	0.73	0.53	0.17
py	10.06	2.00	727	149	0.761	0.76	0.32	0.59
gr	10.75	2.51	782	100	0.518	0.81	-0.03	0.65
alm	10.67	1.57	775	101	0.531	0.80	-0.15	0.05
an	10.57	1.75	782	99	0.452	0.81	-0.06	0.18
tr	11.00	1.67	801	104	0.619	0.74	0.39	0.08
fact	10.60	1.57	790	100	0.538	0.77	-0.41	0.10
ts	10.60	1.57	773	102	0.571	0.79	-0.31	0.10
q	10.65	1.56	781	98	0.568	0.81	0	0
H2O	10.65	1.56	781	98	0.568	0.81	0	0

T = 781¡C, sd = 98,

P = 10.6 kbars, sd = 1.6, cor = 0.568, sigfit = 0.81

Summary DTC15002D

DTC15002D domain 1

	Fe3+ uncorrected		Fe3+ corrected	
All reactions	core	rim	core	rim
P kbar	9.3	9.7	9.3	9.6
P (sd)	1.4	1.5	1.4	1.4
T °C	746	748	747	748
T (sd)	92	92	92	92

DTC15002D domain 2

	Fe3+ uncorrected		Fe3+ corrected	
All reactions	core	rim	core	rim
P kbar	9.5	10.8	9.5	10.8
P (sd)	1.5	1.5	1.5	1.5
T °C	733	779	732	779
T (sd)	88	96	88	96

DTC15002D domain 3

	Fe3+ uncorrected		Fe3+ corrected	
All reactions	core	rim	core	rim
P kbar	9.8	10.6	9.8	10.6
P (sd)	1.4	1.6	1.4	1.6
T °C	715	775	717	781
T (sd)	89	97	89	98

DTC15002D average PT

	Fe3+ uncorrected		Fe3+ corrected	
All reactions	core	rim	core	rim
P kbar	9.5	10.4	9.5	10.3
P (sd)	1.4	1.5	1.4	1.5
T °C	731	767	732	769
T (sd)	90	95	90	95

Appendix F: PT-estimates from classical geothermobarometry

DTC15002D

		D1	D2	D3	Average	SD
	P (kbar)	T (°C)	T (°C)	T (°C)	T (°C)	T (°C)
Hodges and Spear (1982)	1	756	747	694		
	5	772	763	710		
	10	*793*	*784*	*729*	**769**	**35**
	15	814	804	748		
Fe3+ corrected						
	P (kbar)	T (°C)	T (°C)	T (°C)	T (°C)	T (°C)
Hodges and Spear (1982)	1	783	791	709		
	5	800	808	725		
	10	821	829	745	**798**	**46**
	15	842	850	764		

		D1		D2		D3			
	T (°C)	PMg (kbar)	PFe (kbar)	PMg (kbar)	PFe (kbar)	PMg (kbar)	PFe (kbar)	kbar	kbar
Kohn and Spear (1990)	400	8.8	7.7	8.7	8.2	8.2	7.2		
	600	9.5	9.5	9.5	10.3	8.8	9	**9.4**	**0.5**
	800	10.3	11.4	10.2	12.4	9.4	10.7	**10.7**	**1.0**
	1000	11	13.2	11	14.4	10	12.5		
Fe3+ corrected									
	T (°C)	PMg (kbar)	PFe (kbar)	PMg (kbar)	PFe (kbar)	PMg (kbar)	PFe (kbar)	kbar	kbar
Kohn and Spear (1990)	400	8.9	7.7	9	8.4	8.2	7.2		
	600	9.7	9.6	9.8	10.4	8.9	9	**9.6**	**0.6**
	800	10.5	11.5	10.6	12.5	9.5	10.8	**10.9**	**1.0**
	1000	11.3	13.4	11.5	14.6	10.1	12.5		

	D1	D2	D3		
	T (°C)	T (°C)	T (°C)	T (°C)	T (°C)
Graham and Powell (1984)	672	655	648	**658**	**12**
Fe3+ corrected					
	T (°C)	T (°C)	T (°C)	T (°C)	T (°C)
Graham and Powell (1984)	692	687	657	**679**	**19**

DTC15007I

		D1		D2		D3	Average	SD
	P (kbar)	T (°C)	T (°C)	T (°C)	T (°C)	T (°C)	T (°C)	T (°C)
Hodges and Spear (1982)	1	745		662		686		
	5	760		677		701		
	10	780		695		720	**732**	**44**
	15	799		713		739		
Fe3+ corrected								
	P (kbar)	T (°C)	T (°C)	T (°C)	T (°C)	T (°C)	T (°C)	T (°C)
Hodges and Spear (1982)	1	738		780		673		
	5	754		796		688		
	10	774		816		706	**765**	**56**
	15	793		836		724		

		D1		D2		D3			
	T (°C)	PMg (kbar)	PFe (kbar)	PMg (kbar)	PFe (kbar)	PMg (kbar)	PFe (kbar)	kbar	kbar
Kohn and Spear (1990)	400	8.3	7.1	8.2	7.2	8.2	7.2		
	600	9	8.9	8.8	9.1	8.9	9	**9.0**	**0.1**
	800	9.7	10.7	9.5	11	9.5	10.9	**10.2**	**0.7**
	1000	10.4	12.5	10.1	12.9	10.2	12.7		
Fe3+ corrected									
	T (°C)	PMg (kbar)	PFe (kbar)	PMg (kbar)	PFe (kbar)	PMg (kbar)	PFe (kbar)	kbar	kbar
Kohn and Spear (1990)	400	8.5	7.1	8.4	7.3	8.4	7.3		
	600	9.2	9	9.1	9.2	9.1	9.2	**9.1**	**0.1**
	800	10	10.8	9.8	11.1	9.8	11	**10.4**	**0.6**
	1000	10.7	12.6	10.5	13	10.6	12.8		

	D1		D2		D3		
	T (°C)	T (°C)	T (°C)	T (°C)	T (°C)	T (°C)	T (°C)
Graham and Powell (1984)	724		663		661	**683**	**36**
Fe3+ corrected							
	T (°C)	T (°C)	T (°C)	T (°C)	T (°C)	T (°C)	T (°C)
Graham and Powell (1984)	810		690		687	**729**	**70**

DTC15007L

	DTC15007L							
	Domain 1	Domain 2	Domain 3	Domain 4	Average T (°C)	SD (T)	Average P (kbar)	SD (P)
Wood & Bonno (1973)	1062	1056	1050	922	**1023**	**67**		
Holland & Blundy (1994)	830.1	832.6	851.3	791.1	**826**	**25**		
Anderson & Smith (1995)	8.28	8.18	7.4	9.76			**8.41**	**0.99**